RADAR RESOURCE MANAGEMENT TECHNIQUES FOR MULTI-FUNCTION PHASED ARRAY RADARS

A THESIS SUBMITTED TO
THE GRADUATE SCHOOL OF NATURAL AND APPLIED SCIENCES
OF
MIDDLE EAST TECHNICAL UNIVERSITY

BY

ÖMER ÇAYIR

IN PARTIAL FULFILLMENT OF THE REQUIREMENTS
FOR
THE DEGREE OF MASTER OF SCIENCE
IN
ELECTRICAL AND ELECTRONICS ENGINEERING

SEPTEMBER 2014

Approval of the thesis:

RADAR RESOURCE MANAGEMENT TECHNIQUES FOR MULTI-FUNCTION PHASED ARRAY RADARS

submitted by **ÖMER ÇAYIR** in partial fulfillment of the requirements for the degree of **Master of Science in Electrical and Electronics Engineering Department, Middle East Technical University** by,

Prof. Dr. Canan Özgen
Dean, Graduate School of **Natural and Applied Sciences** _____

Prof. Dr. Gönül Turhan Sayan
Head of Department, **Electrical and Electronics Engineering** _____

Assoc. Prof. Dr. Çağatay Candan
Supervisor, **Electrical and Electronics Eng. Dept., METU** _____

Examining Committee Members:

Prof. Dr. Mübeccel Demirekler
Electrical and Electronics Engineering Department, METU _____

Assoc. Prof. Dr. Çağatay Candan
Electrical and Electronics Engineering Department, METU _____

Assoc. Prof. Dr. Umut Orguner
Electrical and Electronics Engineering Department, METU _____

Assist. Prof. Dr. Fatih Kamışlı
Electrical and Electronics Engineering Department, METU _____

Dr. Recep Fırat Tiğrek
REHIS, ASELSAN Inc. _____

Date: **September 3, 2014**

I hereby declare that all information in this document has been obtained and presented in accordance with academic rules and ethical conduct. I also declare that, as required by these rules and conduct, I have fully cited and referenced all material and results that are not original to this work.

Name, Last Name: ÖMER ÇAYIR

Signature :

ABSTRACT

RADAR RESOURCE MANAGEMENT TECHNIQUES FOR
MULTI-FUNCTION PHASED ARRAY RADARS

Çayır, Ömer
M.S., Department of Electrical and Electronics Engineering
Supervisor : Assoc. Prof. Dr. Çağatay Candan

September 2014, 147 pages

Multi-function phased array radars (MFPARs) are capable of executing several tasks without any rotating antenna by jointly optimizing limited time and energy resources. The allocation of radar time resources is usually referred to as scheduling in radar resource management (RRM) literature. In this thesis, two scheduling algorithms, namely multi-type adaptive time-balance scheduler (MTATBS) and knapsack scheduler (KS), are proposed for real-time operations. A resource-aided technique called as the multi-frequency band usage is developed to increase the applicability of task interleaving.

A simulator for MFPAR system is implemented to apply RRM techniques with different optional choices, such as adaptive update-rate, dynamic task prioritization, tracking, task interleaving. The simulator is designed in a way that each of the blocks can be individually modified according to RRM constraints.

Target selection problem emerges when there are more than one target concurrently requesting track update. It is suggested to adopt the solution methods for the well-

known machine replacement problem to the problem of target selection and track update is solved with the method of decision policy (DecP). In addition to this method, two other ad hoc methods based on track quality are described.

Keywords: Radar Resource Management, RRM, Multi-Function Radar, MFR, Task Scheduling, Time-Balance, Adaptive Time-Balance, Knapsack Problem, Task Interleaving, Multi-Frequency Band Usage, Machine Replacement Problem, Target Selection Problem

ÖZ

ÇOK-İŞLEVLİ FAZ DİZİLİ RADARLAR İÇİN RADAR KAYNAK YÖNETİMİ TEKNİKLERİ

Çayır, Ömer
Yüksek Lisans, Elektrik ve Elektronik Mühendisliği Bölümü
Tez Yöneticisi : Doç. Dr. Çağatay Candan

Eylül 2014 , 147 sayfa

Çok-işlevli faz dizili radarlar (MFPARs) dönen herhangi bir anten olmadan sınırlı zaman ve enerji kaynaklarını birlikte eniyileyerek birçok görevi yürütebilme yeteneğine sahiptir. Radar kaynak yönetimi (RRM) literatüründe radar zaman kaynaklarının ayırtımı genellikle zaman çizelgelemesi olarak adlandırılır. Bu tezde, gerçek zamanlı operasyonlar için iki tane zaman çizelgelemesi algoritması, yani çok-tipli uyarlanır zaman-denge çizelgeleyici (MTATBS) ve torba çizelgeleyici (KS) önerilmektedir. Çoklu frekans bandı kullanımı olarak adlandırılan bir kaynak-destekli teknik görev serpiştirmenin uygulanabilirliğini arttırmak için geliştirilmektedir.

Uyarlanır güncelleme-oranı, dinamik görev önceliklendirme, izleme, görev serpiştirme gibi farklı seçimli seçenekler ile RRM teknikleri uygulamaya MFPAR sistemi için bir simülatör gerçekleştirilmektedir. Simülatör, blokların her biri ayrı ayrı RRM kısıtlarına göre değiştirilebilir şekilde tasarımlanmaktadır.

Eşzamanlı iz güncelleme talebinde bulunan birden fazla hedef olduğu zaman hedef seçimi problemi ortaya çıkmaktadır. Karar politikası yöntemi (DecP) ile çözülen

hedef seçimi ve iz güncelleme problemine iyi bilinen makine yerine koyma problemi için çözüm yöntemlerini benimsemeyi önerilmektedir. Bu yönteme ek olarak, iz kalitesine dayalı iki diğer özel yöntem tanımlanmaktadır.

Anahtar Kelimeler: Radar Kaynak Yönetimi, RRM, Çok-İşlevli Radar, MFR, Görev Zaman Çizelgelemesi, Zaman-Denge, Uyarlanır Zaman-Denge, Torba Problemi, Görev Serpiştirme, Çoklu Frekans Bandı Kullanımı, Makine Yerine Koyma Problemi, Hedef Seçimi Problemi

To my loving family

Hüseyin Çayır, Elmas Çayır, Kadir Çayır

ACKNOWLEDGMENTS

First of all, I would like to thank my supervisor, Assoc. Prof. Dr. Çagatay Candan, for his unique encouragement throughout the thesis work. I am deeply indebted for his guidance and interesting theoretical discussions which are the touchstone of my academic life.

I'd like to extend my thanks to all the jury members : Prof. Dr. Mübeccel Demirekler who have taught me the basics of the decision processes for control problems, Assoc. Prof. Dr. Umut Orguner who shares his intelligent experience on tracking methods, especially providing us the IMM simulation codes, with us, Assist. Prof. Dr. Fatih Kamışlı who was one of the evaluators of poster presentation of this work during the Graduate Research Writing and Presentation Workshop (GRWPW), 2014 and Dr. Recep Fırat Tiğrek who motivates us to research on radar systems by his valuable discussions.

I am also very grateful to financial support of TÜBİTAK-BİDEB National Graduate Scholarship Programme for MS (2211).

Very special thanks to Prof. Dr. Nevzat Güneri Gençer and the members of biomedical group who I have met in the office, DZ-10, for their joyful talks and smiling faces.

Lastly, sincerest thanks to my parents, Hüseyin Çayır and Elmas Çayır, and my brother, Kadir Çayır, for supporting and believing in me all the way through my academic life.

TABLE OF CONTENTS

LIST OF TABLES

TABLES

LIST OF FIGURES

FIGURES

LIST OF ALGORITHMS

ALGORITHMS

LIST OF ABBREVIATIONS

AI	artificial intelligence
ATB	adaptive time-balance
CfTUL	method of choosing first target in the update list
CPU	central processing unit
CT	coordinated turn
CV	constant velocity
DecP	method of decision policy
DP	dynamic programming
ECM	electronic countermeasure
FA	false alarm
FCFS	first-come, first-served
GUI	graphical user interface
IMM	interacting multiple model
IMMPDAF	IMM estimator with PDA filter
KF	Kalman filter
KS	knapsack scheduler
LHS	left-hand side
MAB	multi-armed bandit
MFPAR	multi-function phased array radar
MFR	multi-function radar
MHT	multiple hypothesis tracking
MinTE	method of minimizing the tracking error
MTATBS	multi-type adaptive time-balance scheduler
NUPD	not update
PAR	phased array radar
PDA	probabilistic data association
POMDP	partially observable Markov decision process
PPI	plan position indicator
PurMM	method of pursuing the most maneuvering
Q-RAM	QoS based resource allocation model
QoS	Quality of Service
radar	RAdio Detection And Ranging

RHS	right-hand side
RRM	radar resource management
SNR	signal-to-noise ratio
TB	time-balance
TPM	transition probability matrix
UPD	update

CHAPTER 1

INTRODUCTION

Phased array radar (PAR) can steer the beam electronically. This versatile feature allows to control beam adaptively without any rotating antenna, and there is no waiting period to direct the beam or inertia to overcome. Thus, PAR, which is especially employed in military applications [1] owing to capabilities, can carry out multiple functions by exploiting beam agility.

Multi-function radar (MFR) can collectively handle a variety of tasks, such as surveillance, multi-target tracking and missile guidance, which can be performed by separated radars. The illustration of a ship-mounted MFR is shown in Figure 1.1 to visualize the capabilities of an MFR.

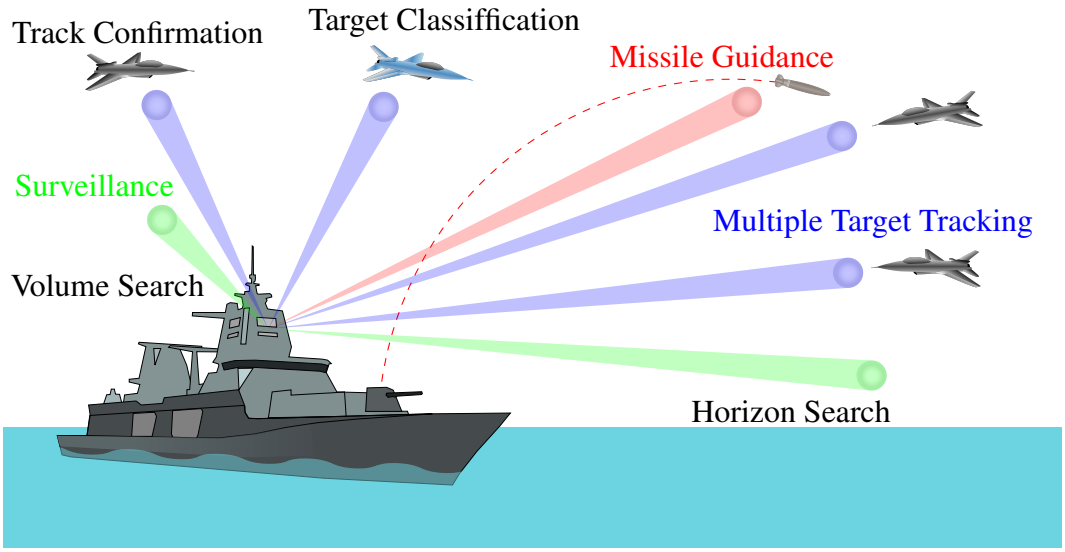

Figure 1.1: A ship-mounted MFR.

The capabilities of MFR come at a significant cost, since MFR contains numerous transmit/receive modules which make the overall system expensive. To use the capabilities efficiently, an effective radar resource management (RRM) is required. The tasks to be executed by MFR, are competing for the limited radar resources which can be mainly classified as time, energy and computation resources [2], as shown in Figure 1.2. This raises the problem of *how to allocate the limited radar resources to handle tasks for the best performance*.

Radar time resources allocation is generally called *scheduling* for RRM applications. The effective scheduling of tasks competing for the radar time resources without significant delays [3] is an important research area of RRM. As an example, there are three targets, an aircraft, an airplane and a missile, to be tracked. There are $3! = 6$ permutations of the set {aircraft, airplane, missile} for tracking queue. One of these will be the worst case operational choice, possibly tracking the missile as the target of interest. The scheduling is crucial for both of time allocation and sustainable operation of radar systems.

1.1 Literature Survey

The resource management is a topic of operational research and is widely used in the area of mathematics, economy, sociology. It can be considered as a planning problem. RRM utilizes algorithms similar to the ones in operations research with some modifications. There are many RRM algorithms in the literature, such as artificial intelligence (AI), stochastic dynamic programming, Quality of Service based resource allocation model (Q-RAM). The preliminary survey of the different algorithms which

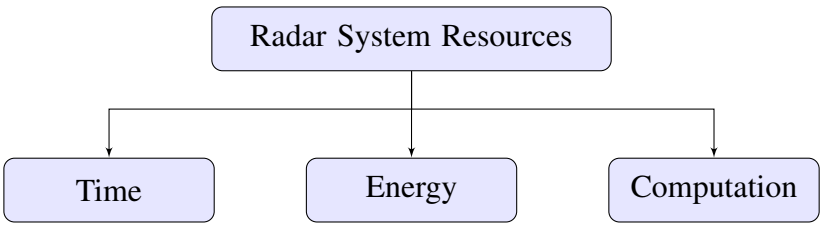

Figure 1.2: Radar system resources.

are described in the numerous publications is briefly provided in [2] and the majority of these algorithms are too complex for real-time implementation.

Scheduling techniques are simply classified in two classes, adaptive and non-adaptive techniques, as shown in Figure 1.3. Non-adaptive scheduling techniques, namely heuristic schedulers, are based on rule-based design [4, 5, 6]. The behavior of schedulers and prioritization (priority assignment) of tasks are pre-defined by rules and they are fixed. By contrast, the adaptive scheduling techniques dynamically determine task prioritization and scheduling to optimize overall performance.

The AI algorithms can be used for task prioritization and scheduling by exploiting different approaches such that neural networks [7, 8], expert systems [9, 10] and fuzzy logic [11, 12, 13, 14]. Neural network approach allows to the value assignment according to learning process within provided data sets. Expert system consists of a knowledge database which contains heuristics, and an inference engine which assigns values according to the knowledge database. Fuzzy logic is applied to characterize the targets through the vague values, i.e. *friendly* or *dangerous* to provide flexibility

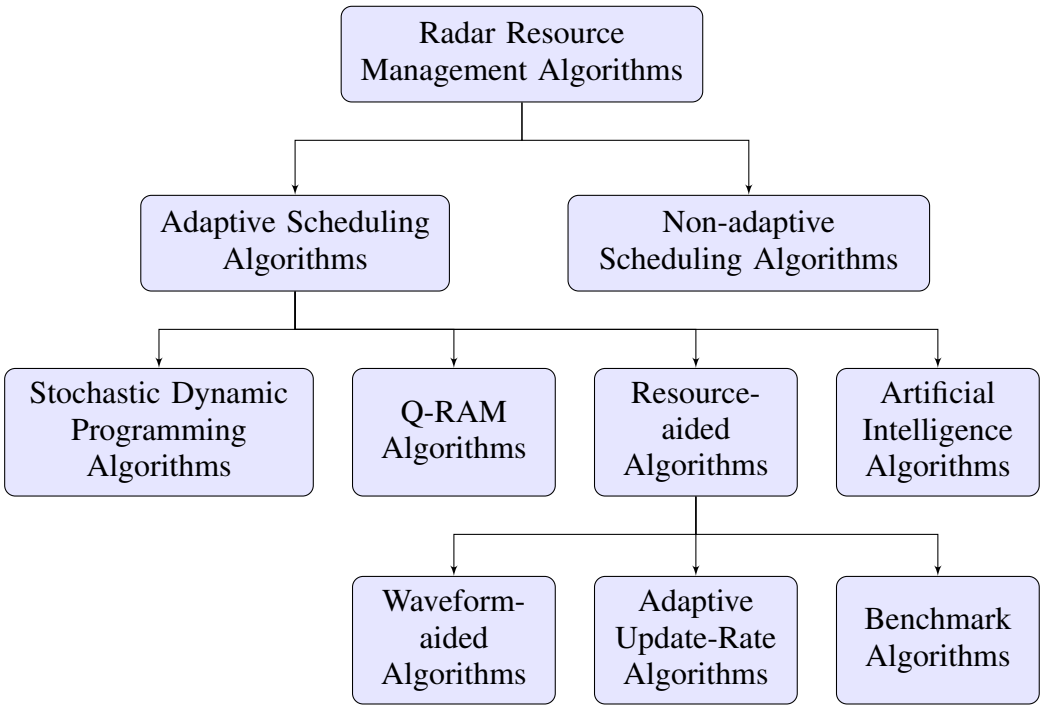

Figure 1.3: Classification of the RRM algorithms.

in task prioritization and scheduling.

Dynamic programming (DP) is a general approach for sequential optimization where decisions are made in stages [15]. For each stage, the outcome of each decision is predictable to some extent before making the next decision through transition probabilities. It is emphasized that the DP comes with heavy of computation load, but can provide the optimal scheduling as in [16] which is one of the first example of DP applications for RRM. In addition to heavy computational load, direct utilization of DP applications, namely without any approximation, can be intractable owing to the *curse of dimensionality* which is inherent in DP [17] for some RRM problems. The stochastic DP algorithms differ in their modeling of the RRM problem, such as multi-armed bandit (MAB) problem in [18], MAB problem with hidden Markov model in [19, 20], restless bandit problem in [21]. In [22, ch. 7], an application of MABs is explained in details of target tracking, and the MAB theory is also briefly explained in [22, ch. 6]. In [17], the RRM problem that the scheduling is decomposed into fast and slow timescales, is translated to a constrained Markov decision process and the algorithm based on Lagrangian relaxation is presented. Further details can be also found in [23].

Resource-aided algorithms are utilized to improve the performance of the radar by modifying the parameters or the features. One of the subclass is the waveform-aided algorithms which provide a noticeable improvement on the radar performance, especially when there are possible jamming resources. In [24], radar detection performance is optimized in a changing environment where performance factors (eclipsing, clutter, propagation and jamming) are analyzed and utilized to select the optimum waveform parameters within a neural network approach. In [25], waveforms are adaptively scheduled to detect a new target by using stochastic DP and it is noted that the time to detect a new target decreases with described method.

Waveforms can be selected according to the features of tasks by using fixed or variable waveform libraries. In [26], waveform is selected from a pre-designed library by using the information states and it is noted that acceptable limits of tracking error are achieved with the decreased number of revisits. Similarly, the effects of waveform scheduling is analyzed for target tracking in [27] and target classification in [28].

Another subclass of resource-aided algorithms is the adaptive update-rate algorithms which are studied to improve tracking performance of radars, in comparison to the traditional trackers that use uniform update-rates for the case of clutters and maneuvering targets. In [29], the revisit time, which depends upon the estimated lack of information corresponding to the target, is computed. In addition, the radar parameters such as signal-to-noise ratio (SNR), track sharpness and detection threshold, are optimized with respect to the radar load for tracking in the same work. In [30], a method is proposed to control the revisit time and adjust the energy level of the radar by exploiting the interacting multiple model (IMM)[1]. In [31], an adaptive update-rate algorithm that is based on IMM for target tracking, is proposed. The IMM algorithm has already been capable to estimate target state and tracking error covariance. Thus, update intervals are computed with respect to these tracking error covariances to decrease the number of track updates by providing the acceptable beam positioning losses, in the same work. In [32], the radar energy resource, which is required for track maintenance, is minimized by optimally computing track update time and SNR pairs.

The last subclass of resource-aided algorithms comprises the benchmark algorithms which are studied to cope with the benchmark problems. The benchmark problem is a scenario that converts the dynamics of radar environment into a simulation concept, in order to test the behavior of described algorithms without implicitly running on a radar system. In [33], a benchmark problem is proposed for tracking maneuvering targets where the features of a PAR such as beam-shape, finite resolution, and other restrictions that occur in a real-world environment such as target maneuvers, missed detections, track loss are handled by the simulation test-bed. The work, [33], is extended to cover the effects of false alarms (FAs), namely false detections, and electronic countermeasures (ECMs) in [34]. Furthermore, multiple waveforms are included to allocate the radar energy with tracking algorithms in the same work. Many of the deficiencies which are associated with [34] are rectified in [35, 36]. In [35], a documentation for the computer program, which is written in MATLAB®[2] to simulate the radar system, is also provided. In [37], IMM/MHT method which combines IMM for tracking, and MHT for data association, as described in [38],

[1] The algorithm is described in Appendix A

[2] MATLAB is a registered trademark of the The MathWorks, Inc. www.mathworks.com.

is presented for the benchmark problem that is given in [34]. In [39], IMMPDAF method, as described in [38], which combines IMM for tracking, and PDA filter for data association, is presented for the benchmark problem that is given in [36].

Q-RAM algorithms are utilized to allocate radar resources by managing Quality of Service (QoS) [40]. The main aim of a Q-RAM model is to allocate system resources between applications, namely tasks, in order to make overall system utility maximized while meeting the minimum needs of applications [41]. The Q-RAM approach gets more complex, when the system has more constraints. Thus, the algorithms have been developed to approximately solve the problem or to exploit its useful features in the last decades. The PARs are convenient to present the capabilities of Q-RAM which is described in the pioneer work [41]. In [42], real-time scheduling of a PAR system, which is described in [43], is developed by using Q-RAM. In [44], a dwell scheduling scheme that is based on Q-RAM, is proposed for a radar tracking system where the physical and environmental factors are incorporated to manage QoS for the same PAR system. In [45], Q-RAM is evaluated and the shortcomings of the method are identified for RRM problem.

There is another scheduling method called as the time-balance method which does not exactly fit into any category shown in Figure 1.3 [2]. This method is described as a measure of the radar time which is requested by a task to be scheduled. The algorithms based on this method are presented in [46, 47, 48].

1.2 Main Scope of the Thesis

Main purpose of this thesis is to realize the RRM techniques for a multi-function phased array radar (MFPAR). The entire of the radar system is taken into account to attain this purpose. It should be noted that the existing works are usually too specific such that they consider only task prioritization or revisit time without completely remarking the effect of other components on RRM. This makes a comparison of the suggested algorithms quite difficult. Furthermore most of these methods utilizes specific test-beds which are insufficient to model stochastic nature of radar environment. Hence, randomized scenarios are generated and RRM is applied to almost all compo-

nents of MFPAR. The simulation environment is built on the MATLAB software, and contains adaptive update rate, dynamic task prioritization, tracking and task interleaving features.

Here, the problem presented in [17] is studied to understand the main aspects of the RRM problem. The ideas given in [23], such as target dropping, track quality, two timescales, utility function are also utilized in this work. The time-balance approach described in [48] is preferred instead of the DP approaches, owing to its simplicity and applicability in real-time operation. Moreover, a scheduling method based on binary integer programming is studied to solve the RRM problem as an optimization problem and to present comparisons with the previous approach.

1.3 Outline of the Thesis

The radar system model is described in Chapter 2. Then, the time-balance technique based schedulers in literature, are briefly explained in Chapter 3. Furthermore, the scheduling algorithms, multi-type adaptive time-balance scheduler and knapsack scheduler, are described in the same chapter. Next, in Chapter 4, the decision making problem that occurs, when two or more targets concurrently request track update, is mentioned and some analytical methods are described to handle this problem. The experimental results are provided in Chapter 5. Finally, conclusions and future work are given.

CHAPTER 2

RADAR SYSTEM MODEL

A general MFR system model shown in Figure 2.1 is used for simulation and analyzing the scheduling techniques. The given model is mainly focused on surveillance and tracking tasks, since the other types of tasks (i.e. missile guidance, calibration) are used less frequently in comparison to these tasks.

In this chapter, every block of the system model is briefly described and a resource-aided technique, multi-frequency band usage, is presented for the utilization of radar timeline effectively.

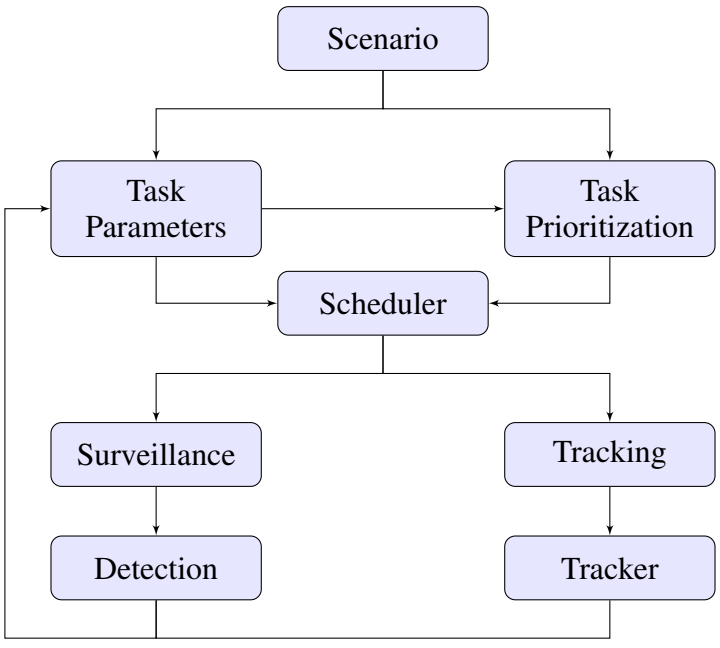

Figure 2.1: Radar system model.

2.1 Scenario

Scenario is formed with a surveillance task and tracking tasks of N targets. Targets are generated by a Markovian model which has constant velocity (CV) and coordinated turn (CT) states by randomly choosing one of the following TPMs

$$\begin{bmatrix} 0.65 & 0.35 \\ 0.35 & 0.65 \end{bmatrix}, \begin{bmatrix} 0.8 & 0.2 \\ 0.2 & 0.8 \end{bmatrix}, \begin{bmatrix} 0.9 & 0.1 \\ 0.1 & 0.9 \end{bmatrix}, \begin{bmatrix} 0.95 & 0.05 \\ 0.05 & 0.95 \end{bmatrix}, \begin{bmatrix} 0.99 & 0.01 \\ 0.01 & 0.99 \end{bmatrix},$$

and one of the turn-rates, ω, from the set, $\{-0.02\,\text{rad/s}, -0.01\,\text{rad/s}, 0\,\text{rad/s}, 0.01\,\text{rad/s}, 0.02\,\text{rad/s}\}$, for duration of t_{max} and the sampling interval, $T = 1$ s. The details of target generation can be found in [49].

An example scenario, which contains $N = 15$ targets moving for the duration of $t_{max} = 500$ s, is shown in Figure 2.2. On the figure, "Tn" denotes target n, and inside of the red dashed circle with radius 200 km denotes the region of interest to detect targets. Hereafter, the maximum range, r_{max}, is assumed to be equal to 200 km.

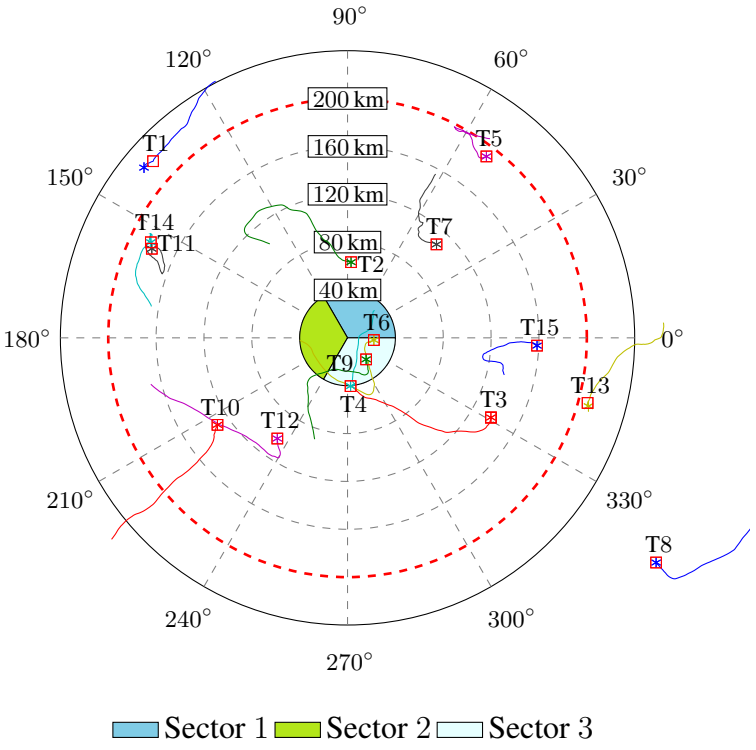

Figure 2.2: A scenario contains $N = 15$ targets moving for $t_{max} = 500$ s.

2.2 Task Parameters

Task parameters contain *task id*, *task time*, *task update time*, *allowable lateness*, *scheduling value* and *priority*. By notifying that the declarations may not be realistic to reflect the real-world, the parameters are described as follows:

- Task id is an integer between 1 and N and associated with a target. Therefore the task id, n, is reserved for target n, even if target n is dropped after a while. It is the only fixed parameter. The task id of a surveillance task is always associated as $N + 1$.

- Task time is the elapsed time to complete transmitting and receiving cycle for a task. Task time of a surveillance task is fixed as 2 s. Task time of tracking task is thought to depend on the range of corresponding target. This idea is inspired from the range equation,

$$R = \frac{cT_R}{2}, \tag{2.1}$$

given in [1, ch. 1], where $c = 3{\times}10^8$ m/s is the speed of light and T_R is the round-trip travel time which is the elapsed time when pulse has to travel to the target and back. Task time, $\mathcal{T}_i$, of the tracking task for target i is computed as

$$\mathcal{T}_i = (0.95\,\text{s}) + (0.05\,\text{s}) \left\lceil \frac{r_i}{40\,\text{km}} \right\rceil . \tag{2.2}$$

where the constants are intuitively chosen and r_i is the range of corresponding target. Considering the range which can take any value from 0 to 200 km for detection, $\mathcal{T}_i$ can take any value which belongs to the set, $\{0.95\,\text{s}, 1.00\,\text{s}, 1.05\,\text{s}, 1.10\,\text{s}, 1.15\,\text{s}, 1.20\,\text{s}\}$, with respect to the range of target i.

- Task update time is the elapsed time between sequential updates for a task, namely it is the desired period value for a task. Task update time of surveillance task is assumed to be 25 s, and it can be dynamically changed to decrease idle time of radar. Task update time of a tracking task is initialized with a value which depends on the speed of corresponding target, and it can be dynamically

changed to keep maneuvers and to track the target more accurately. Task update time, $\mathcal{U}_i$, of the tracking task for target i is computed as

$$\mathcal{U}_i = (17\,\text{s}) - \left\lceil \frac{v_i}{25\,\text{m/s}^2} \right\rceil . \tag{2.3}$$

where the constants are intuitively chosen and v_i is the speed of corresponding target. Considering the speed which can take any value from 10 to 340 m/s for detection, $\mathcal{T}_i$ can take any value which belongs to the set, $\{3\,\text{s}, 4\,\text{s}, \ldots, 16\,\text{s}\}$, with respect to the speed of target i. Indeed, (2.3) can be modified as

$$\mathcal{U}_i = \max\left((17\,\text{s}) - \left\lceil \frac{v_i}{25\,\text{m/s}^2} \right\rceil , 3\,\text{s}\right) . \tag{2.4}$$

to detect a target, speed of whom is greater than 340 m/s. However, it may be improper to assign the same task update time for two targets which have the speeds 340 m/s and 1000 m/s respectively. Hence, it is beyond the scope of this work at this level.

- Allowable lateness is a tolerable time, in other words, it is the time difference between update time at which the task can be scheduled, and due time by which it must be scheduled to successfully accomplish, for late update and it is assumed to be equal to 20% of the task update time. If update time of a tracking task exceeds the allowable lateness, the tracked target is counted as *probably dropped*. Therefore another aim of scheduling is to reduce the number of probable drops.

- Scheduling value refers the state of task, i.e. how much time is left to new update, after scheduling epochs. Its function is directly related to scheduler. Hence, it is defined to help scheduler to choose the most convenient task for scheduling.

- Priority refers the importance of scheduling a task. Its range is defined to be between 1 and 5. Assuming that the maximum range is 200 km, the priority is decreased from 5 to 1 by 1 through each ring has 40 km thickness for tracking tasks. If a target is 50 km away from radar which is at the origin, its priority is associated as 4. Target prioritization levels according to regions are shown in Figure 2.3. Surveillance task has the minimum priority that is 1.

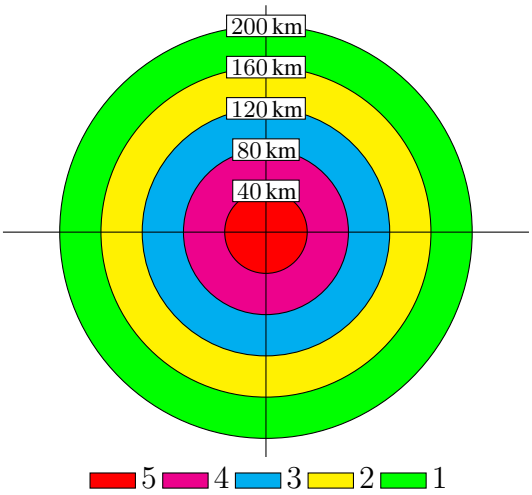

Figure 2.3: Target prioritization regions.

2.3 Task Prioritization

Task prioritization is applied so that each one of the targets has an initial priority based on its range for tracking tasks (targets closer to base are more important) and surveillance task has the minimum priority.

If task prioritization process is not dynamically changed, every aspect of MFR performance may be sub-optimal. For example, assuming surveillance tasks have the lowest priority level, the total occupancy of surveillance tasks is set as $\mathcal{O}_S$ and the remaining part, $100\% - \mathcal{O}_S$, of the resource is set as free in case of detection. Assuming that there is not any initialized track, the system is run. Then, scheduler allows surveillance tasks to share all of the resource, since there is not any tracking task to be scheduled. However, as number of tracks becomes higher, available resources may not be sufficient to sustain tracks after the first detection. Since priority of a tracking task is usually higher than surveillance task, scheduler should transfer some amount of the resource which is reserved for surveillance to tracking tasks and the detection performance of system decreases, as shown in Figure 2.4. This simple example demonstrates the importance of dynamic task prioritization. To avoid such problems or to reduce their negative effects, task prioritization should be dynamically

performed. If surveillance task cannot be scheduled at the desired time, its priority is increased temporarily to a level which is higher than the highest priority of available tasks. Similarly, if a tracking task cannot be scheduled at the desired time, its priority can be increased temporarily to a level which is higher than the highest priority of available tasks. Thus, the dynamic task prioritization process is applied to avoid lateness and to enhance system performance.

If a target has a range which is associated with a different priority level, then its priority is immediately updated. This is explained with a scenario shown in Figure 2.5. By choosing the sector 3 as a region of interest and the priority threshold as 2, namely the targets with priority levels higher than 1 can be detected, the target 2 and the target 3 are going to be tracked. Figure 2.5(a) shows that the tracking is handled at a desired level when the feature, dynamic task prioritization, is enabled. However, the Figure 2.5(b) shows that the tracking tasks are not scheduled to meet the constraints. The target 2 is tracked until the maximum range. The target 3 is not tracked until the detection of target 5, since the system only updates the task list whenever a detection occurs.

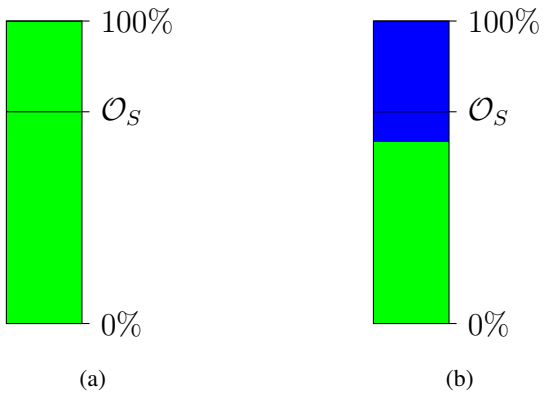

Figure 2.4: Detection performance degradation due to task prioritization. (a) Surveillance task completely utilizes radar resources, since there is initially no tracks to schedule a tracking task. (b) Surveillance task cannot maintain the desired detection performance, since radar is overloaded by detections and some amount of reserved resource for surveillance task is transferred to tracking tasks.

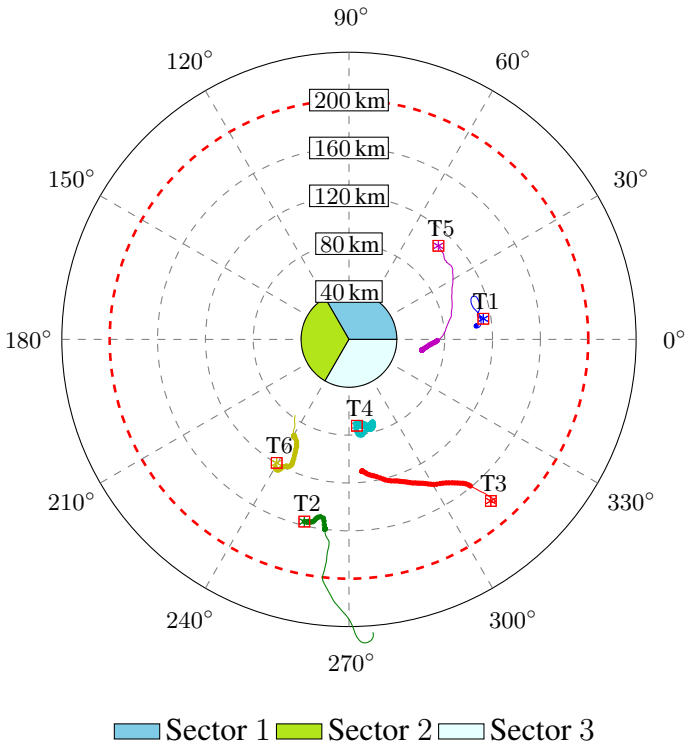

(a) Dynamic task prioritization is enabled.

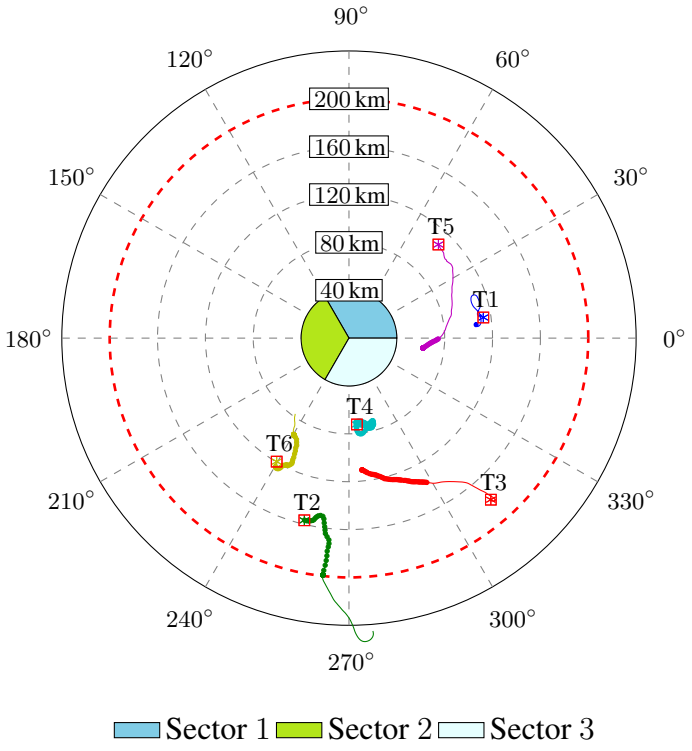

(b) Dynamic task prioritization is disabled.

Figure 2.5: Effect of dynamic task prioritization.

2.4 Scheduler

Scheduler block controls the performance of the radar. Here, the performance is measured by the factors which are defined as follows:

- The number of probable drops is the number of updates which are too late to track target accurately. The probable drop occurs when the update interval exceeds the sum of task update time and allowable lateness.
- Cost is the sum of squared lateness values after each scheduling epochs.
- Average of errors is simply the average of the trace of tracking error covariance matrices of all targets.
- Occupancy is the ratio of utilized radar time to the total available time interval.

The following sections describe several resource-aided techniques for the scheduling algorithms which are described in detail in Chapter 3 to enhance the overall performance of the radar.

2.4.1 Task Interleaving

Tasks mentioned here are coupled-tasks [50] that consist of transmitting, idle time and receiving parts, as shown in Figure 2.6. Task interleaving technique is applied to insert the transmitting and receiving parts of a coupled-task into the idle time part of other coupled-tasks. The time when radar is idle, can be reduced so that radar time-line is effectively utilized by this technique. However, it increases the consumed radar energy, since radar processes more tasks for the same interval.

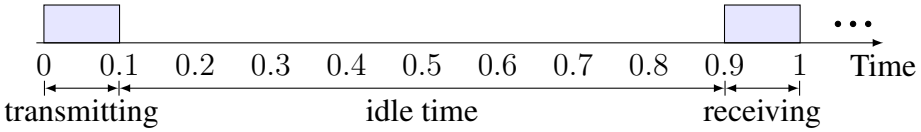

Figure 2.6: A coupled-task.

In this work, transmitting and receiving intervals are assumed to be equal to 10% of the task time. Thus, idle time interval is assigned as 80% of the task time. Task queue shown in Figure 2.7 where "Tn" denotes the tracking task for target n, and "Surv" denotes the surveillance task, is obtained by exploiting task interleaving technique for a scenario.

The task queue starts with surveillance task which is not interleaved. Then, tracking tasks for target 11 and target 1 are scheduled respectively. Since task times are not identical, a gap, which is labeled as "Idle" on the figure, appears between the receiving parts of these tasks. Task interleaving process continues in this manner.

Task interleaving cannot be always handled in a proper way, as shown in Figure 2.7. When tasks are closely interleaved, this interleaving may cause interference and other problems in a real radar systems. A practical method of using multiple frequency bands is suggested to interleave the tasks without any negative side effects. This method is described in the next section.

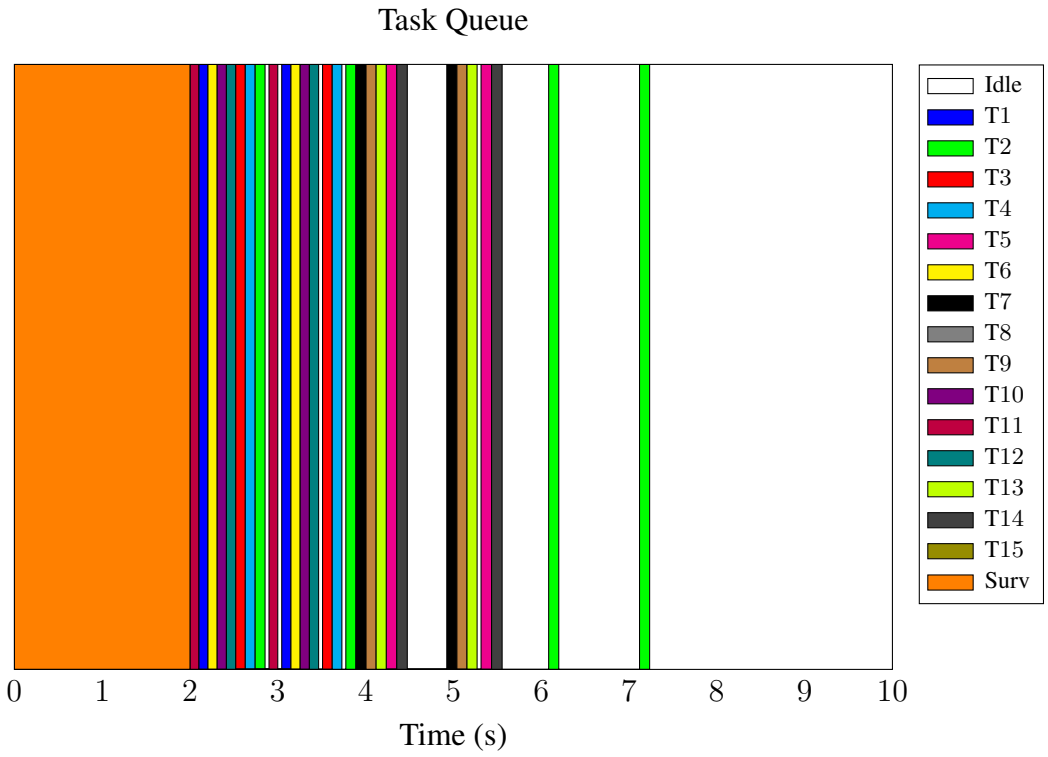

Figure 2.7: Task queue by exploiting task interleaving technique.

2.4.2 Multi-Frequency Band Usage

The interleaving of tasks is valuable choice to decrease the idle time for radar. However, the interleaving of tracking tasks between closer targets can bring wrong target association problems, physical layer problems, etc. There are many methods, i.e. waveform selection, to solve these problems. Unfortunately, these methods are too complex for implementation. Thus, the idea of *frequency re-usage* has emerged to deal with tracking of the high number of targets and to avoid the track mixing of closer targets. In this method, it is supposed to have multiple distinct frequency bands. Each of the frequency bands is reserved for a single tracking task.

The method is explained via a scenario shown in Figure 2.8. It is supposed that there are 2 frequency bands (f_1 and f_2), 4 targets and target priorities makes the scheduling sequence as target 1, target 2, target 3 and target 4 respectively. Here, the critical point is that the two of targets are referred to as *closer targets*, if their azimuth difference is less than the frequency re-usage angle, θ_{fr}.

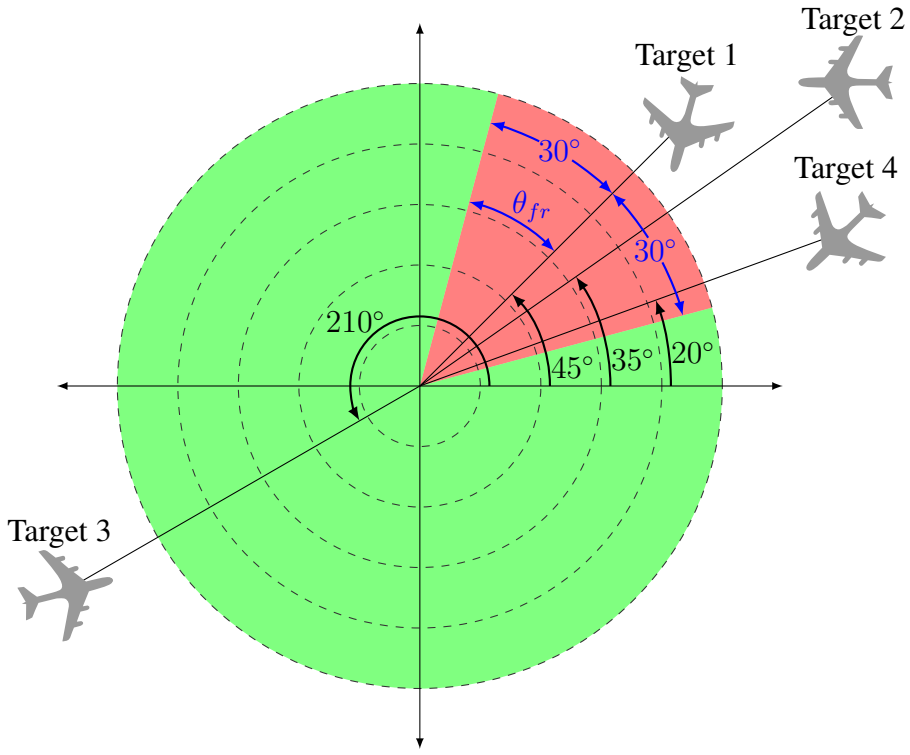

Figure 2.8: A scenario for multi-frequency band usage technique.

According to Figure 2.8, azimuth angles are given as $45°$, $35°$, $210°$ and $20°$ for each target respectively. Thus,

- target 1 and target 2,
- target 2 and target 4,
- target 1 and target 4

becomes closer targets by choosing θ_{fr} to be $30°$.

Herewith, task scheduling times are determined with respect to these assumptions. The frequency bands f_1 and f_2 are assigned to target 1 and target 2 respectively, since target 1 and target 2 are closer targets. There is no harm in assigning f_1 and f_2 to target 3, since it is too "far from" the other targets. Lastly, target 4 needs to wait for f_1 or f_2 until one of them becomes free, since target 4 is one of the closer targets with target 1 and target 2 respectively. If there were 3 frequency bands, there would not be any need for waiting. Task queue example is shown in Figure 2.9 by using 2 (above) and 3 (below) frequency bands. Moreover, the same scenario utilized in the previous section is revisited, as shown in Figure 2.10. Previously, all of the detected targets are scheduled at least one time within 5.5 s, as shown in Figure 2.7. Next, all of the detected targets are scheduled at least one time within 10 s, as shown in Figure 2.10. The number of frequency bands limits the task interleaving to avoid mixing tracks.

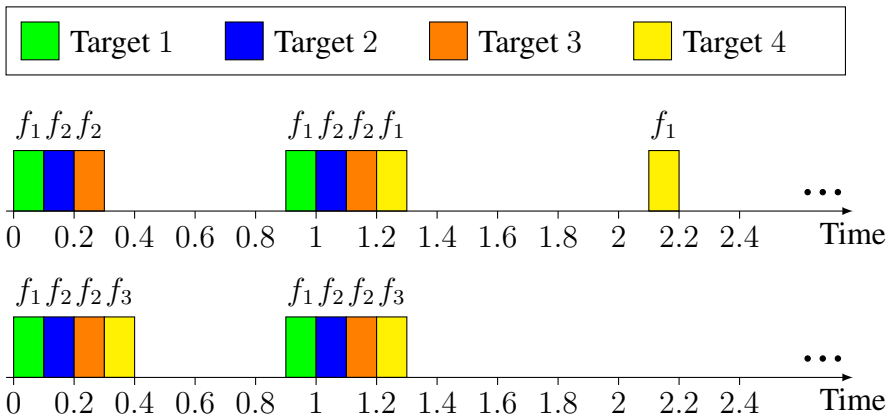

Figure 2.9: Task queue example for multi-frequency band usage technique.

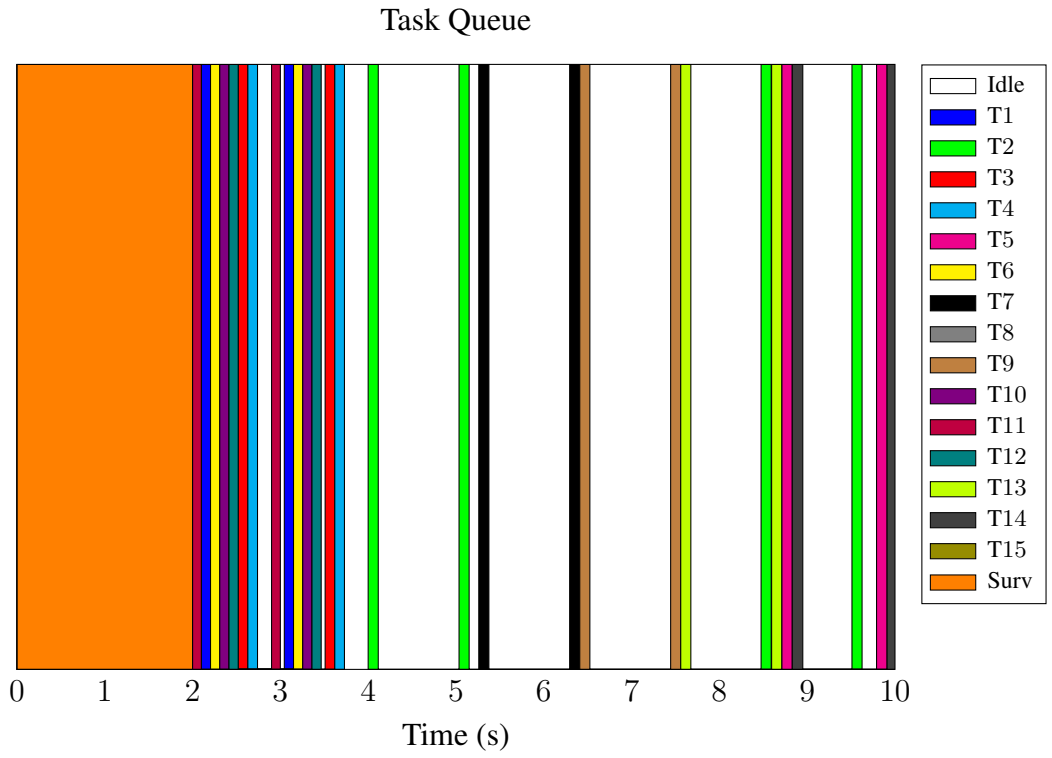

Figure 2.10: Task queue by exploiting multi-frequency band usage technique for 2 frequency bands.

2.4.3 Adaptive Update-Rate

Task update time, $\mathcal{U}_n$, of the tracking task for target n is modified to decrease the tracking error in the following way,

$$\mathcal{U}_n = \begin{cases} 1 + \left\lceil \dfrac{m-\ell}{m-1}\mathcal{U}_n \right\rceil, & \dfrac{m-\ell}{m-1} < 0.5, \\ 1 + \left\lfloor \dfrac{m-1}{m-\ell}\mathcal{U}_n \right\rfloor, & \text{otherwise} \end{cases} \tag{2.5}$$

where $m-1$ denotes the number of time samples between two consequent measurements and $m-\ell$ denotes the number of predictions that their trace of error covariances on target position do not exceed the threshold, Υ, as shown in Figure 2.11. In this work, Υ is assumed to be $2{\times}10^4$ m^2.

In (2.5), the constant, 1, and the least integer function [51] are utilized to make $\mathcal{U}_n$

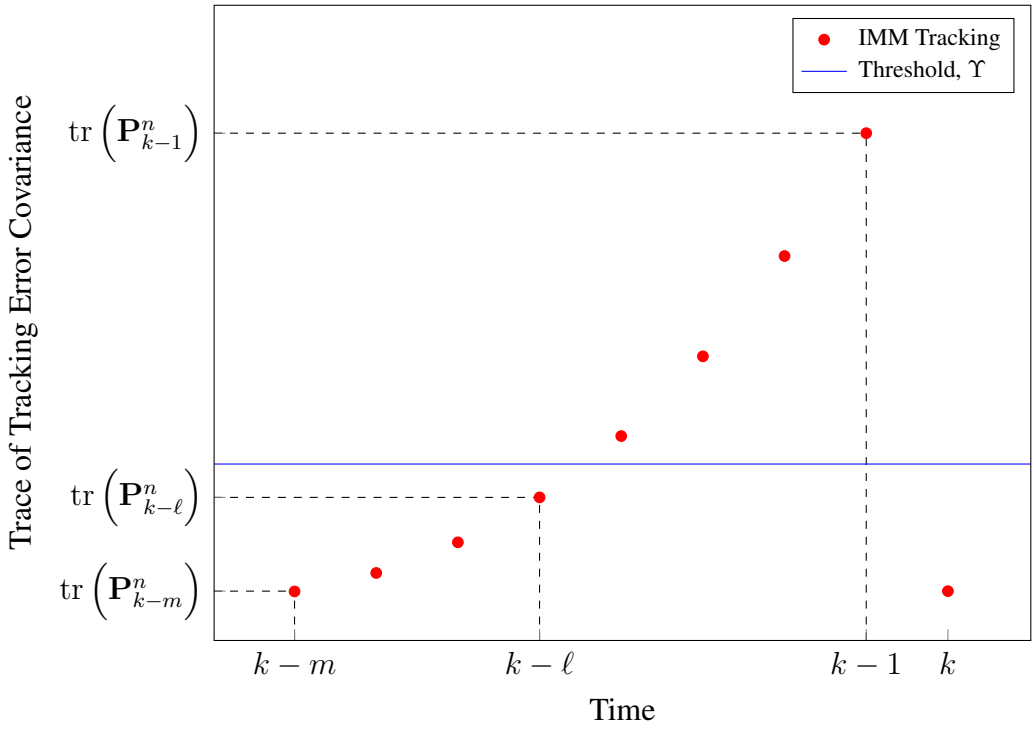

Figure 2.11: Description of parameters used by adaptive update-rate technique.

is always higher than $\mathcal{T}_n$, since task time can be greater than 1 s. When the case $(m-\ell)/(m-1) < 0.5$ which denotes the higher tracking error is valid, the task update time is decreased for the next track update to decrease the tracking error. If the other case $(m-\ell)/(m-1) \geq 0.5$ which denotes the smaller tracking error is valid, the task update time is increased for the next track update to decrease the tracking load of radar.

The adaptive update-rate technique extends the domain of task update time from $\{3\,\text{s}, 4\,\text{s}, \ldots, 16\,\text{s}\}$ to $\{2\,\text{s}, 3\,\text{s}, \ldots, 33\,\text{s}\}$ by using (2.5).

The TB scheme which is described in Chapter 3, as shown in Figure 2.12, compares two cases when adaptive update-rate technique is disabled and enabled. If adaptive update-rate technique is disabled, as shown in Figure 2.12(a), tracking tasks are scheduled with respect to fixed task update time. Otherwise, tracking tasks are scheduled with respect to variable task update time, as shown in Figure 2.12(b). The technique is emphasized through the line labeled as "T3" which denotes the tracking task for target 3, and task update time, $\mathcal{U}_3$, is adaptively decreased and increased.

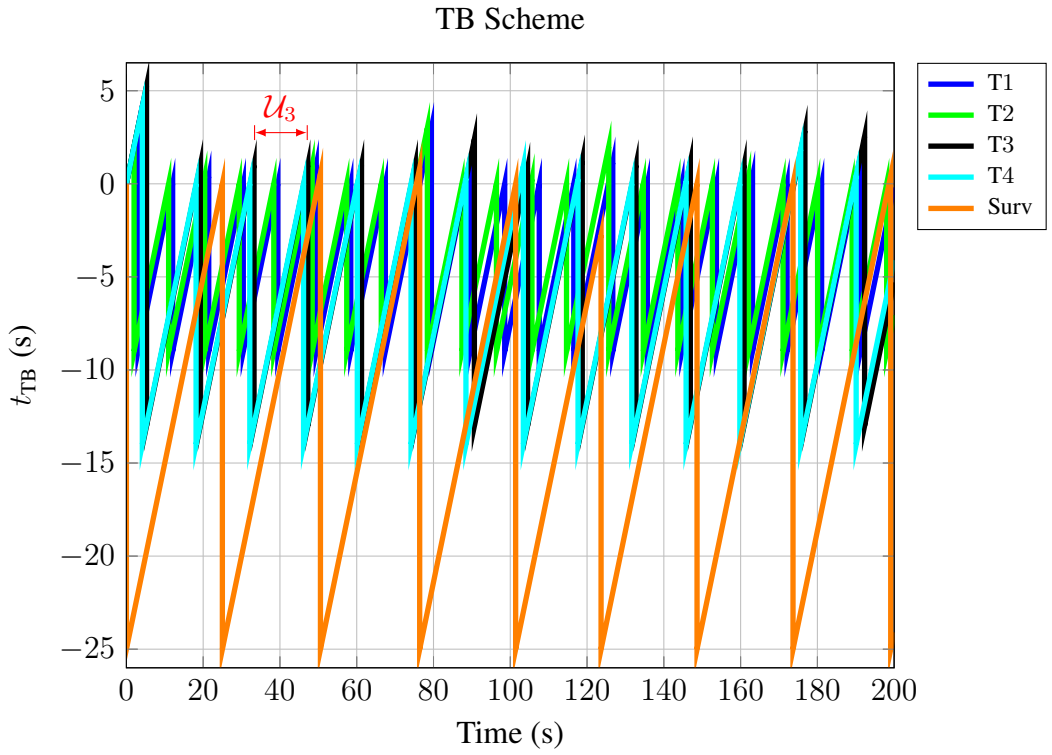

(a) Adaptive update-rate technique is disabled.

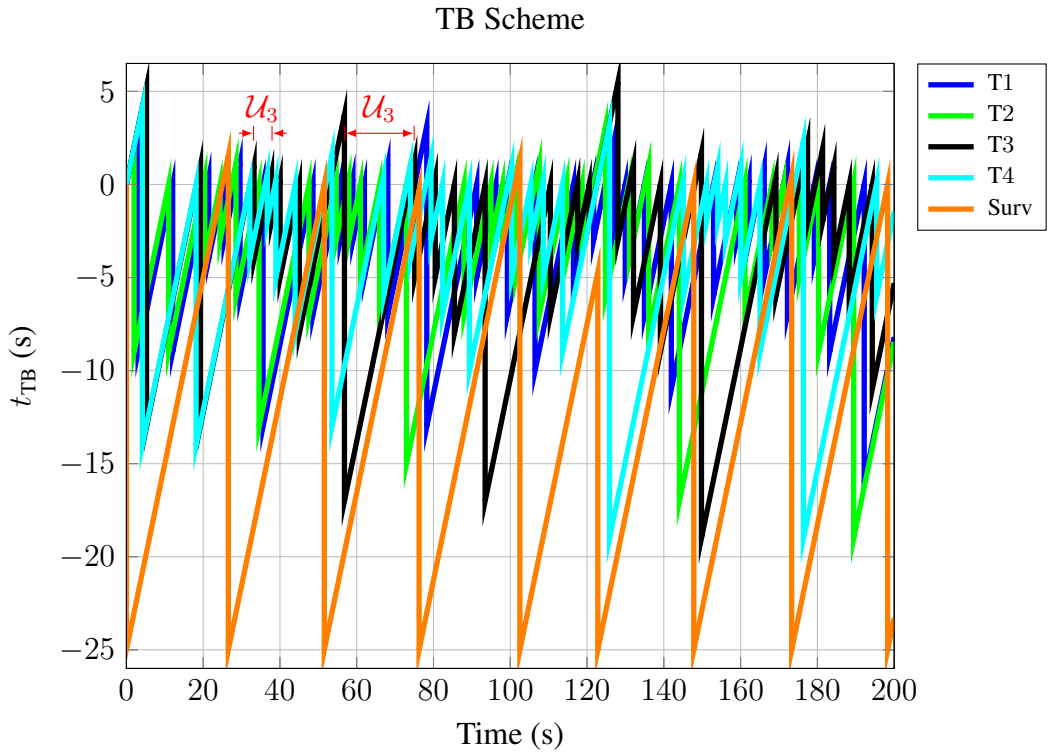

(b) Adaptive update-rate technique is enabled.

Figure 2.12: Effect of adaptive update-rate technique on TB scheme.

2.5 Surveillance

Surveillance task can be a single task or can be a task that can be fragmented with tracking tasks [48]. The fragmented surveillance task is supposed to be handled in the idle time when there is no task to schedule. The fragmented surveillance task is assumed to be completed when all fragments summed up to a given surveillance task time. However, task update time for this case is not fixed, if there is not sufficient idle time for the surveillance.

2.6 Detection

The instrumented detection range of radar is up to r_{max}, and hence, the targets are assumed to be detected within this range. It is crucial to remind that the detections in this work are assumed to be perfectly associated with the targets.

The effects of the sectoring and priority threshold on detections are shown in Figure 2.13. Here, only sector 2 is the region of interest and the priority threshold is 2, namely the targets with priority levels higher than 1 can be detected.

2.7 Tracking

A tracking task is associated for every target in track mode. A target which is previously detected is assumed to be perfectly associated, if it stays in the out of range for a while and comes back to the region of interest. Therefore tracks are not mixed during the scheduling process.

2.8 Tracker

The utilization of the tracker can be seen as the most important phase of RRM. Because its performance effects the future tracking load of the radar. The tracker, in this work, utilizes IMM algorithm which is briefly described in Appendix A. The IMM

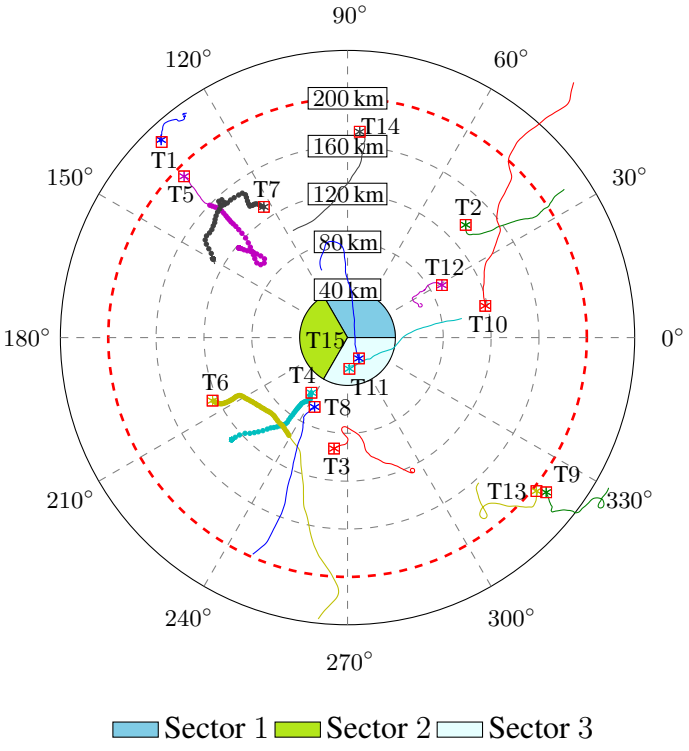

Figure 2.13: Effects of the sectoring and priority threshold on detections.

provides the information about the maneuver state of targets, and this information is useful for RRM in target selection, adaptive update-rate.

2.9 Summary

In this chapter, the general MFR system and its environment are modeled for simulation. The methods for parameter assignment, task prioritization and adaptive update-rate are explained. A resource-aided technique called as the multi-frequency band usage, is proposed to increase the applicability of task interleaving. Thus, the elements of the simulation model are described to emphasize each phase of the scheduling. However, the scheduling techniques are not covered, while describing the scheduler phase. Hence, they are described in the next chapter.

CHAPTER 3

SCHEDULING TECHNIQUES

In this chapter, time-balance technique based schedulers and two suggested scheduling algorithms, namely multi-type adaptive time-balance scheduler (MTATBS) and knapsack scheduler (KS), are described. MTATBS and KS are implemented on the simulation model described in the previous chapter.

3.1 Time-Balance Technique Based Schedulers

The time-balance (TB) is described as a measure of how much time which is owed to a task to perform it by radar [46]. The TB actually indicates the *degree of urgency* corresponding to the next scheduling of a task, and hence, TB is continually updated to indicate the actual and required use of radar time [52].

General idea of TB technique is very simple. Each task is associated with a TB value, t_{TB}, which is varying with time and there is a TB scheme which maintains t_{TB}'s. A task is thought to be delayed for scheduling, if it has a positive t_{TB} which indicates to request radar time. Similarly, a task is thought to wait radar time for scheduling, if it has a negative t_{TB} to indicate that it is not ready. A task has zero t_{TB} when it is exactly ready for scheduling. Moreover, new tasks can be inserted to a radar task list with a negative t_{TB} in order to delay the new task until its due time of execution. If a task is scheduled, its t_{TB} is decreased by its task update time. The t_{TB} of other tasks which are not scheduled is increased by an amount that is determined in accordance with the algorithm of scheduling. This process continues in this way until the end of operation.

In the following sections, the TB technique based algorithms are presented in an increasing order of complexity and a non-historical order. Various versions of the suggested TB scheduler are described in the remaining parts of this work.

3.1.1 Time-Balance Scheduler

This type is the simplest scheduler based on TB technique and it is described in [53]. The TB scheduler chooses the task which has higher t_{TB} than other tasks to be processed next. The scheduler is designed to schedule mainly tracking tasks, and hence, surveillance task is not associated with a t_{TB}. The surveillance task is scheduled whenever all tracking tasks have negative t_{TB}. Thus, surveillance task can be scheduled if radar is underloaded. The underloaded radar cannot perform a complete surveillance task if there is not a sufficient idle time after performing tracking tasks. Therefore the surveillance task is fragmented by task fragment time, $\mathcal{T}_F$, in order to interleave with tracking tasks. When total time of the scheduled fragments is equal to task time of surveillance, a surveillance task is completely scheduled.

3.1.1.1 Algorithm of TB Scheduler

Flow diagram of the TB scheduler algorithm is shown in Figure 3.1. The step 1 gets parameters for each task. Tracking task parameters contain the number of targets, N, task time, $\mathcal{T}_n$, and task update time, $\mathcal{U}_n$, for $n = 1, 2, \ldots, N$, and surveillance task parameter is only task fragment time, $\mathcal{T}_F$. The step 2 assigns t_{TB} as zero for new tasks. The step 3 finds out that if there is any task with positive t_{TB}. The step 4 chooses a task which has the highest t_{TB}, if there is at least one task with positive t_{TB} after step 3. The step 5 decreases t_{TB} of task, which is chosen by step 4, by task update time of this task. Here, the critical point is that t_{TB}'s of other tasks are not updated. The step 6 schedules task chosen by step 4. The step 7 increases t_{TB}'s of all tasks by task time of the scheduled task. If there is not any task with positive t_{TB} found by step 3, then step 8 is executed. The step 8 schedules a surveillance fragment. The step 9 increases t_{TB}'s of all tasks by $\mathcal{T}_F$. After processing step 7 or step 9, the next step is again step 1, and scheduling continues in this way.

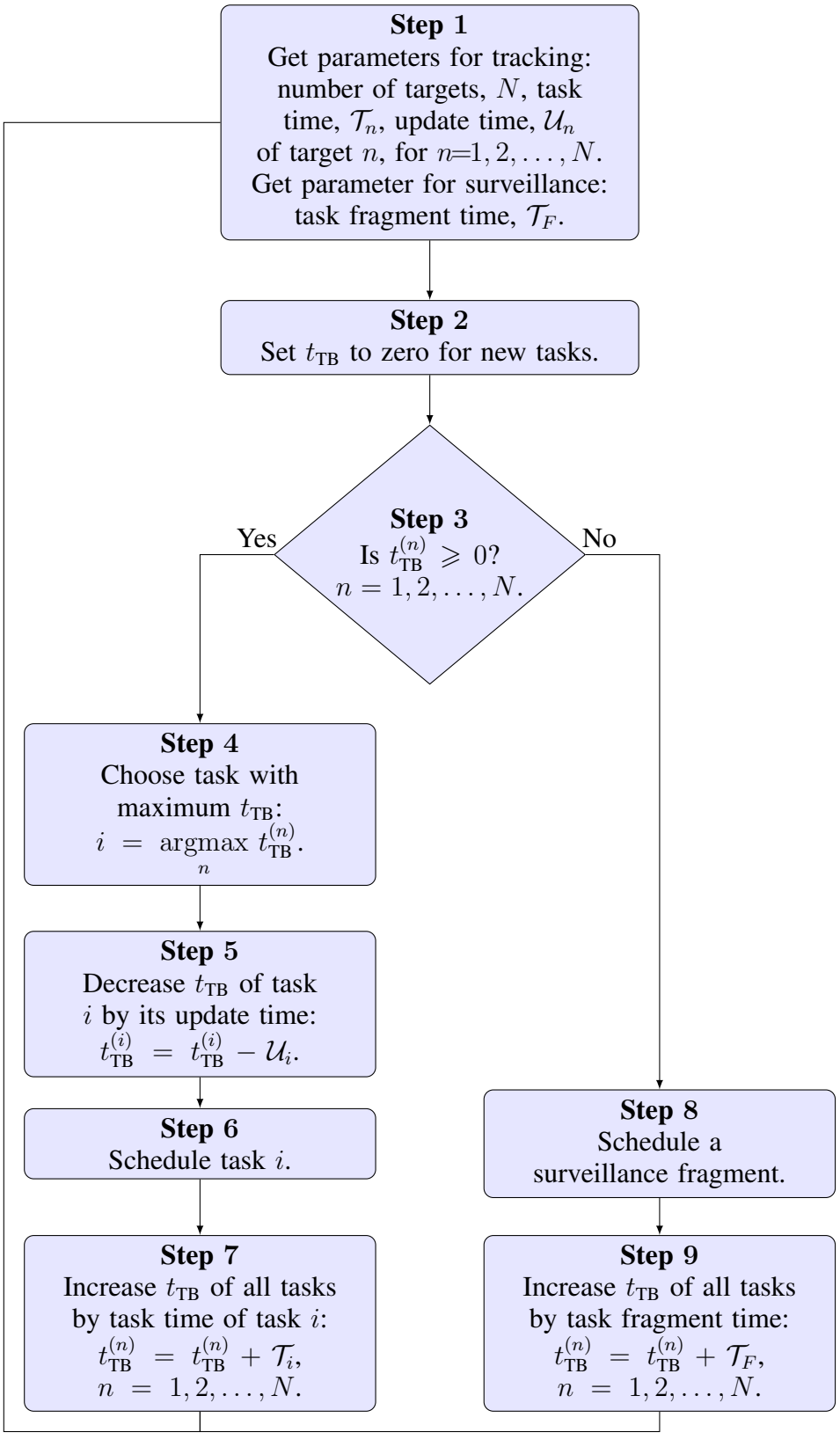

Figure 3.1: Flow diagram of TB scheduler algorithm.

3.1.1.2 An Example

A scheduling example for two tracking tasks is shown in Figure 3.2. Task time and task update time for tracking task 1 are assigned as $\mathcal{T}_1 = 6$ s and $\mathcal{U}_1 = 24$ s, and for tracking task 2 are assigned as $\mathcal{T}_2 = 9$ s and $\mathcal{U}_2 = 15$ s. According to these parameters, the occupancies, $\mathcal{O}_n = \mathcal{T}_n \mathcal{U}_n^{-1}$, are computed as 25% and 60% for each task respectively. Task fragment time, $\mathcal{T}_F$, is assigned as 1 s, so that surveillance task fragments can be scheduled when both of tracking tasks have negative t_{TB}.

After processing step 1, as given in previous paragraph, step 2 is processed to assign t_{TB} as 0 for both of tracking tasks, at $t = 0$. Thus, t_{TB}'s are not negative in step 3 and either task 1 or task 2 can be chosen in step 4. In step 5, t_{TB} of task 1, $t_{\text{TB}}^{(1)}$, is decreased with $\mathcal{U}_1$, as depicted by blue line on TB scheme shown in Figure 3.2. Meanwhile, t_{TB} of task 2 is depicted by green line on TB scheme. In step 6, task 1 is scheduled. In step 7, t_{TB} for both of tracking tasks are increased with $\mathcal{T}_1$. The first

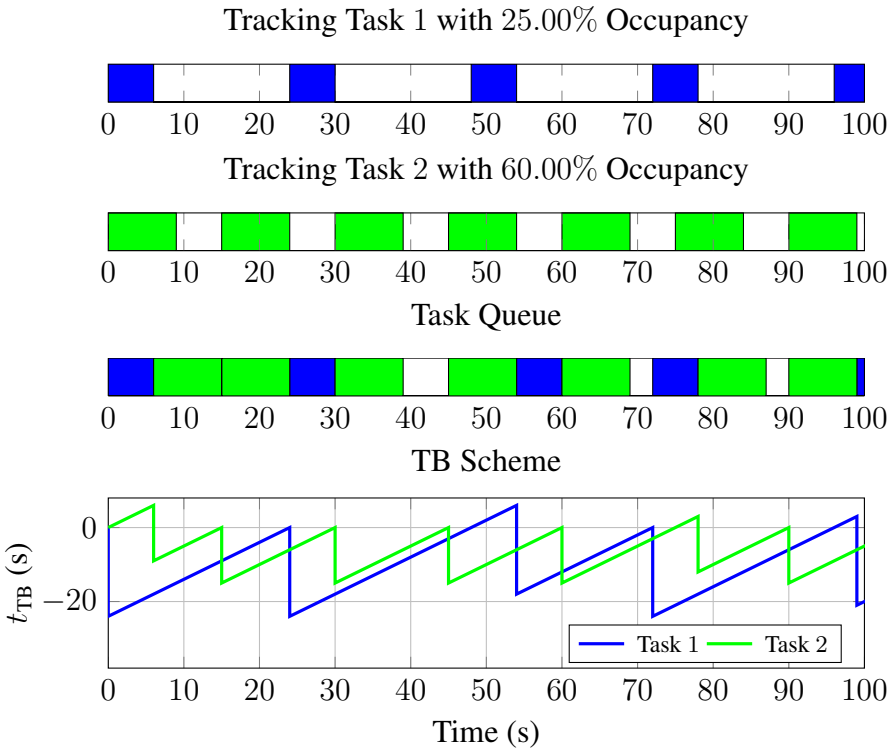

Figure 3.2: TB scheduler example.

cycle of scheduling ends at $t = 6$ s, and $t_{\text{TB}}^{(1)} = -18$ s and $t_{\text{TB}}^{(2)} = 6$ s, as shown on TB scheme. In the second cycle of scheduling, task 2 is chosen since task 1 has a negative t_{TB}. The second cycle of scheduling ends at $t = 15$ s, and $t_{\text{TB}}^{(1)} = -9$ s and $t_{\text{TB}}^{(2)} = 0$ s by processing all steps, as shown on TB scheme. Radar time is completely utilized until $t = 39$ s. Here, $t_{\text{TB}}^{(1)} = -9$ s and $t_{\text{TB}}^{(2)} = -6$ s, and hence, step 8 is processed after step 3. Then, a surveillance task fragment, as depicted by the white areas on task queue shown in Figure 3.2, is scheduled. In step 9, t_{TB} for both of tracking tasks are increased with $\mathcal{T}_F$. Surveillance task fragments are successively scheduled until $t = 45$ s, since both of tracking tasks have negative t_{TB}, as shown on TB scheme. The scheduling process continues in this way.

The requested task queue of each tracking task is individually shown in Figure 3.2, and task queue after scheduling is also shown in the same figure below of them. Here, the main aim is compare the actual and requested occupancies. Task 1 and task 2 actually utilize radar time for 25 s and 63 s respectively until $t = 100$ s. These values indicate that the actual occupancies are 25% and 63% for task 1 and task 2 respectively. Thus, there are minor differences which is negligible for longer durations between the actual and requested occupancies.

3.1.2 Scheduler Developed for MESAR

A scheduler algorithm which utilizes TB technique is briefly explained in [46] for real-time control of Multifunction Electronically Scanned Adaptive Radar (MESAR). In addition to some improvements on this algorithm, the work [47] describes TB technique in a detailed manner. This section describes the original and modified version of scheduling algorithms, as explained in [47], developed for real-time task scheduling with MESAR. Before delving into scheduling algorithms, it is more convenient to give some aspects briefly related to MESAR.

The resource management of MFR can be applied efficiently by achieving the following processes.

- All tasks must be ranked in a priority order. Note that the priorities of tasks may change throughout an engagement.

- Tasks must be formed into a timeline for MFR to perform. This is the main task of the scheduler.

The scheduler's task in constructing scheduling timeline in real-time is complicated due to the constraints which apply to each task as follows:

- Tasks vary in the criticality of the time period in which they must be scheduled. Some may have a small window of opportunity which must be met for the task to be successful, while others may have looser time constraints.
- Tasks differ significantly in length.
- Tasks may become suddenly necessary or urgent, or may become unnecessary.
- Tasks may have to adhere to some constraint such as close to array broadside operation in a rotating system.

Thus, the following broad objectives are suggested for resource management and task scheduling effectively.

- Schedule each task as near to the requested time as possible.
- Schedule each task as close to array broadside as possible.
- Schedule each task to minimize the radar idle time.
- Schedule each task to maximize the tactical benefit of MFR.

3.1.2.1 Algorithm of MESAR

The task is thought as a single entity in Section 3.1.1. However, it is known that tasks can be divided into subtasks, i.e. coupled-tasks consist of transmitting, idle time and receiving parts [50]. In addition, the resource manager sometimes needs interruptions to serve the resources to the tasks with higher priority. Therefore the algorithm of MESAR allows to divide tasks into subtasks that can be interleaved to manage radar time efficiently and decrease the delays for the highly prioritized tasks. The flow diagram of the algorithm of MESAR is shown in Figure 3.3.

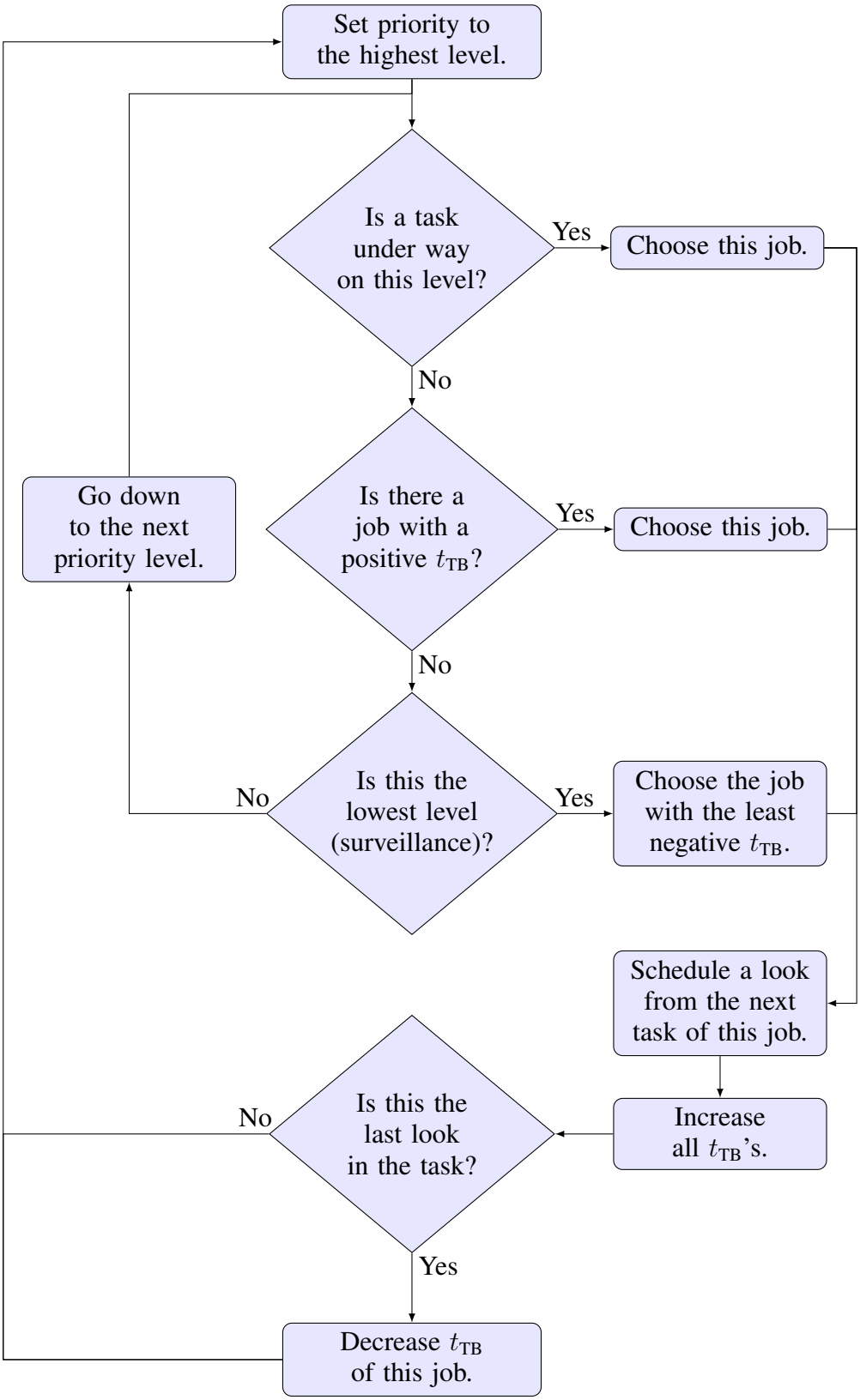

Figure 3.3: Flow diagram of scheduler algorithm for MESAR.

According to Figure 3.3, it should be clear that the description of a job, a task and a look in MESAR must be clarified. A job may be surveillance of a region, or maintaining track on a specific target and it usually consists of several tasks, i.e. searching a single surveillance beam position, or performing one track update. Then, each task usually consists of several activities which are non-coherently integrated to give a detection. The last definition, a look is one or more activities from a task that are transmitted coherently by the radar. The described terms and time intervals are illustrated in Figure 3.4.

Description of the figure by starting from the highest priority level;

1. If a job is already under the process on that level, then that job is chosen for scheduling of looks. This means that tasks from each level will be completed sequentially, rather than many tasks from the same level being interleaved, and thus drawn out in time.

2. If no task is executed then the task on the same priority level is chosen with the highest positive t_{TB}.

3. If no task has a positive t_{TB} then move down to the next level and repeat (1)-(3).

4. If no task has a positive t_{TB} on the job table, then choose the surveillance task with the smallest negative t_{TB}.

5. Schedule one look from the chosen task, and increase all other t_{TB}'s by a fraction of this task.

6. If that was the last look of a task decrease the job's t_{TB} by the task dwell time.

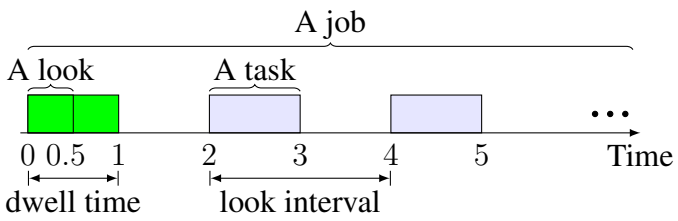

Figure 3.4: Illustration of job, task, look terms and time intervals.

The idea is deduced from the given description that resource management, handled in real-time, schedules jobs (or tasks) within the fixed time intervals. The elapsed time for a look, and tasks are said to be complete after all of the corresponding looks processed, while the previous algorithm described in Section 3.1.1 adds task times to or subtracts task update times from t_{TB} variables. Then, it schedules tasks only after the task under the process is completely executed.

3.1.2.2 Modified Algorithm of MESAR

It has been mentioned that the simplest TB algorithm only used to determine whether a task is ready for scheduling, i.e. if the job has a t_{TB} that is not negative then this job is ready to be executed. Here, the modified version of the algorithm of MESAR is the same as the algorithm described in Section 3.1.1 with an addition of priority assignments.

The simplifications of the algorithms with respect to MESAR are as follows:

- The t_{TB} unit is seconds.
- Tasks are scheduled as a single entity.
- Scheduler uses the task look interval (the time between implementations of successive tasks, e.g. the track update interval, or the surveillance beam revisit time), and the task time (the dwell time of the task) to control the scheduling of tasks.

In addition to these simplifications, once a task has been scheduled one of two things may happen to the task t_{TB} which are different in their result.

- The t_{TB} is decreased by the task look back interval.
- The t_{TB} is reset to minus the task look back interval, so that the next task will not occur until the desired time has elapsed.

In the first case, if the task was late then it is possible that t_{TB} of that job would still be positive after it was decreased. Therefore more tasks may be scheduled for that

job straight away, without waiting for maximum interval. This case may be useful when surveillance tasks are considered. For example, where if the search of a region is running late due to overload, the search may catch up by searching several beams very rapidly. This is not a useful property for all functions however. When updating a track for example, there is little benefit accrued from scheduling two or more track updates in rapid succession. In this instance, t_{TB} should be reset to negative of the task interval, so that all track updates are scheduled periodically with the look interval. It should be noted that the look interval can adaptively be changed.

Currently the algorithm resets the t_{TB} of tracking jobs and surveillance job time balances are decreased by the task look back interval, so that if they are running late, they may catch up by scheduling several looks.

3.1.3 Adaptive Time-Balance Scheduler

The adaptive time-balance (ATB) scheduler is proposed in [48]. The ATB scheduler extends some ideas behind the TB technique. Here, surveillance task can be associated with a t_{TB} so that it is scheduled with respect to task update time to detect new targets. Task time of surveillance, $\mathcal{T}_S$, is not divided into fragments. Furthermore, task update times can be adaptively changed to mitigate the overload conditions or to increase the revisit improvement factor. The ATB scheduler supports user defined priority levels for each task, and tasks are scheduled according to these priority levels and t_{TB}'s.

3.1.3.1 Adjusting Task Update Times

The occupancy, $\mathcal{O}$, is expressed as $\mathcal{T}\mathcal{U}^{-1}$ that is the ratio of task time, $\mathcal{T}$, and task update time, $\mathcal{U}$, for each task. In this approach, the total occupancy of all tasks is fixed at 100% so that radar time is completely utilized. That is

$$\mathcal{O}_T + \mathcal{O}_S = \sum_{n=1}^{N} \mathcal{O}_n + \mathcal{O}_S = 100\%, \tag{3.1}$$

where $\mathcal{O}_T$ denotes the total occupancy of all tracking tasks, N is the number of targets, $\mathcal{O}_n = \mathcal{T}_n\mathcal{U}_n^{-1}$ denotes the occupancy of tracking task for target n, and $\mathcal{O}_S$ denotes the occupancy of surveillance task. Task time of surveillance, $\mathcal{T}_S$, is the elapsed time for a complete search in the region of interest, and task update time of surveillance, $\mathcal{U}_S$, is determined from $\mathcal{O}_S = \mathcal{T}_S\mathcal{U}_S^{-1}$. If $\mathcal{O}_T$ exceeds 100% then radar is overloaded. Hence, tracking tasks will be unavoidably delayed and the surveillance task, which usually runs with a lower priority, will not run until the overload condition disappears. This becomes a serious problem since it is desired that the surveillance task is executed within a time interval not too long so that it can keep the current tracks and achieve early detection of new tracks. Therefore two approaches are presented in [48] to maintain surveillance execution while handling the overload condition.

The first step to adjust task update times is to set task update time of surveillance equal to the task update time for a conventional search, $\mathcal{U}_C$, namely maximum allowable task update time for surveillance, and then estimate the remaining occupancy based on (3.1) as

$$\mathcal{O}_T^* = 100\% - \mathcal{T}_S\mathcal{U}_C^{-1}, \tag{3.2}$$

where $\mathcal{O}_T^*$ is the total occupancy available for tracking tasks after allocating the occupancy for surveillance task. The estimation of $\mathcal{O}_T^*$ leads to three different radar resource load conditions. $\mathcal{O}_T^* < \mathcal{O}_T$ the radar is said to be overloaded, if $\mathcal{O}_T^* = \mathcal{O}_T$ it is fully loaded, otherwise it is underloaded. For the overload condition, it is necessary to decrease the total requested tracking task occupancies. A total occupancy correction factor, C_f, can be computed as

$$C_f^{-1}\mathcal{O}_T = \mathcal{O}_T^*. \tag{3.3}$$

Then, the new occupancy distribution for N tracking and surveillance tasks is described as

$$\mathcal{O}_T^* + \mathcal{O}_S^* = \sum_{n=1}^{N} \mathcal{T}_n(C_f\mathcal{U}_n)^{-1} + \mathcal{T}_S\mathcal{U}_C^{-1} = 100\%, \tag{3.4}$$

where the term $C_f\mathcal{U}_i$ is the adjusted task update time for tracking task for target n, and $\mathcal{O}_S^*$ is the surveillance occupancy corresponding to $\mathcal{U}_C$.

It is simple to understand that $C_f \geqslant 1$ and task update times for tracking tasks increase for the overloaded case, $C_f \leqslant 1$ and task update times for tracking tasks decrease for the underloaded case.

3.1.3.2 Task Prioritization

Task prioritization is critical for the selection the best task within multiple tasks competing for radar resources are present. If there is not sufficient radar time, namely radar is overloaded, one or more of these tasks have lower priority levels may be executed late. Therefore the operator can assign higher priority to some tasks to execute them on time.

The priority level, $P_n \in \mathbb{Z}^+$, is associated with tracking task for target n and the minimum priority level is 1, for $n = 1, 2, \ldots, N'$. Here, $N' = N + 1$ so there are N tracking tasks and one surveillance task with associated priority levels.

Priority levels can also be changed according to defined constraints, as described in Section 2.3. For example, if surveillance has not been executed for a time period of $\mathcal{U}_C$, it must be forced by maximizing its priority level so that the track identification and tracking can be effective.

3.1.3.3 Quality Measurement for Update Times

The TB algorithm is extended to handle the two overload mitigation approaches described above. Approach 1 is adjusting task update times which is described in Section 3.1.3.1, and approach 2 is task prioritization which is described in Section 3.1.3.2. A quality measurement is described as

$$I = \frac{\sum_{i=1}^{N} \mathcal{U}_m \mathcal{U}_i^{-1}}{N \mathcal{U}_m \mathcal{U}_C^{-1}}. \tag{3.5}$$

This measure shows the improvement on the number of scheduled tasks after adjusting update times. First it is assumed that N tasks have a constant update time $\mathcal{U}_C$, then the update times are adjusted to individual values, $\mathcal{U}_i$'s and $\mathcal{U}_m$ is the time interval, region of interest, for scheduled tasks.

3.1.3.4 Algorithm of ATB Scheduler

The step 1, the process of acquiring and/or setting parameters for surveillance and tracking tasks is described in Figure 3.5. In step-a, tracking parameters such as number of tracks , N, task time ,$\mathcal{T}$, task update time $\mathcal{U}$, priority level, P for each track and the maximum surveillance update time $\mathcal{U}_C$ are loaded from database. Step-b, if a t_{TB} is not associated with surveillance, then surveillance is fragmented and update times are adjusted as suggested by approach 1 is named as step-e and shown in detail in Figure 3.6. If the requested update times are to be controlled, the update time for surveillance is estimated based on (3.1), and its value determines whether or not radar resources are overloaded. For an overload condition, the update time correction factor is estimated based on (3.3) and update times are increased as shown in (3.4). For a non-overload condition, if the surveillance update time is set to $\mathcal{U}_C$, then tracking update times are decreased using (3.4). Third, when a t_{TB} is associated with surveillance, (shown in the right branch of Figure 3.5), surveillance is not longer fragmented and its task time is denoted by $\mathcal{T}_{N'}$. Also, priority level assignments are evaluated as suggested by approach 2 is named as step-h and shown in detail in Figure 3.7. If the radar resources are insufficient, the surveillance task update time is forced to be the same as for conventional radar, $\mathcal{U}_C$. In addition, if surveillance t_{TB} is positive, its priority is set to be larger than the maximum of all P_i. Otherwise, surveillance update time and surveillance priority are not modified.

The ATB scheduler algorithm flow chart is shown in Figure 3.8. After step 1 is processed, priority levels and t_{TB}'s for all tasks are evaluated. The output of this process is indicated by three branches in the same figure. The step 5 runs if there is at least one task of tracking or surveillance that has a positive t_{TB} at the current priority level. The task which has the highest positive t_{TB} is scheduled next. Here, it should be noted that tasks are analyzed in decreasing order of priority. The step 12 runs if all tracking

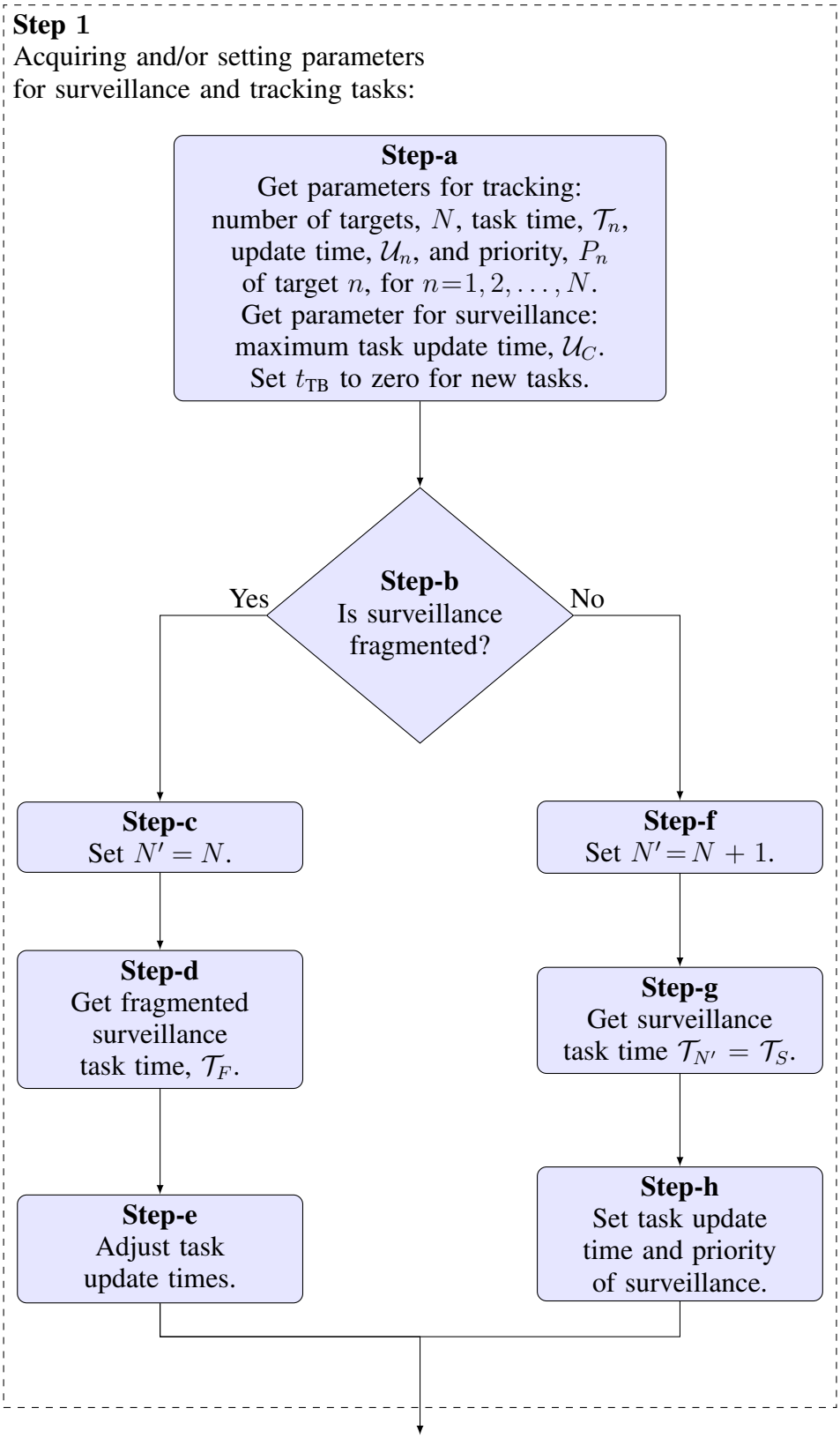

Figure 3.5: Step 1 of ATB scheduler algorithm.

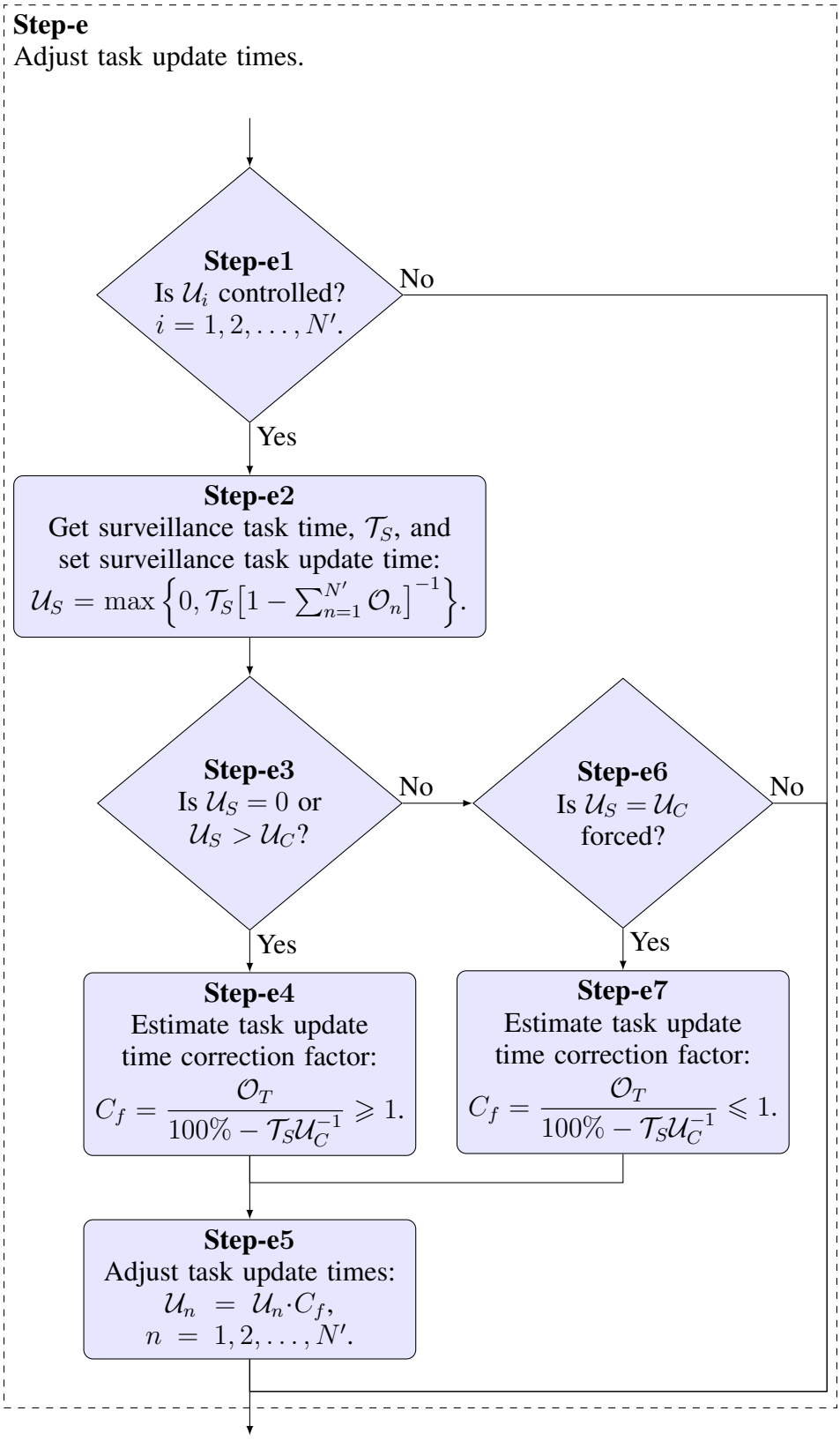

Figure 3.6: Step-e of ATB scheduler algorithm.

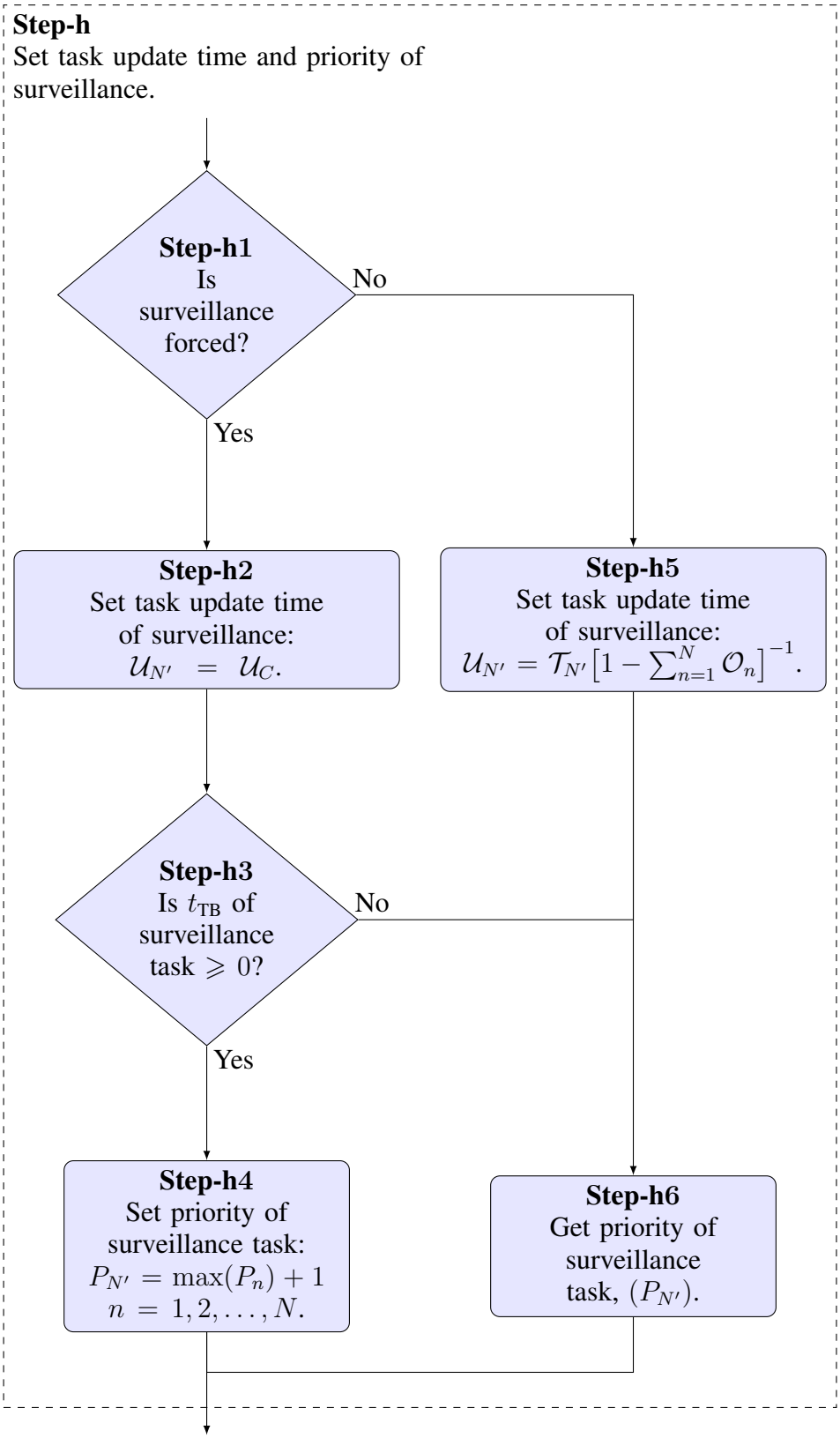

Figure 3.7: Step-h of ATB scheduler algorithm.

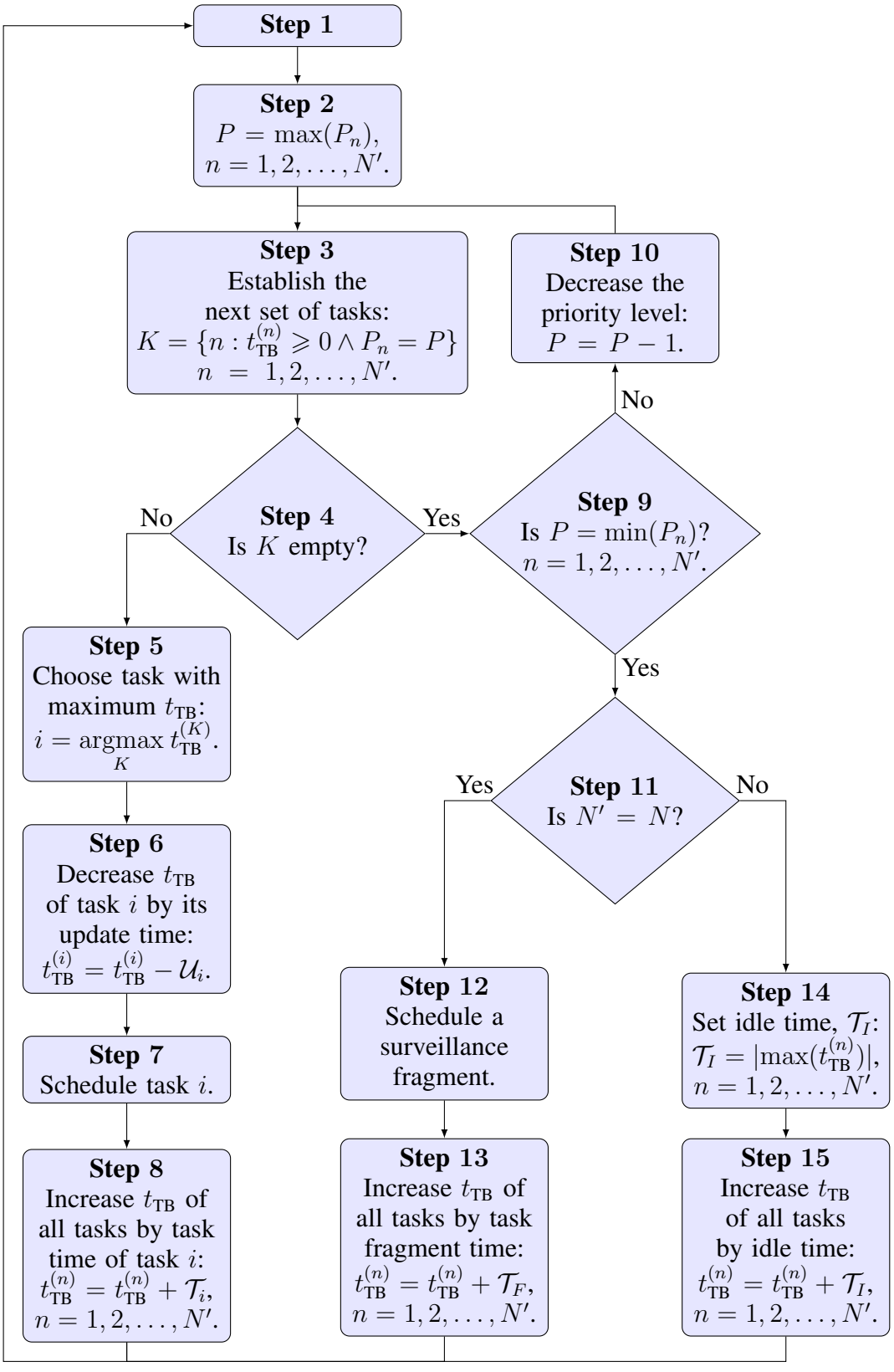

Figure 3.8: Flow diagram of ATB scheduler algorithm.

tasks have negative t_{TB} and surveillance fragments need to be executed until t_{TB} of a tracking task becomes positive. The step 14 runs if both tracking and surveillance tasks have a negative t_{TB}, and so all of them are on time. In this case, the radar is idle until the largest t_{TB} becomes zero or positive. The t_{TB} changes with time as the algorithm provided in [53] for left and center branches. This procedure is repeated until no more tasks are to be scheduled.

The tasks shown in Figure 3.2 is scheduled with ATB scheduler. The task 2 is highly prioritized and it is scheduled before task 1, as shown in Figure 3.9(a). If update times are controlled, total occupancy can be set as 100%, as shown in Figure 3.9(b).

The general idea of the ATB algorithm is to schedule each task as it was requested by balancing the available radar time and the requested update time of each tracking task. When radar resources are not enough, the ATB algorithm can adaptively change requested update times or schedule tasks based on both priority levels and t_{TB}'s.

The TB technique based schedulers are described up to this point and a method which combines the useful features of these described schedulers is proposed in the following section.

3.2 Proposed Schedulers

In this section, the proposed schedulers are explained. The performance measures are,

- the occupancy,
- the number of completed tasks, (tracking+surveillance),
- the number of probable drops and
- the average of errors

on the scenario which contains 15 targets moving for the duration of $t_{max} = 500$ s, as shown in Figure 3.10, are given with the distribution of scheduled tasks.

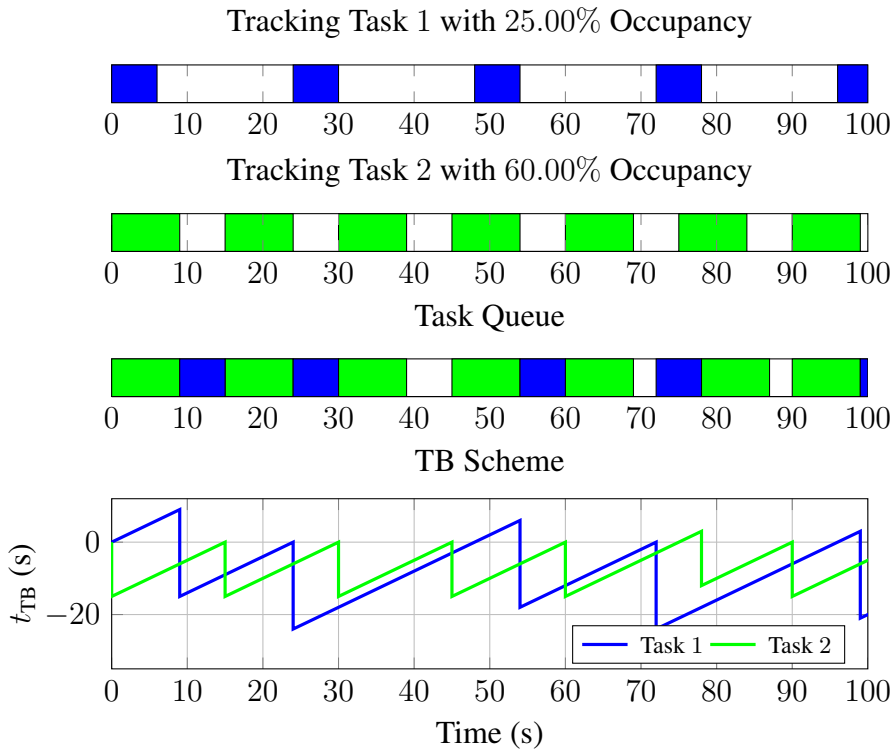

(a) Task 2 is highly prioritized.

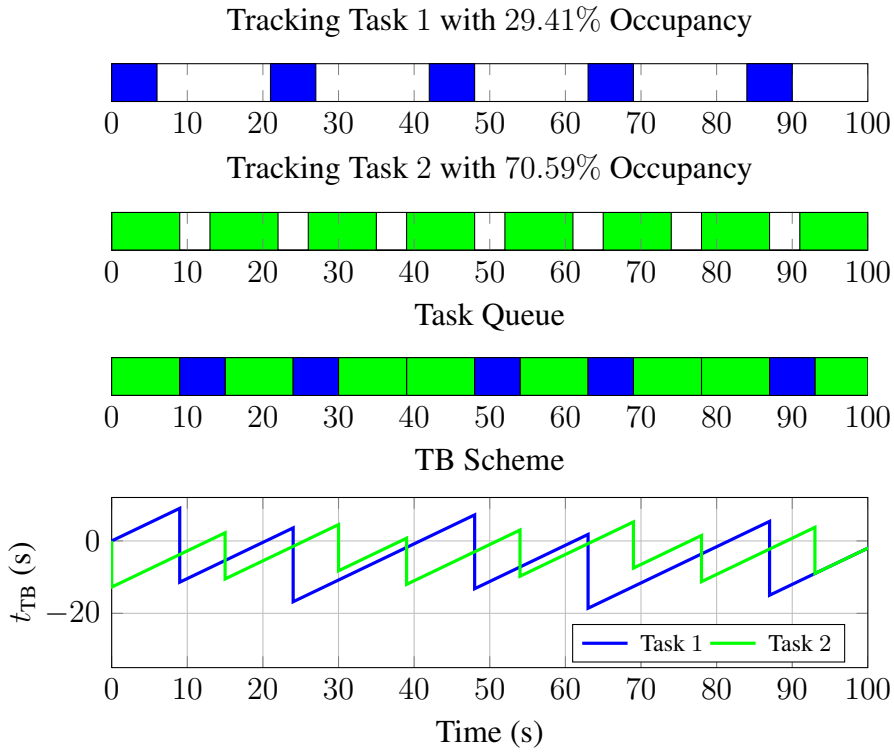

(b) Task 2 is highly prioritized and task update times are controlled.

Figure 3.9: ATB scheduler example.

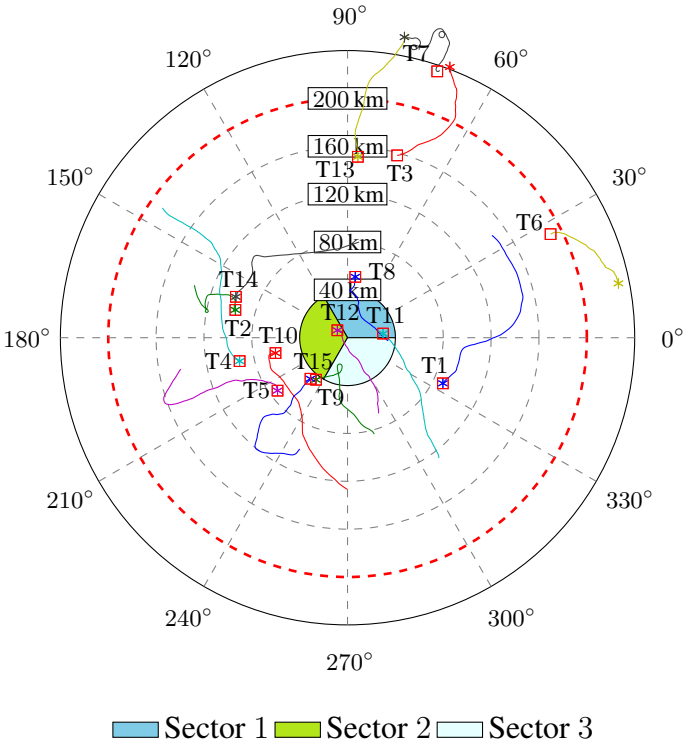

Figure 3.10: The scenario used to measure the performance of proposed schedulers.

3.2.1 Multi-Type Adaptive Time-Balance Scheduler

The multi-type adaptive time-balance scheduler (MTATBS) consists of four different types of ATB scheduler differ with updating t_{TB}'s and task selections. The following sections describe these types.

3.2.1.1 MTATBS-Type 1

The MTATBS-Type 1 tries to update all available targets for positive t_{TB}. It utilizes the dynamic task prioritization to temporarily increase the priority of less important task to the highest priority level. Hence, this task is scheduled for the next cycle of scheduling. However, the scheduling of less important tasks that have less priority can cause to increase t_{TB}'s of other more important tasks. Thus, t_{TB} of each target monotonically increases, and the cost of each target also increases with the time goes

on. Since it tries to schedule all of available tasks, lateness values are smaller and the distribution of scheduled tasks is usually more similar to a uniform distribution.

Figure 3.11, 3.12 and 3.13 show the performance measures of MTATBS-Type 1.

3.2.1.2 MTATBS-Type 2

The MTATBS-Type 2 mainly schedules more important tasks. Thus, t_{TB} and the cost of less important tasks increase rapidly. Lateness values are higher for MTATBS-Type 2 than MTATBS-Type 1, since MTATBS-Type 2 delays less important tasks.

Figure 3.14, 3.15 and 3.16 show the performance measures of MTATBS-Type 2.

3.2.1.3 MTATBS-Type 3

The MTATBS-Type 3 is similar to MTATBS-Type 1, except the decrement in t_{TB} of the scheduled task. It assigns the new t_{TB} of the scheduled task as negative of update time of this task instead of subtracting task update time from current t_{TB}, in other words, it resets the new t_{TB}, after each update. This process avoids the monotonically increment of t_{TB}.

Figure 3.17, 3.18 and 3.19 show the performance measures of MTATBS-Type 3.

3.2.1.4 MTATBS-Type 4

The MTATBS-Type 4 is similar to MTATBS-Type 2, except the decrement in t_{TB} of the scheduled task. It assigns the new t_{TB} of the scheduled task as negative of update time of this task instead of subtracting task update time from current t_{TB}, in other words, it resets the new t_{TB}, after each update. Hence, the cost of MTATBS-Type 4 is always less than the cost of MTATBS-Type 1 and MTATBS-Type 2. The smaller t_{TB}'s also makes lateness values smaller. Lateness values are higher for MTATBS-Type 4 than MTATBS-Type 3, since MTATBS-Type 4 usually delays less important tasks.

Figure 3.20, 3.21 and 3.22 show the performance measures of MTATBS-Type 4.

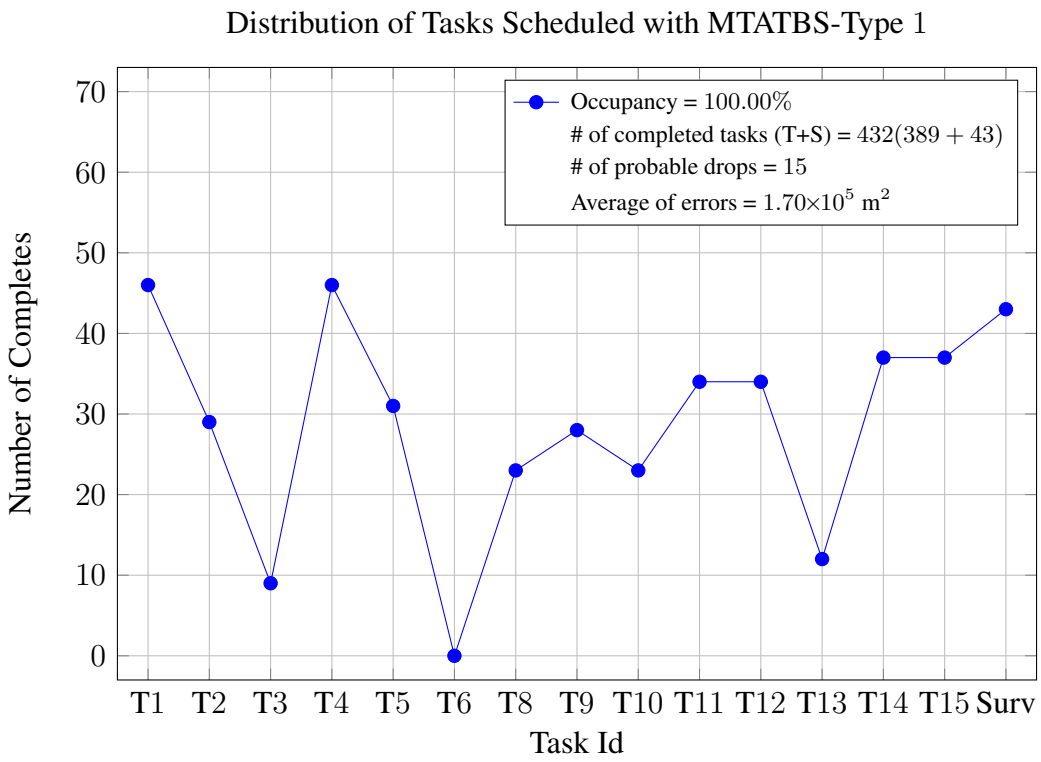

(a) Task interleaving technique is disabled.

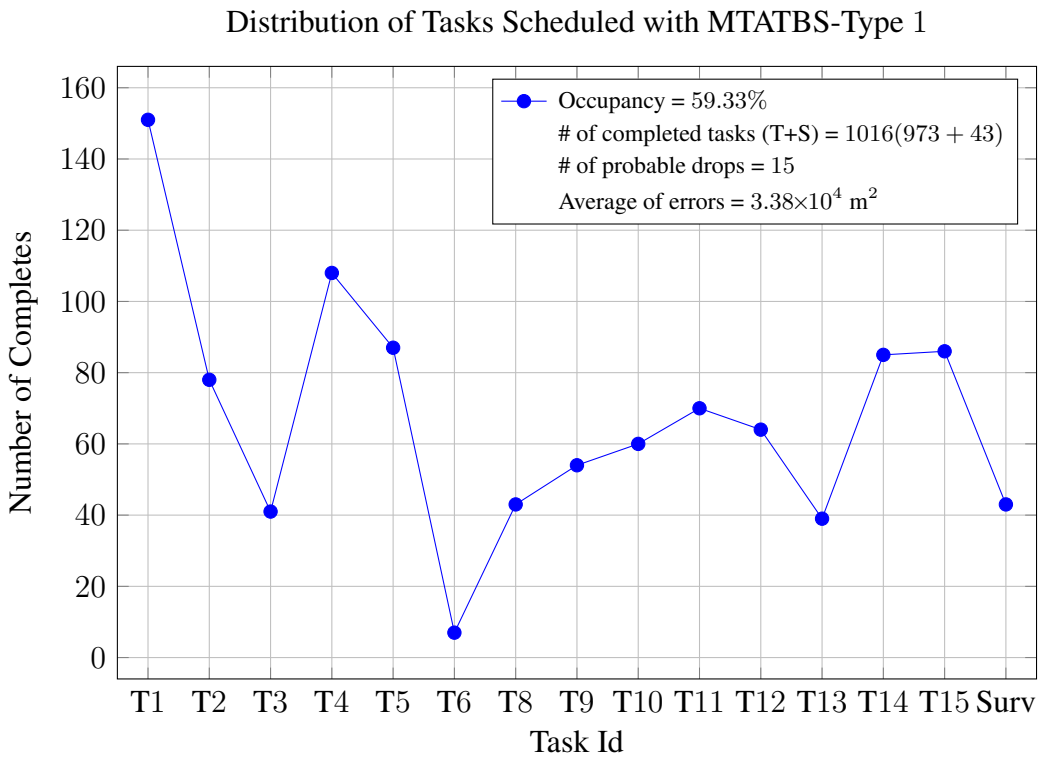

(b) Task interleaving technique is enabled.

Figure 3.11: Distribution of tasks scheduled with MTATBS-Type 1.

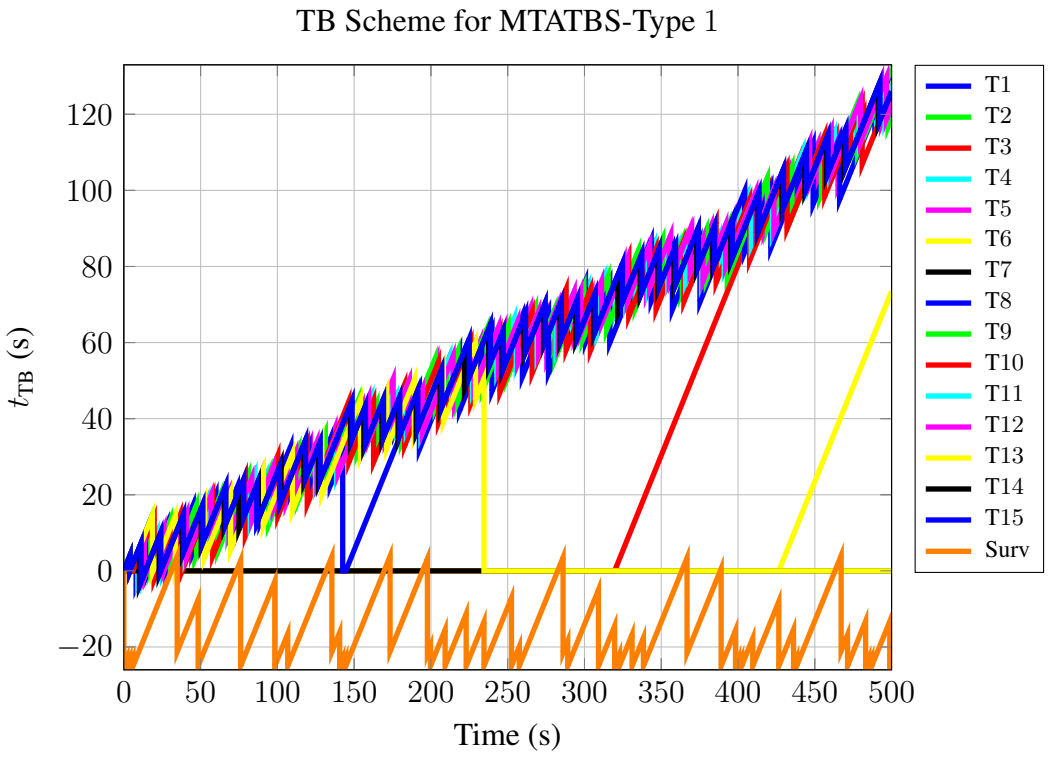

(a) Task interleaving technique is disabled.

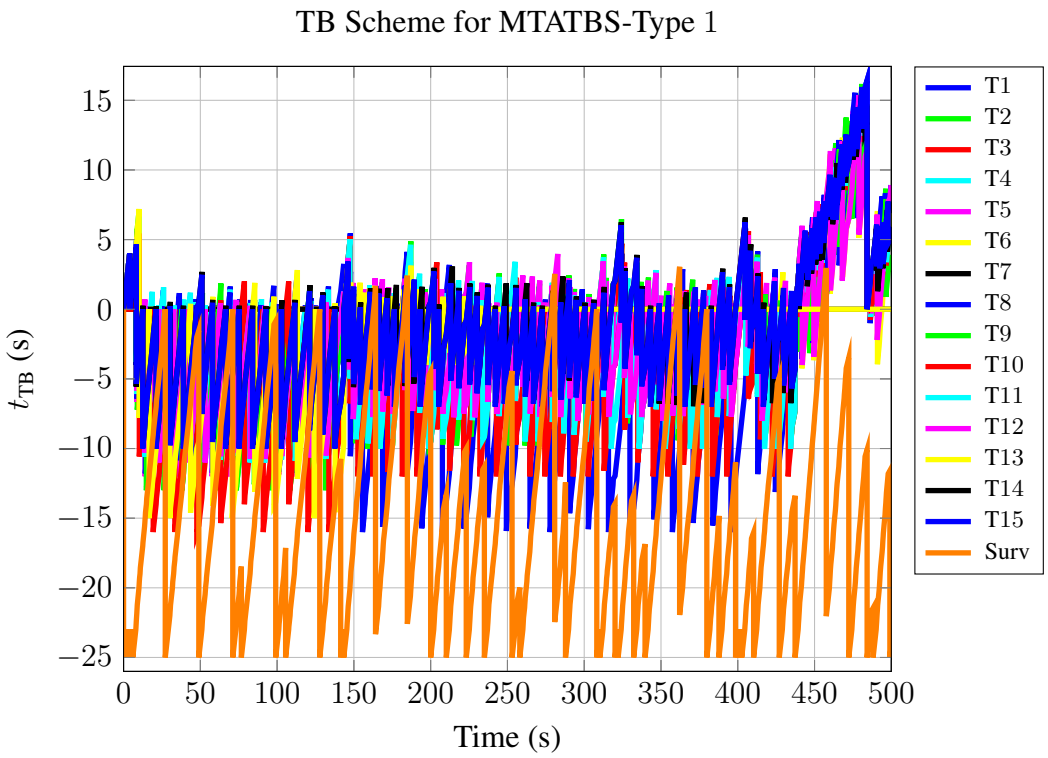

(b) Task interleaving technique is enabled.

Figure 3.12: TB schemes for MTATBS-Type 1.

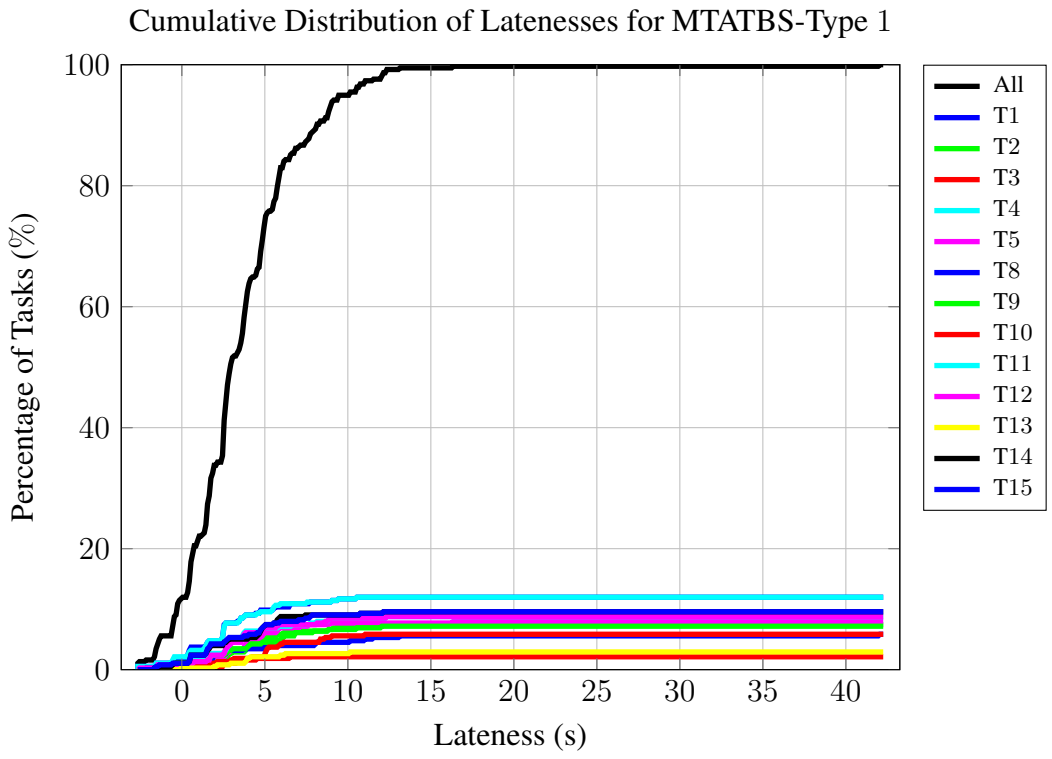

(a) Task interleaving technique is disabled.

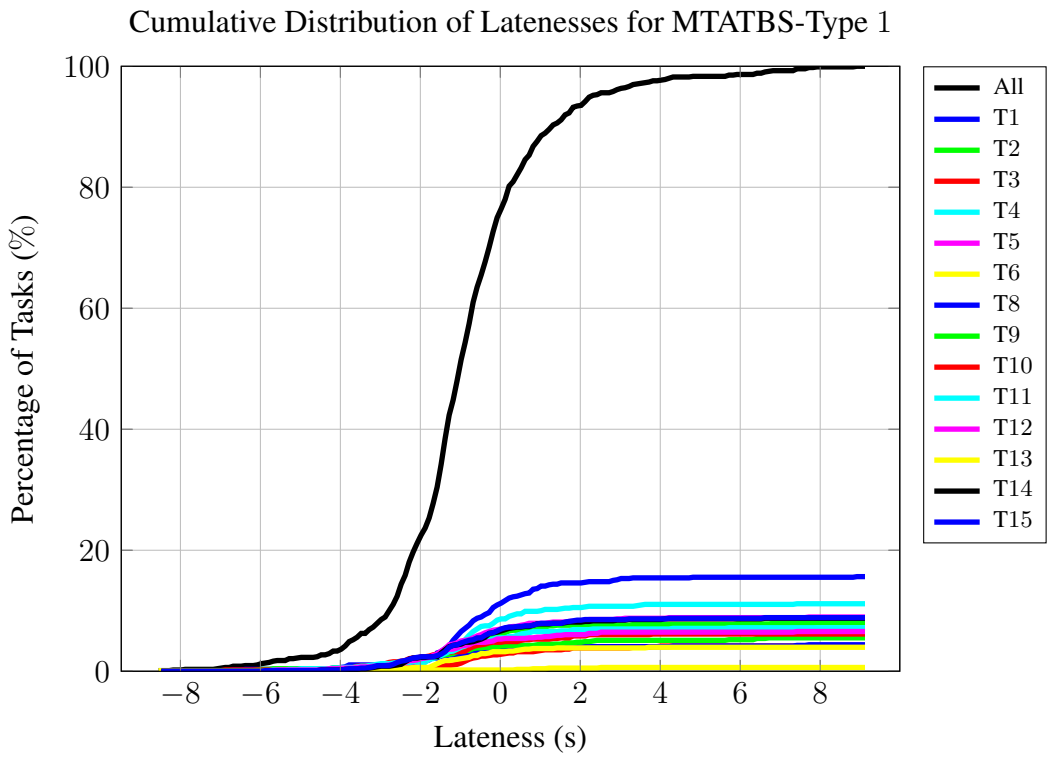

(b) Task interleaving technique is enabled.

Figure 3.13: Cumulative distribution of latenesses for MTATBS-Type 1.

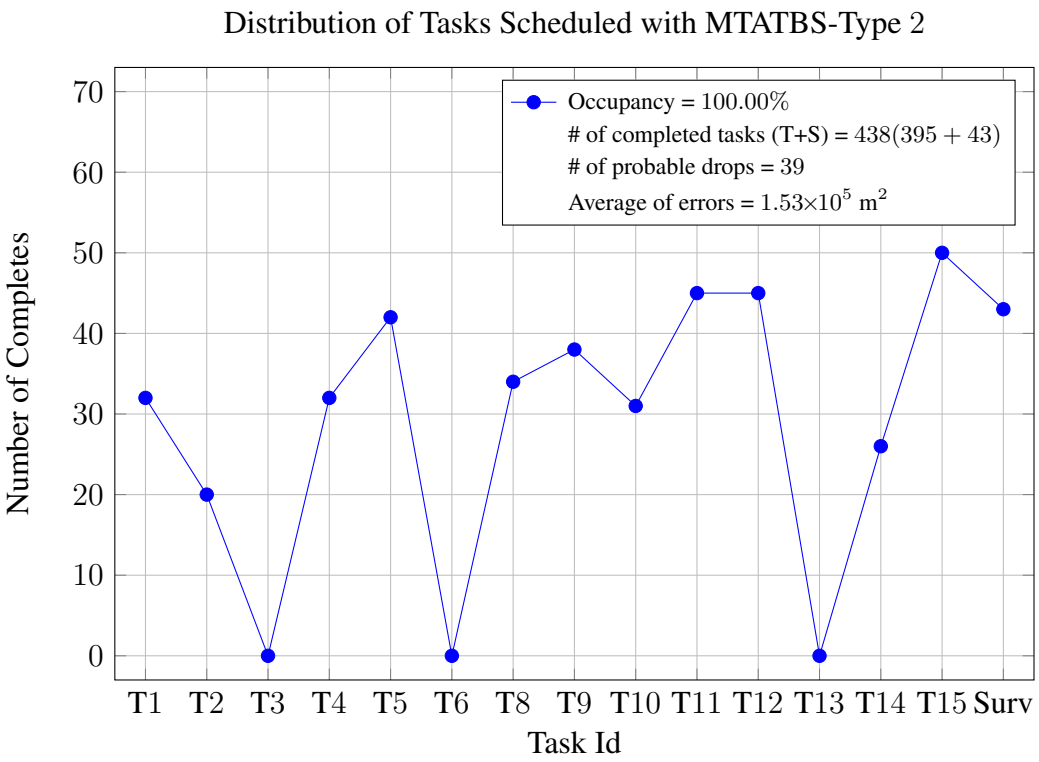

(a) Task interleaving technique is disabled.

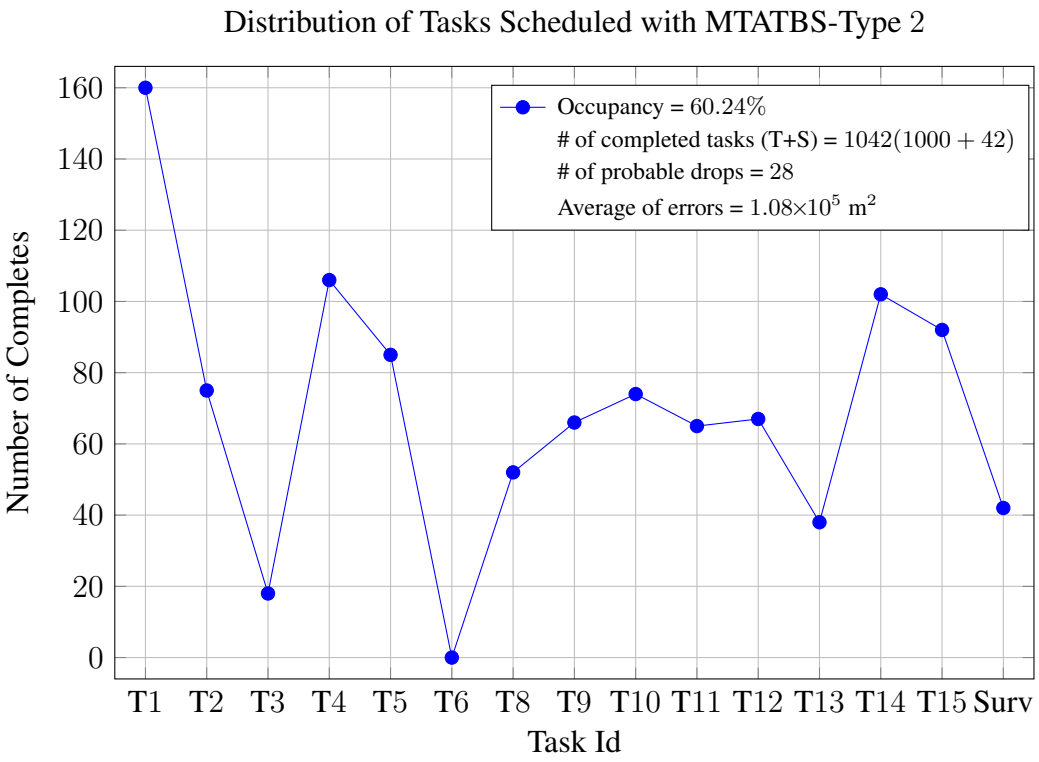

(b) Task interleaving technique is enabled.

Figure 3.14: Distribution of tasks scheduled with MTATBS-Type 2.

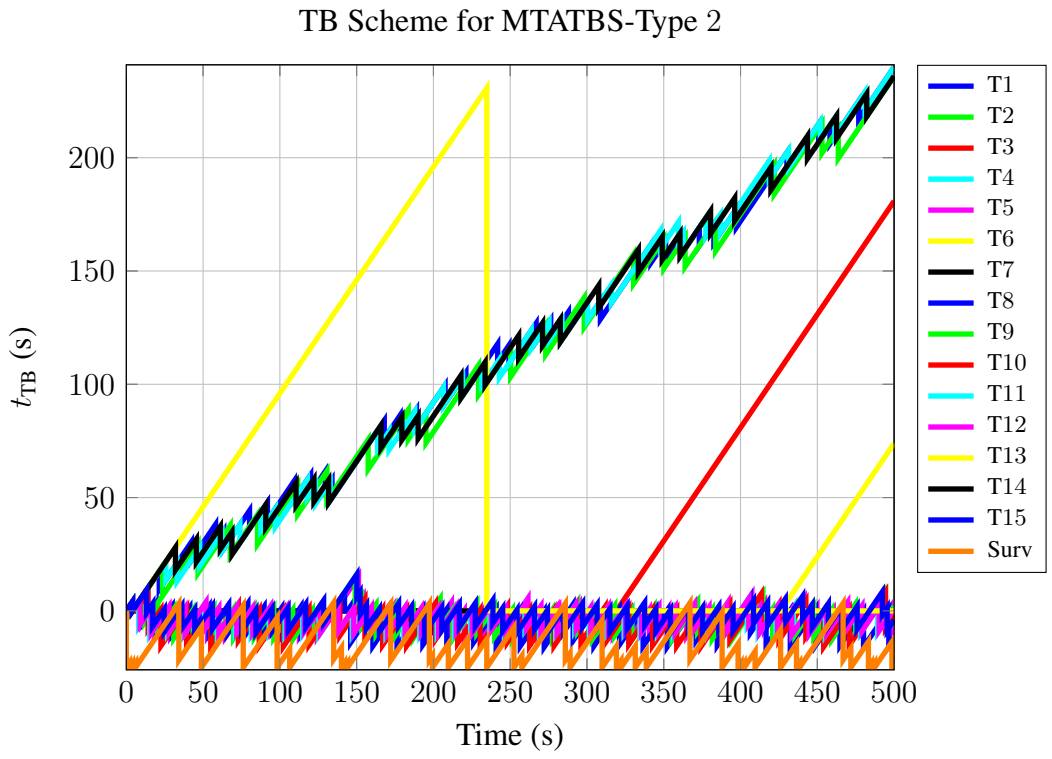

(a) Task interleaving technique is disabled.

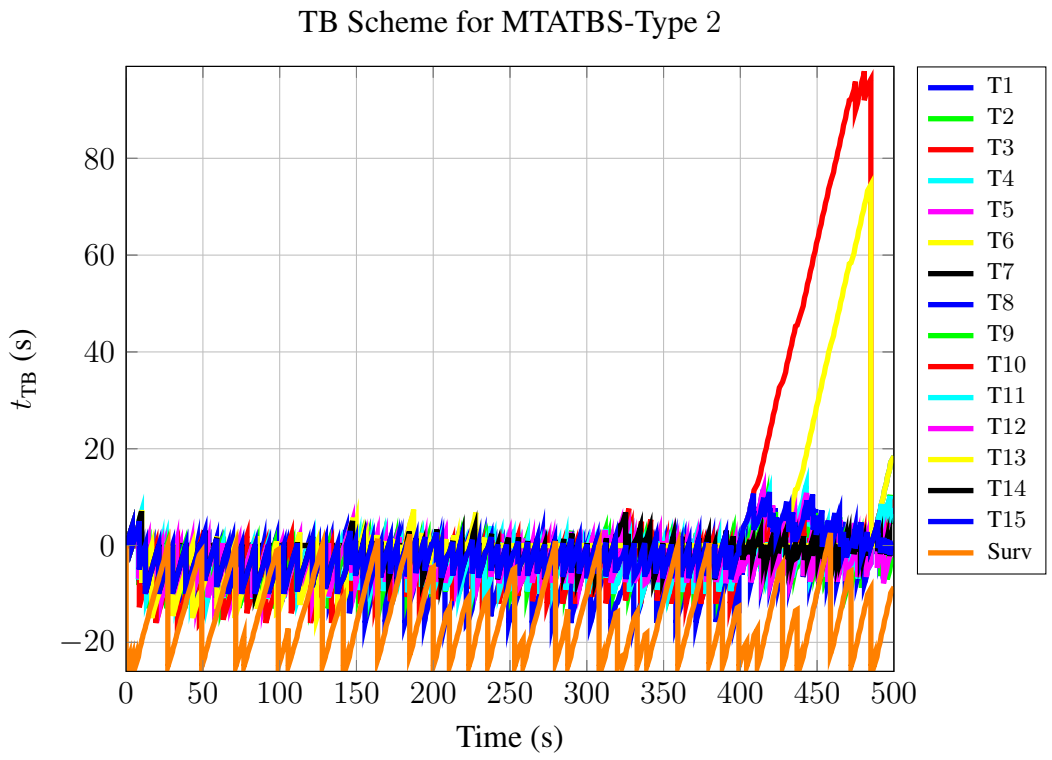

(b) Task interleaving technique is enabled.

Figure 3.15: TB schemes for MTATBS-Type 2.

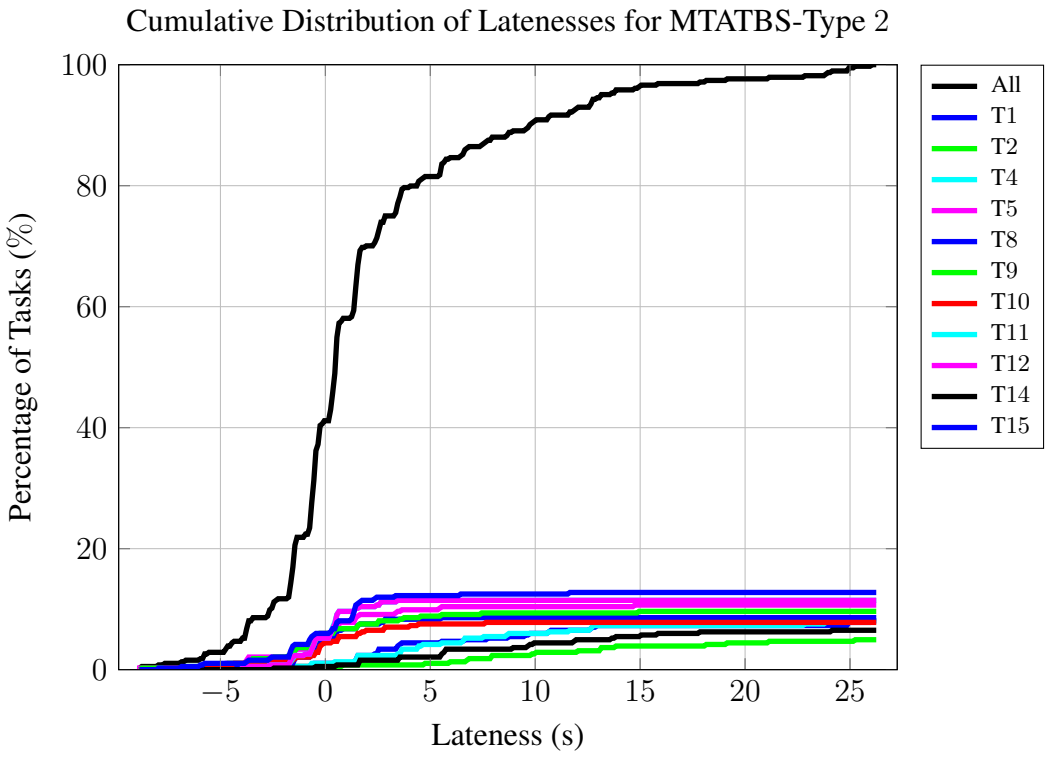

(a) Task interleaving technique is disabled.

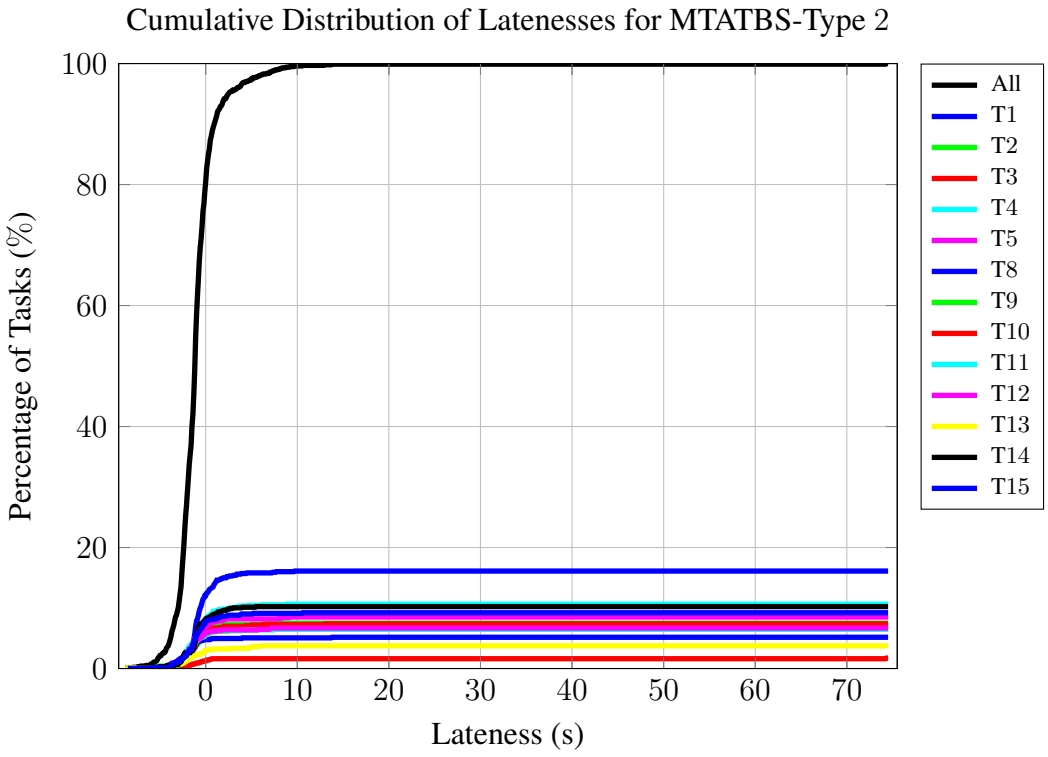

(b) Task interleaving technique is enabled.

Figure 3.16: Cumulative distribution of latenesses for MTATBS-Type 2.

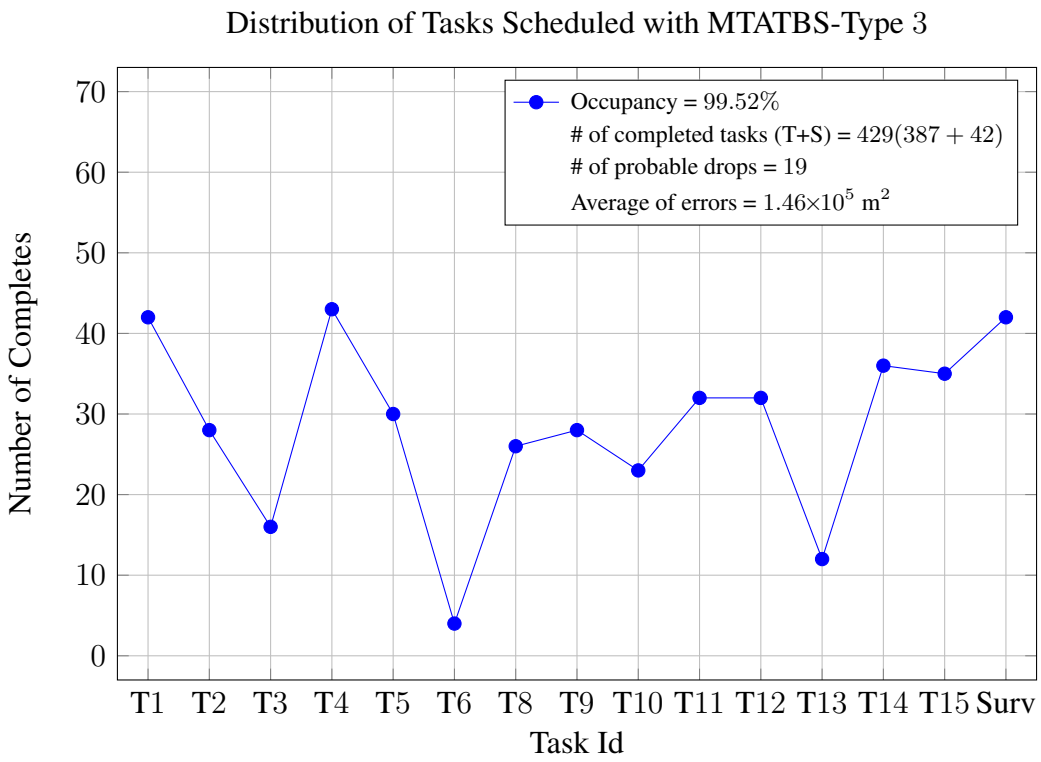

(a) Task interleaving technique is disabled.

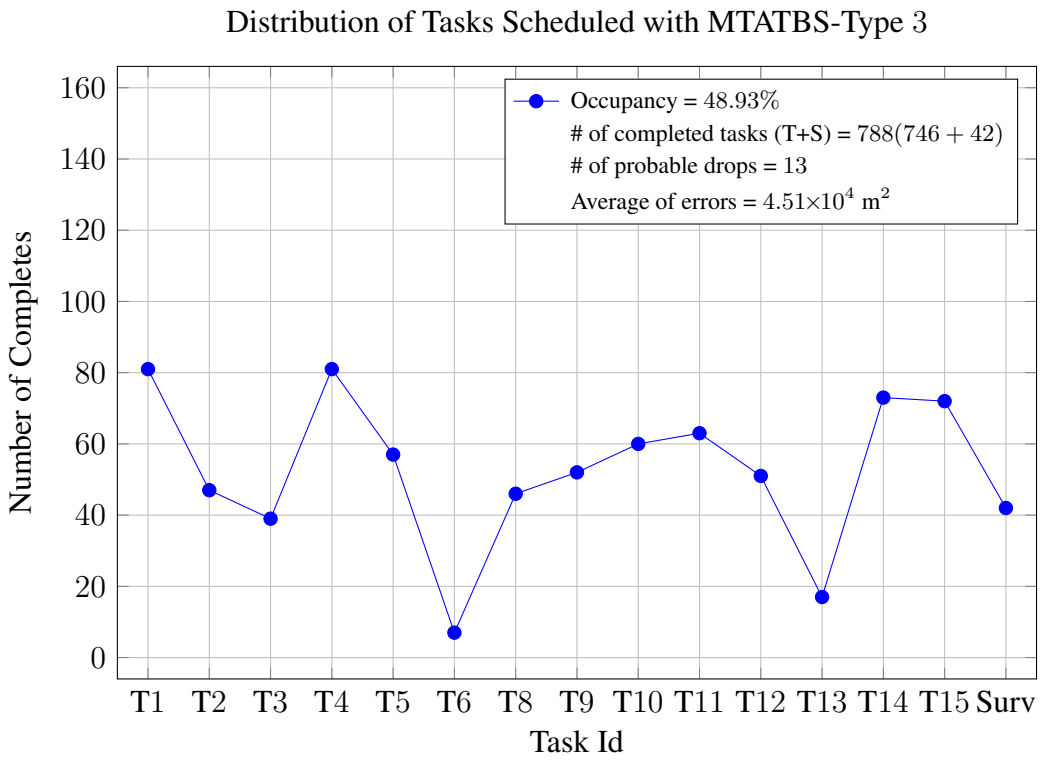

(b) Task interleaving technique is enabled.

Figure 3.17: Distribution of tasks scheduled with MTATBS-Type 3.

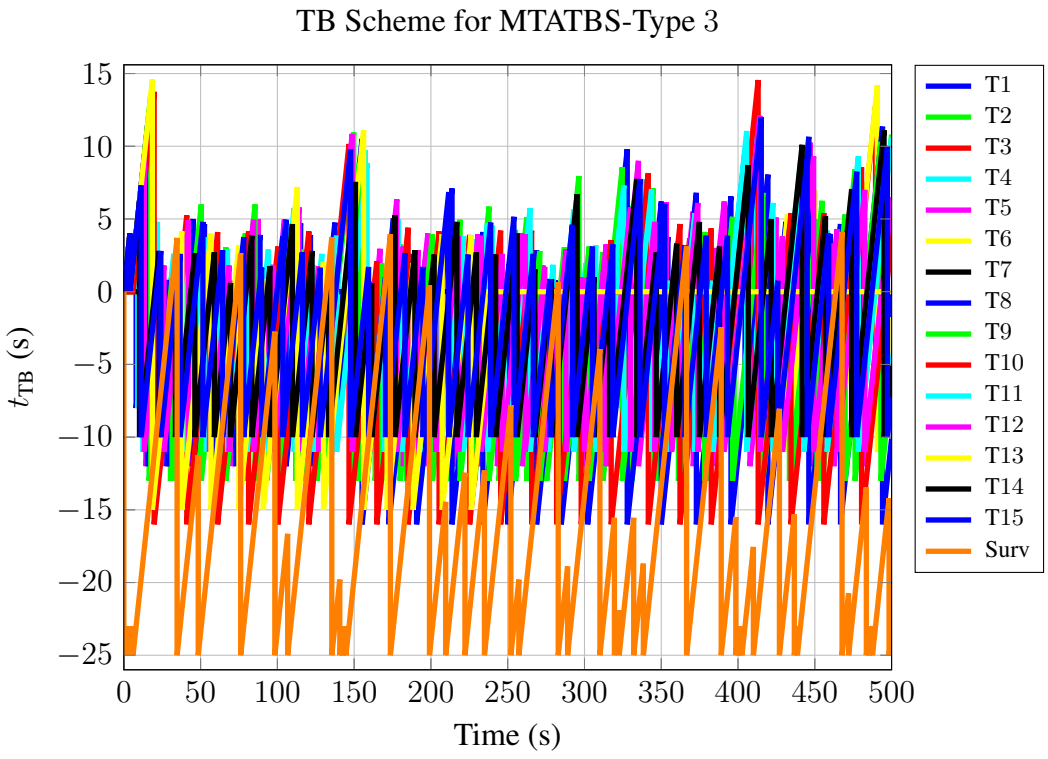

(a) Task interleaving technique is disabled.

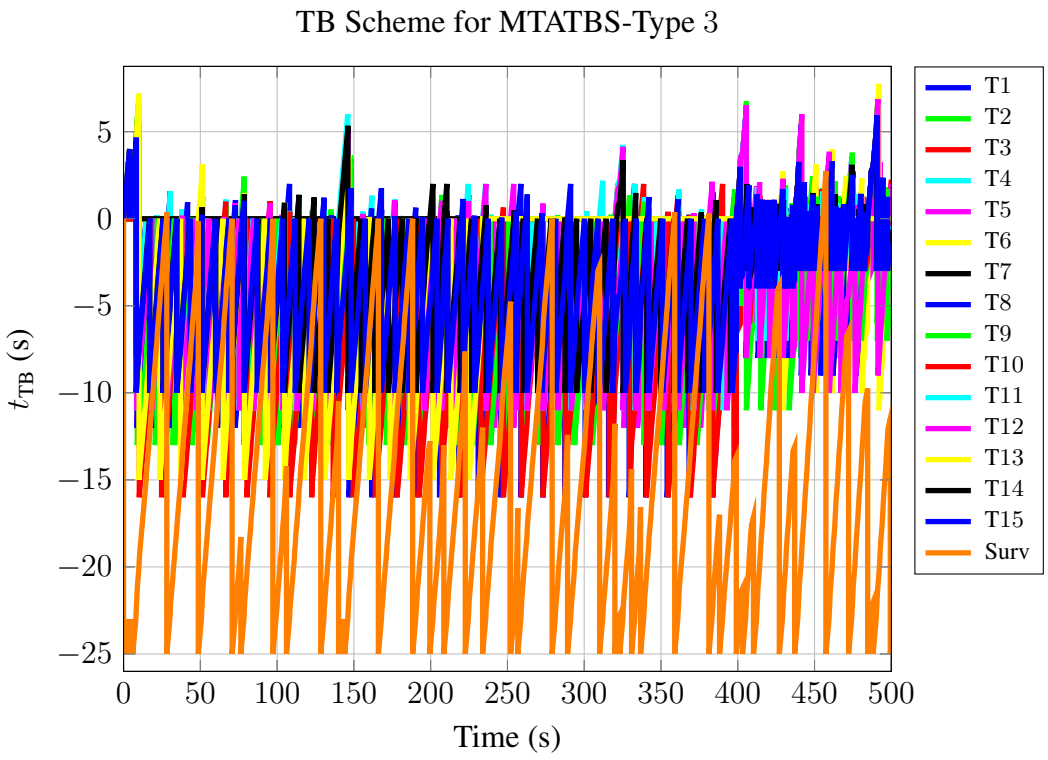

(b) Task interleaving technique is enabled.

Figure 3.18: TB schemes for MTATBS-Type 3.

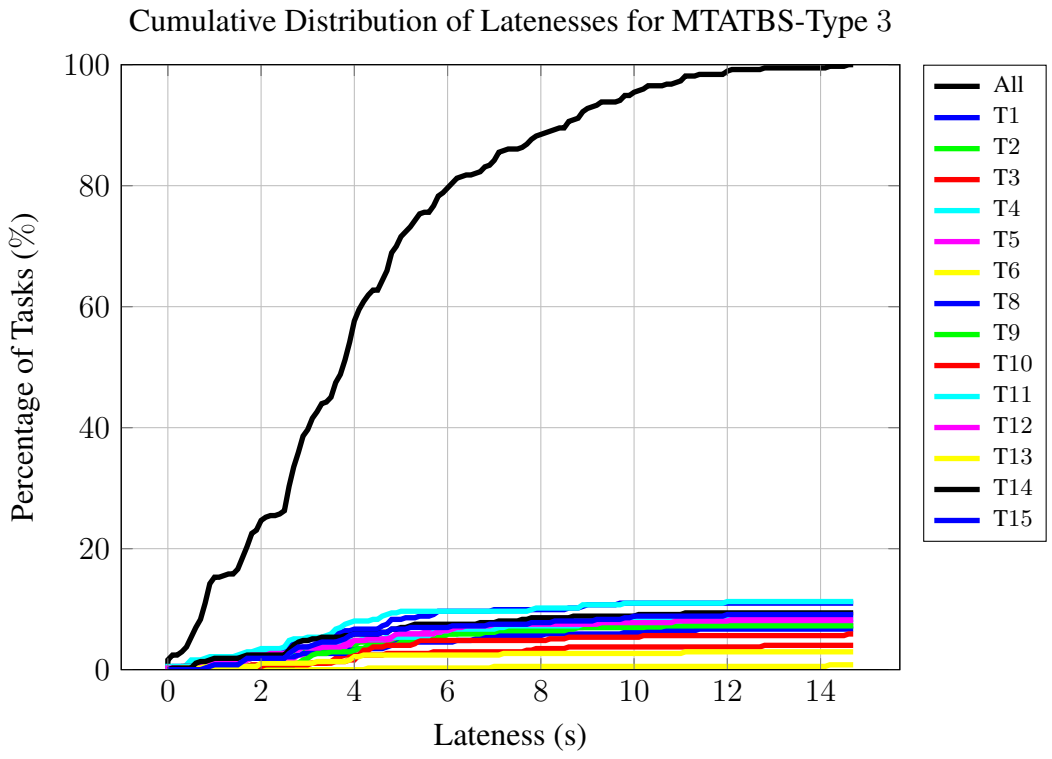

(a) Task interleaving technique is disabled.

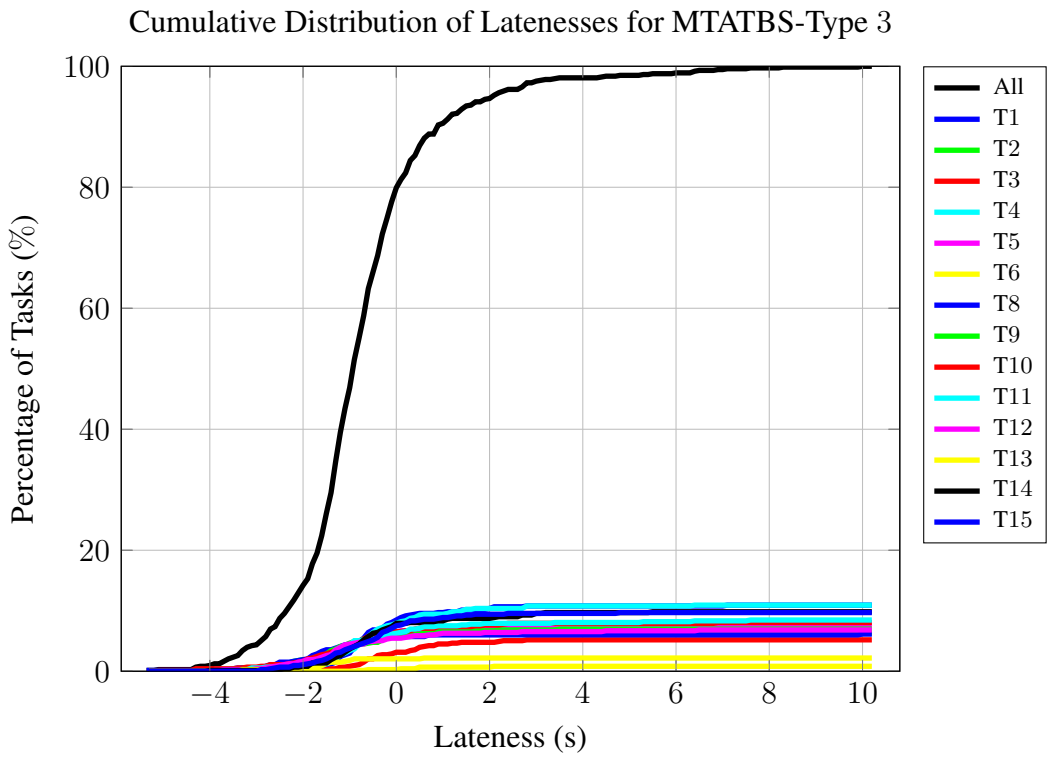

(b) Task interleaving technique is enabled.

Figure 3.19: Cumulative distribution of latenesses for MTATBS-Type 3.

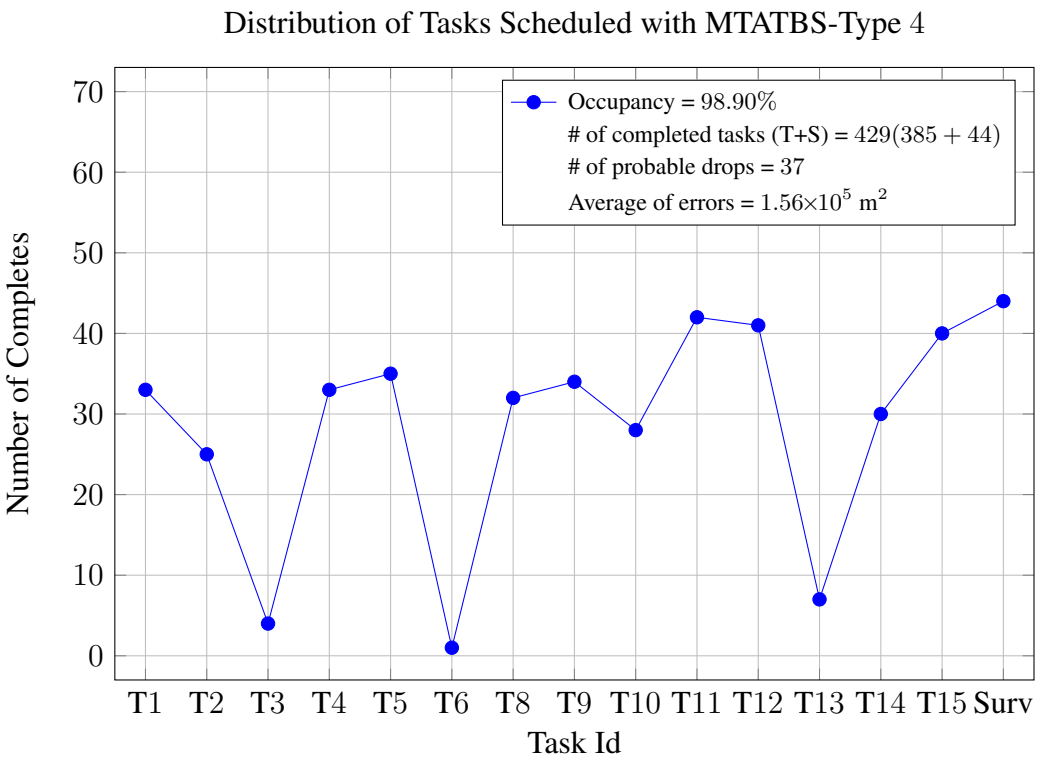

(a) Task interleaving technique is disabled.

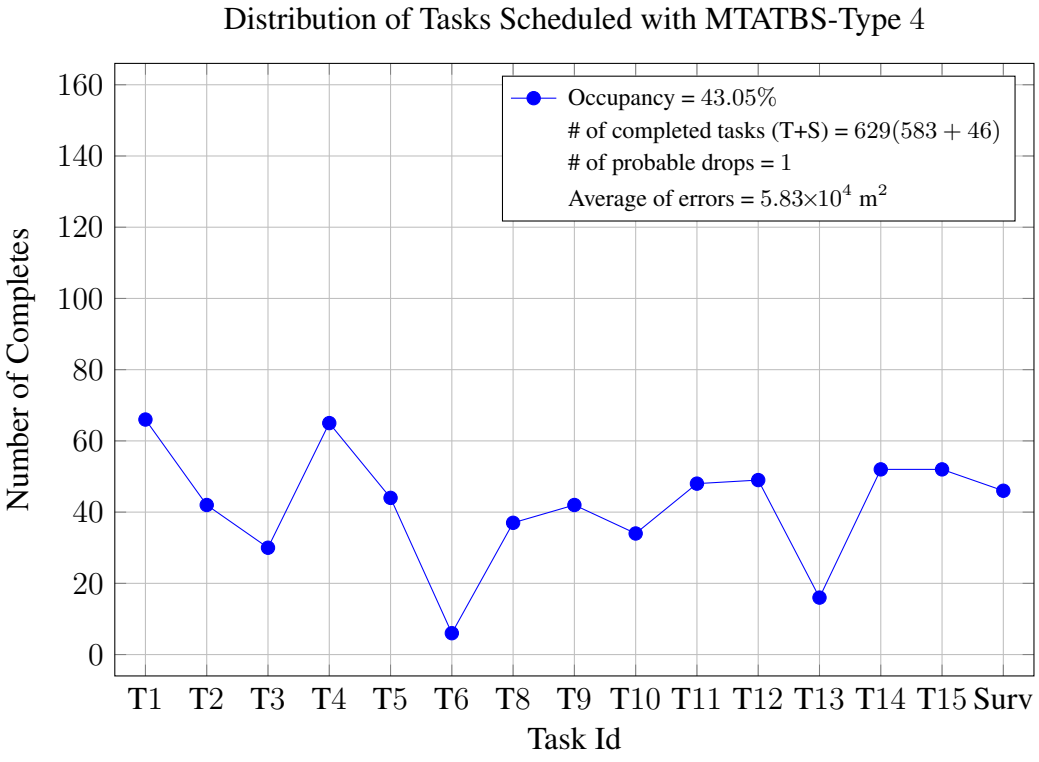

(b) Task interleaving technique is enabled.

Figure 3.20: Distribution of tasks scheduled with MTATBS-Type 4.

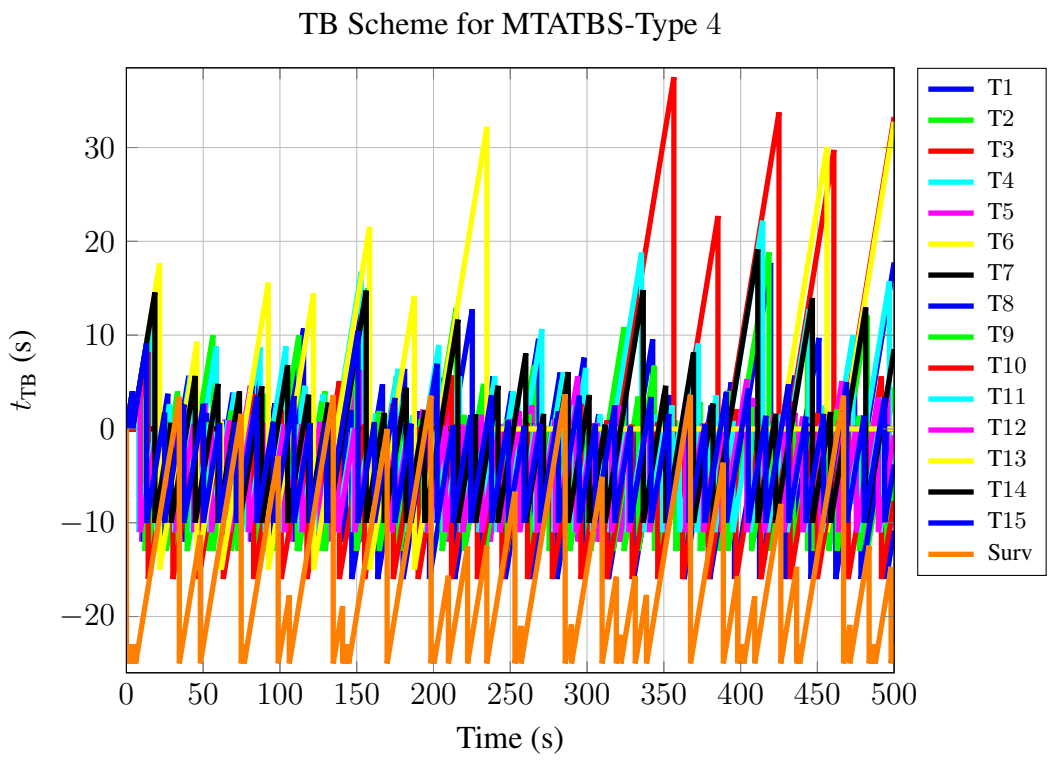

(a) Task interleaving technique is disabled.

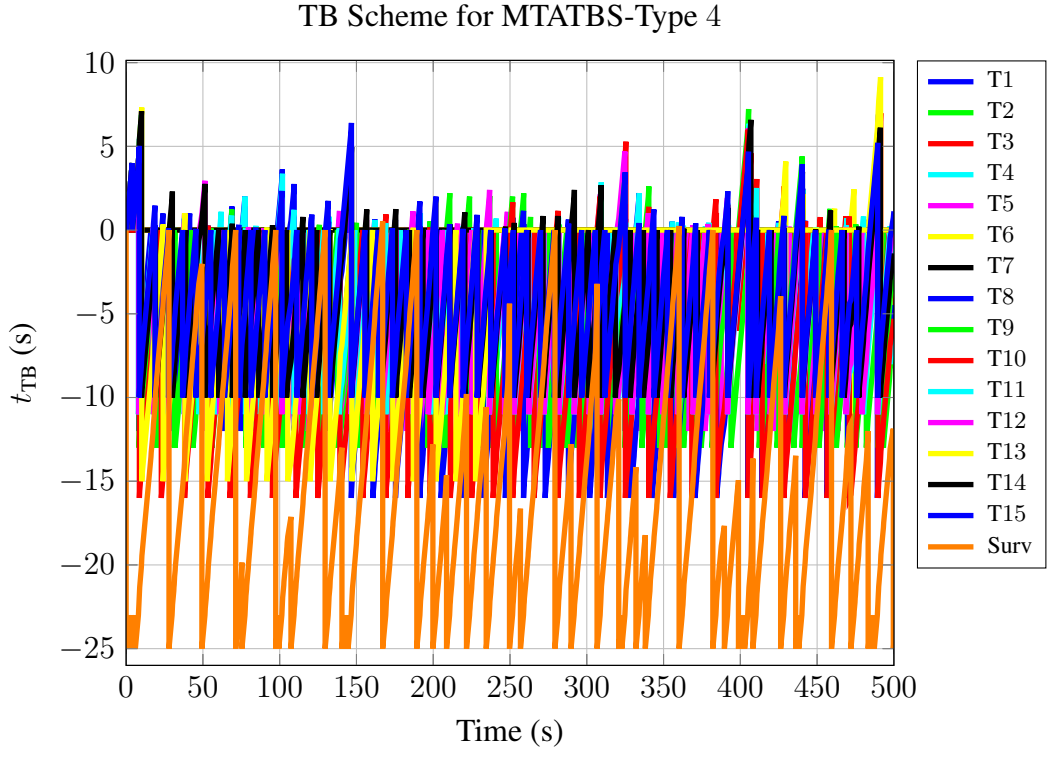

(b) Task interleaving technique is enabled.

Figure 3.21: TB schemes for MTATBS-Type 4.

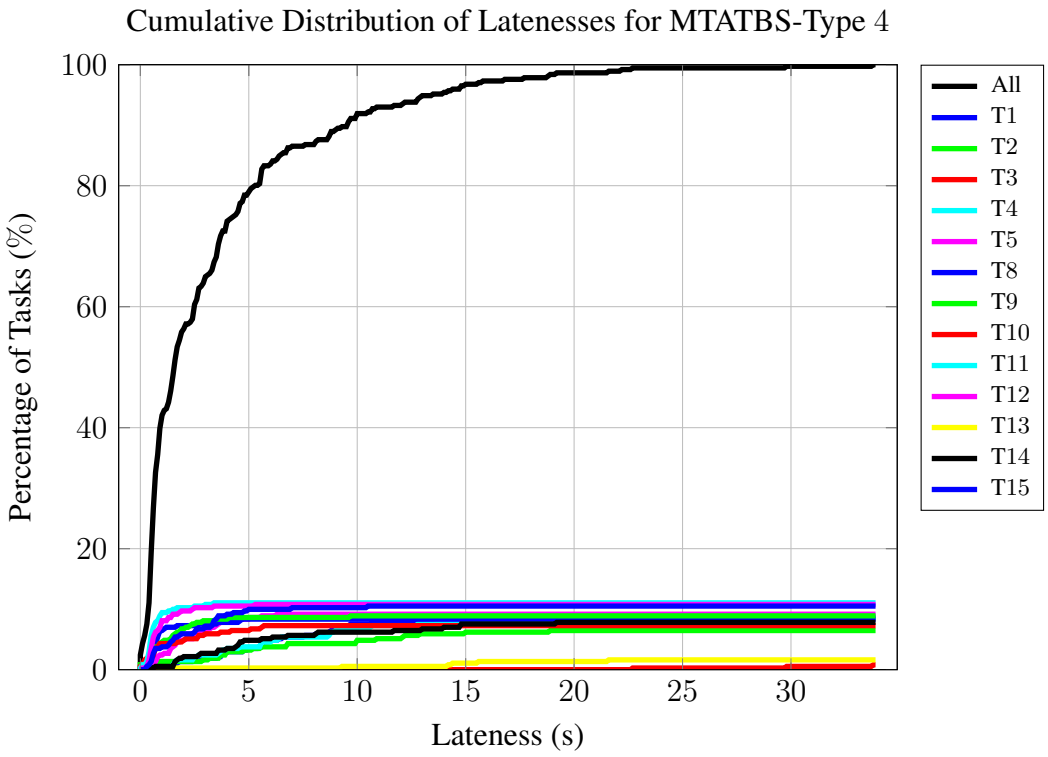

(a) Task interleaving technique is disabled.

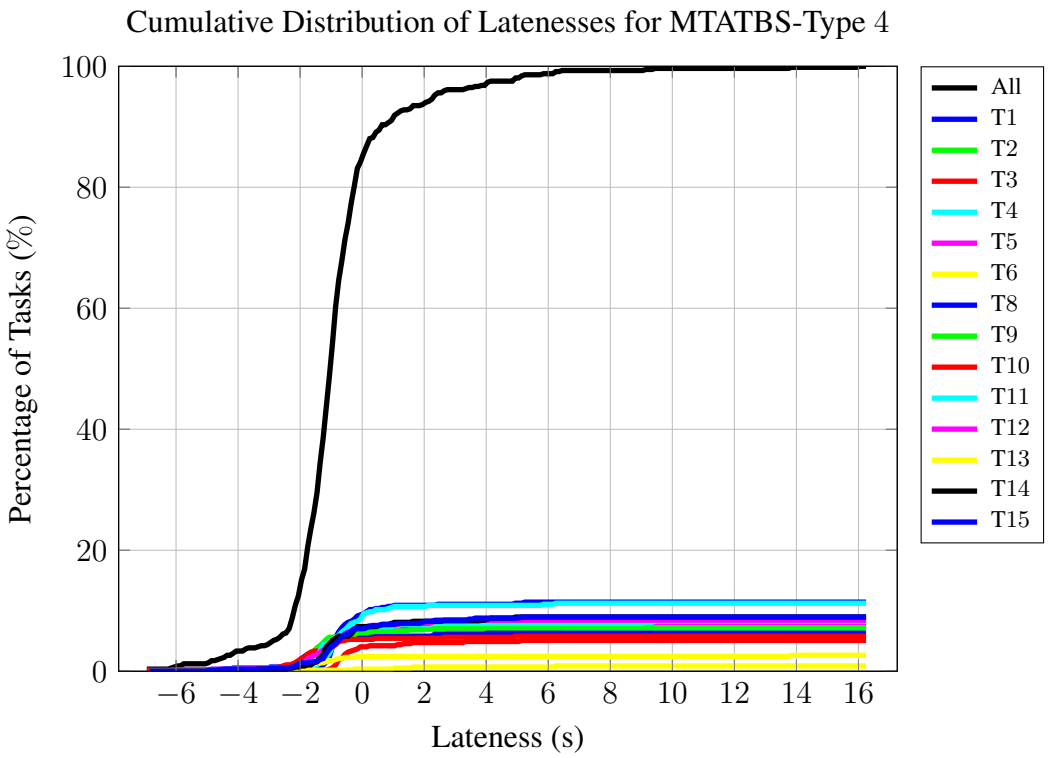

(b) Task interleaving technique is enabled.

Figure 3.22: Cumulative distribution of latenesses for MTATBS-Type 4.

3.2.1.5 Explanation About TB Schemes

As a remark to the readers, it should be interpreted that the dropping directly to zero and not changing after a time level means that the target is dropped at that time. Furthermore constant t_{TB}'s equal to zero shows that the target is out of radar scope. The target 2 and target 6, as shown in Figure 3.23(a), are dropped at ~ 420 and ~ 430 s respectively. The target 1, range of whom is always higher than r_{max} as shown in Figure 3.23(b), is not detected within the simulation interval.

Negative lateness values usually appear, when type 1 and type 2 of MTATBS is utilized. It is the result of t_{TB} update procedure. Decreasing t_{TB} by task update time does not guarantee that the task will not be scheduled for a while that is equal to update time. If it's current t_{TB} is larger than its update time, new t_{TB} after subtraction will already be positive. Therefore the same task may be chosen at the next scheduling cycle. It is very easy to see it from TB scheme shown in Figure 3.23(a). If a task with a t_{TB} starts to decrease monotonically after a few scheduling cycles, the task must have negative lateness values. In the Figure 3.23(a), t_{TB} of target 7 decreased to 0 from ~ 220 between ~ 430 and ~ 480 s. It is the result of frequent scheduling, namely consecutively updating, of target 7, while there is no need to do so. These consecutive updates may be viewed as the waste of sources.

The effect of priorities is revisited by using the type 2 scheduler which is said to schedule only more important tasks. By disabling dynamic task prioritization, the case is emphasized in Figure 3.23(a). The target 5 and target 14 have the priority level 1, when they are detected. Then, the scheduler could not share the radar time resource until ~ 480 s, while target 7 is unnecessarily scheduled. Hence, t_{TB} of less important tasks usually increases monotonically.

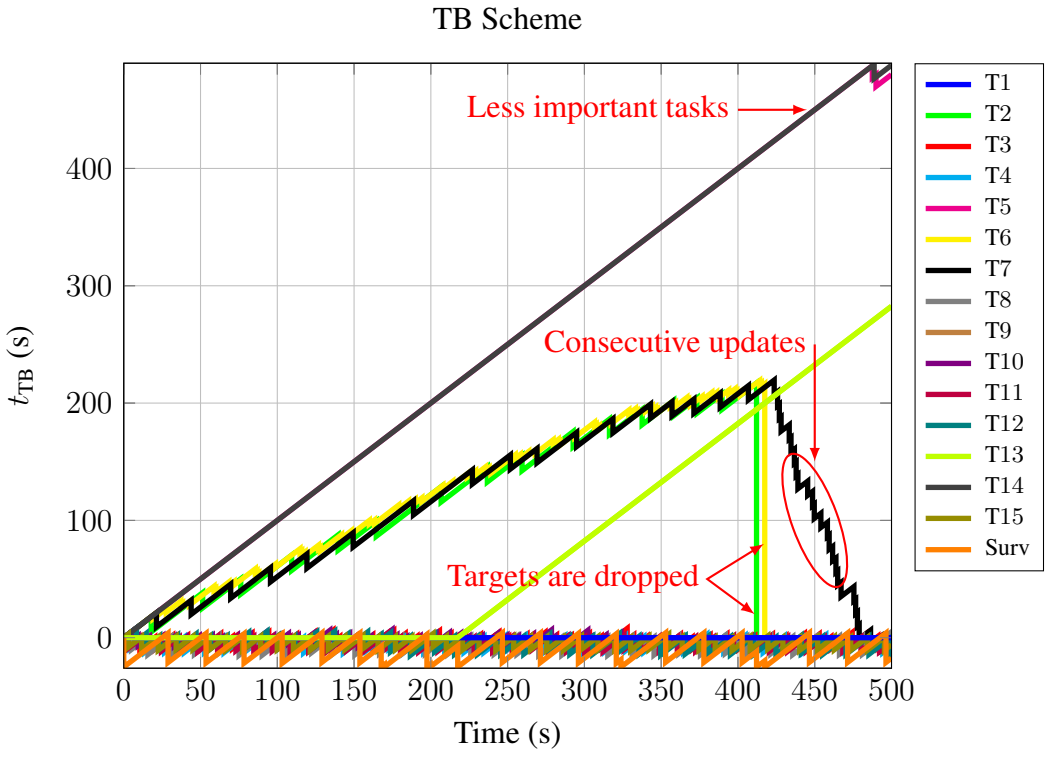

(a) TB scheme.

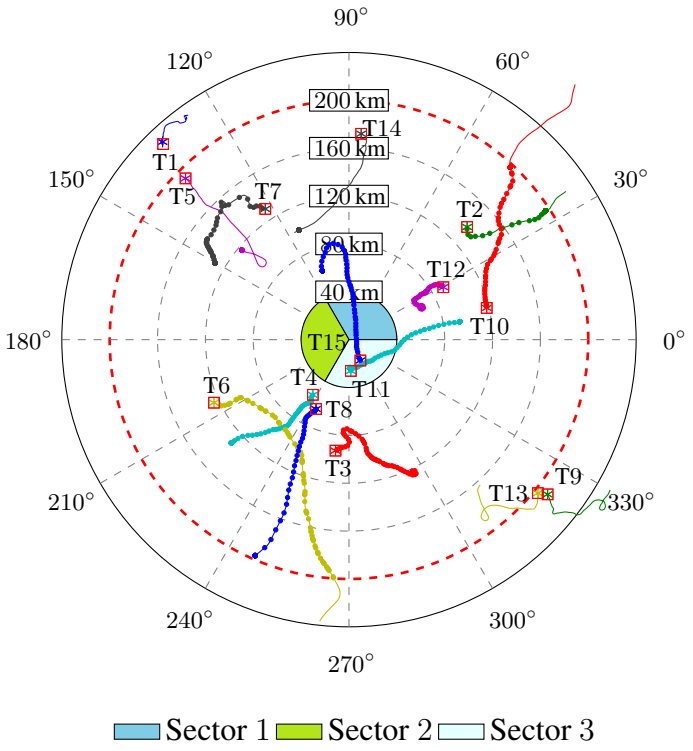

(b) Tracking PPI.

Figure 3.23: Explanation about TB schemes.

3.2.2 Knapsack Scheduler

In combinatorial optimization field, a well-known problem, *knapsack problem*, is studied to make a selection within available items that each item has a value and a weight so that the total value is maximized and the total weight does not exceed the allowed weight for selected items [54]. Its name is thought to come from a problem which usually arises in daily life whenever one wants to pack a suitcase or knapsack with useful objects in a proper way.

The applicability of knapsack problem for financial and industrial applications where resource management is the main concern increases the research on solution methods in many areas, such as applied mathematics, operational research. After the pioneer work [55] that discusses knapsack problem and presents some solution methods for it, there are many algorithms, most of them are described in [56], to solve this problem.

A simple example of knapsack problem is shown in Figure 3.24. Here, there are 4 different gifts and a knapsack for carrying them, but it is allowed to carry a maximum of only 10 kg in knapsack. Thus, the aim is to carry gifts that have maximum total weight less than 10 kg and maximum ratio of total value per total weight.

Since it is a toy example, its solution is too simple with greedy algorithm. Firstly, the ratio of value per weight for each gift is computed as follows:

$$\text{Gift-}1 : \frac{36}{6} = 6, \quad \text{Gift-}2 : \frac{20}{4} = 5, \quad \text{Gift-}3 : \frac{24}{3} = 8, \quad \text{Gift-}4 : \frac{24}{8} = 3.$$

Then, the gift which has the highest ratio, is chosen. After choosing gift-3, gift-1 or gift-2 can be chosen. As gift-1 has higher ratio than gift-2, gift-1 is chosen.

Knapsack scheduler (KS) is built on the solution methods of knapsack problem. The scheduling problem is solved by maximizing the total value of N tracking tasks and the surveillance task. Total value may be referred as the total utility or negative of the total cost for each scheduling epoch. This method only help to select tasks to be processed, while sorting the selected tasks is another problem. Thus, KS uses two-step scheduling method where the first step is *macro scheduler* and the second step is *micro scheduler*, to schedule the tasks. The following sections briefly describe these schedulers.

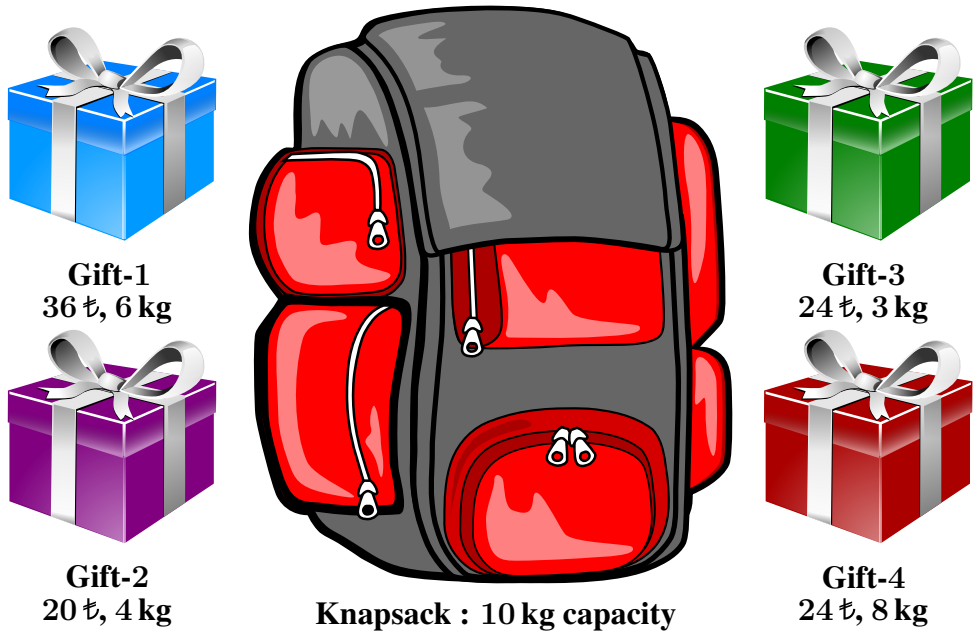

Figure 3.24: Knapsack problem.

3.2.2.1 Macro Scheduler

Macro scheduler determines the set of tasks so that the total value is maximized. Here, value of a task is defined as the utility of scheduling the task. Then, the proposed optimization problem for the first step is

$$\max \sum_{n=1}^{N'} \mathcal{V}_{n,k} x_n, \tag{3.6}$$
$$\text{subject to} \sum_{n=1}^{N'} \mathcal{T}_n x_n \leqslant \mathcal{T}_{interval}, \quad x_n \in \{0,1\}$$

where $N' = N+1$ if surveillance task is not scheduled as a fragmented task, otherwise $N' = N$.

In (3.6), weight, $\mathcal{T}_n$, corresponds to task time of task n and sum of $\mathcal{T}_n$'s for selected tasks must not exceed $\mathcal{T}_{interval}$ which is the time interval of scheduling epoch and is determined as

$$\mathcal{T}_{interval} = \min \{\mathcal{U}_n\}_{n=1}^{N'} . \tag{3.7}$$

Thus, $\mathcal{T}_{interval}$ is chosen as the minimum of the task update times to reduce the probability of target dropping. Assignment of the value of task i, $\mathcal{V}_{i,k}$ at time k, is more complex and it is too crucial to choose the well-defined function for the value. Initial utility value of each tracking task is equal to task priority for detected targets. If target is not detected, its value is assumed to be zero. At the end of each cycle for the first step, the utility of unscheduled targets are increased by their priorities while the utility of scheduled targets are fixed. This process reduces the probability scheduling the same targets in a cascaded order and increases the probability of scheduling previously unscheduled targets.

The macro scheduling problem is solved by using `bintprog` function comes with MATLAB. This function solves the problem by minimizing the total value and hence, the values are assigned as the negative of utilities for simulation.

3.2.2.2 Micro Scheduler

Micro scheduler sorts tasks selected by macro scheduler, according to their priorities, in a way that task with highest priority is sorted as first, to make this step simpler.

There is a trade-off between simplifying micro scheduler and sharing the much of CPU to macro scheduler. Since macro scheduler has more crucial effects on the performance, much of the CPU is reserved for the first step, and sorting process at the second step usually results with too earlier or too later scheduled tasks than optimal. Hence, the number of probable drops is higher.

3.2.2.3 Time-to-Go Value

The time-to-go value is defined for each task that is scheduled at least once. This value stores how much time to left after a scheduling with the micro scheduler. In addition, time-to-go values are directly related to the macro scheduler. If there is a task that has a time-to-go value larger than $\mathcal{T}_{interval}$, the task is not considered for the optimization problem at this level.

3.2.2.4 An Example

The scenario shown in Figure 3.25 is scheduled by KS. Time-to-go scheme is shown in Figure 3.26(a) and value vs. time graph is shown in Figure 3.26(b). The KS always schedules more tracking tasks, as it is sometimes not aware of scheduling surveillance tasks.

The KS is slower than the other types of scheduler. Since increasing the number of detected targets by one, exponentially increases the computation load. Therefore the maximum number of targets must be limited. Furthermore, a modification is to schedule the targets with respect to their sectors is proposed. For example, if there are 30 targets and detection region is bounded by sector 1 and sector 2, KS considers targets in sector 1 ahead to targets in sector 2 by using common $\mathcal{T}_{interval}$. This modification is very useful to schedule more targets in a limited processing time, since scheduling problem is solved among targets in each sector individually.

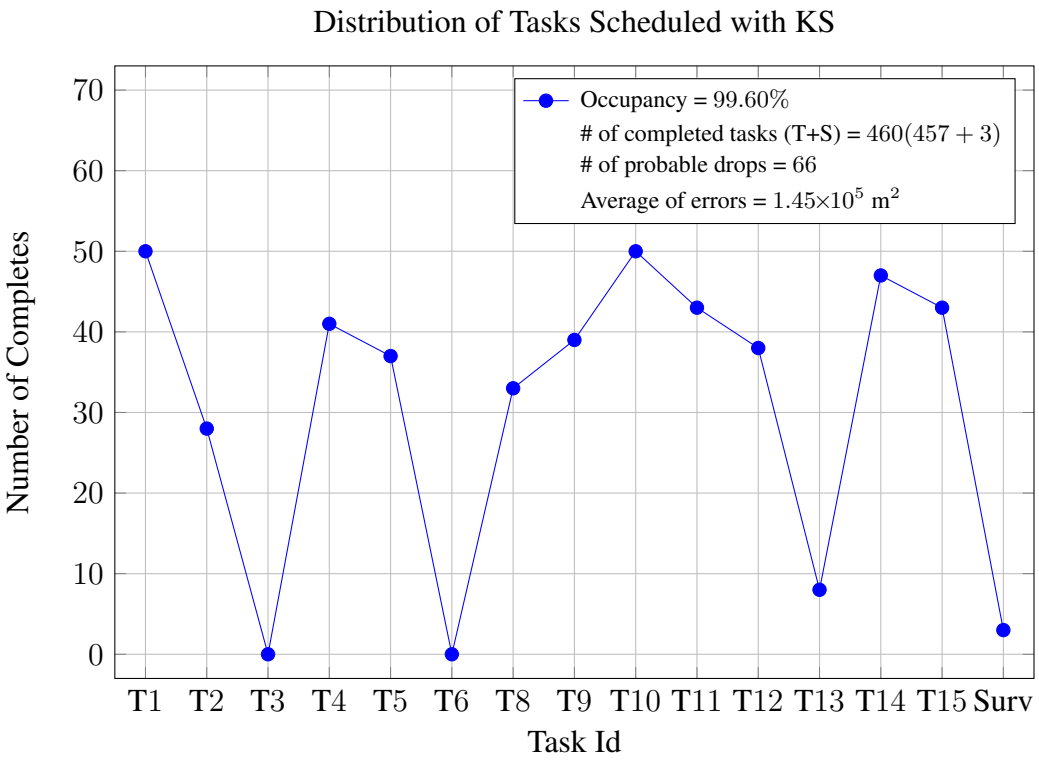

Figure 3.25: Distribution of tasks scheduled with KS.

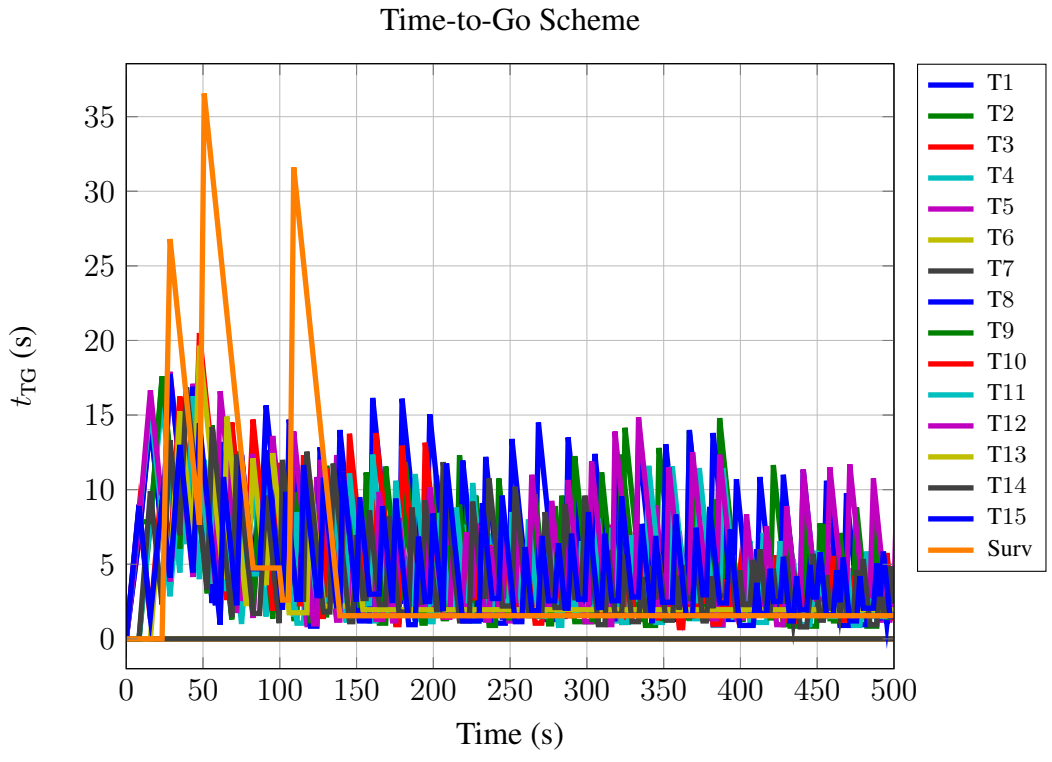

(a)

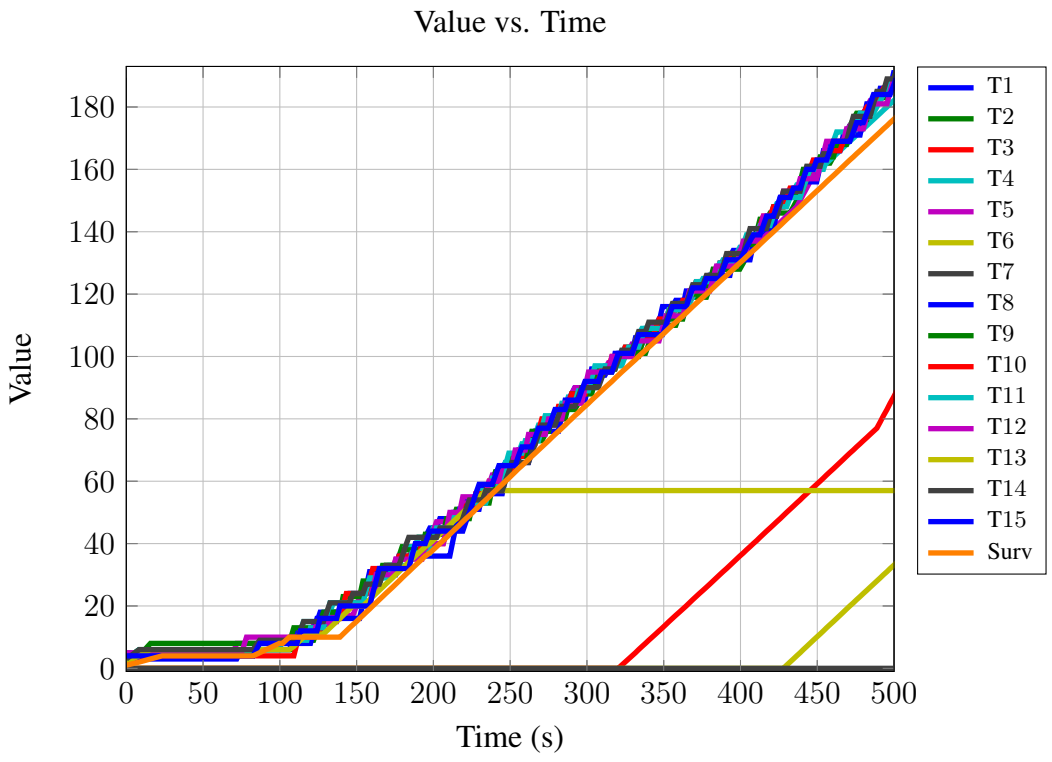

(b)

Figure 3.26: (a) Time-to-Go scheme and (b) value vs. time graph for KS.

3.3 Summary

In this chapter, time-balance technique based schedulers found in [47, 48, 53] are described. Then, a scheduler referred to as MTATBS is proposed. The MTATBS covers the appropriate features of the scheduler described in [48] and handles the optional techniques described in the previous chapter.

In the final part of this chapter, an optimization-based method, KS, utilizing binary integer programming, is proposed to make a comparison with MTATBS, and it is seen that KS is not capable of task interleaving due to computational complexity.

Up to here, MTATBS is not well-defined for target selection, when there are more than one targets which request track update. Hence, the suggested methods for target selection are described in the next chapter.

CHAPTER 4

DECISION METHODS FOR TIME-BALANCE SCHEDULERS

Target selection problem emerges when there are more than one target requesting track update. If MTATBS is forced to make a selection, it firstly selects the targets with the highest priority level. Then, it looks for the targets which have the highest t_{TB} within these targets. If there are more than one target after the second stage, it selects a target which has smaller task id than the others. This target selection procedure is not reliable for the real systems, since task id does not reflect track informations.

In this chapter, the methods to handle the target selection problem are described. To do this, the well-known machine replacement problem is examined. Then, the analogies between target selection and machine replacement problems are emphasized. The method for target selection is adopted from a solution of the machine replacement problem, found in [57], by conducting the analogies and modifications which are related to tracking performance. In addition to this method, two other ad hoc methods which only depend on tracking information are given.

The machine replacement problem is the uncertainty of the time when the existing machine should be replaced. For example, there is only one oven (machine) at a bakery and the bread (product) can be delicious (conforming) or tasteless (defective), if this oven is used. The cooking performance of the oven deteriorates due to aging (deterioration) process, and the oven can be in good or bad state due to its cooking performance. Hence, a delicious bread can be cooked by an oven, state of which is not exactly known. This case is valid, when the bread is tasteless. Therefore it is possible to say that an oven which is in good state can cook a tasteless bread. The cost of a new oven (replacement cost) is too expensive to frequently renew the oven.

Despite the complexity of problem, the baker can estimate the time when the existing oven should be replaced with a new one by utilizing one of the solution methods for the machine replacement problem.

Returning to the target selection problem, a target can be in one of the states, "Good" and "Bad" owing to track quality during the track updates. The target supposed to be in "Good" state tells scheduler that there is no need to update its track at that time, since the update is not necessary, in other words it is a waste of radar time that can be better put into use by doing another task. The target in a "Bad" state alerts the scheduler that it is important to do update the track, since the scheduler knows that the target will be probably dropped for the next scheduling time, if its track is not updated as soon as possible.

It is easily concluded from above that assigning a state to each target helps the scheduler decide which one of the targets currently deserves the track update. Especially, it will be crucial for the scheduler, when the radar is in overloaded case. Executing an unnecessary task may decrease the tracking performance by causing an increase in the delay of other tasks in the queue. Therefore the state dependent target selection is crucial for both of cases, while the main goal of the state assignment is to deal with overloaded case.

4.1 Method of Decision Policy

The RRM problem is examined in analogy with machine replacement problem. The machine replacement, machine maintenance and quality control applications are widely popular in decision making literature. The discussed method is adopted from [57] that analyzes the binomial observation model for machine replacement problem. The binomial observation is the classification of the quality of products as *conforming units* or *defecting units* according to measurements while production process is in either "Good" or "Bad" state. True state of the process is assumed to be unobservable and only the measured quality of the produced units gives the tips about the true state which the process is most likely to be in. Thus, the production process is modeled as a partially observable Markov decision process (POMDP) with control limits.

The most interesting part of [57] is the proof for that the infinite-horizon control limit which is defined as a function of probability of obtaining conforming unit can be calculated by solving a finite set of linear equations. Because POMDPs are known to be usually hard to solve due to prohibitively large size of the state space [58]. It is also known that the length of time horizon effects the tractability of the problem, i.e. a 5-horizon problem is harder than 2-horizon problem.

One-to-one adoption from the machine replacement problem to the target selection problem of RRM is really hard. Because procedures of the referred machine replacement problem consider only one machine. In addition, cost of renewing the machine is fixed and decision making policy can become a degenerate policy, such as always *continue with the same machine* when chosen cost value makes the other action, *replace the machine* the worst selection for infinite-horizon case.

In the case of target selection problem, there are many targets and each target is thought to represent a single machine. At each instant of decision making, only one target can be chosen to update its track. Therefore decision making process specifies targets that need track update, and then it selects one of them which improves at most of the tracking performance of radar.

Another difficulty is to specify the cost value associated with each target. At each instant, the scheduler can choose only one of available targets to update its track. Thus, it would be almost impossible to define cost value of each target as independent from the other targets.

Furthermore, it is necessary to explain how to obtain "Good" or "Bad" state information. To do so, IMM algorithm in Appendix A, is utilized through advantage of providing mode-probabilities. Mode-probabilities tell tracker how motion model of moving targets is distributed at each instant. For example, it is given that there are 2 motion models which obey the constant velocity model (CV) with different process noise covariances, $\mathbf{Q}^1$ and $\mathbf{Q}^2$. There is a relation between these covariances as follows:

$$\mathbf{Q}^2 = 100^2\mathbf{Q}^1.$$

Hence, the model-1 with $\mathbf{Q}^1$ indicates non-maneuvering motion and the model-2 with $\mathbf{Q}^2$ indicates maneuvering motion. If the mode-probabilities are distributed as 0.7

and 0.3 for model-1 and model-2 respectively, tracker presumes that the target is not probably maneuvering. For both the tracker and scheduler, the main concern is to know that the target is maneuvering or not maneuvering. Owing to this knowledge, the tracker can predict tracks of a target with less error for an interval when there is not any measurement provided, and the scheduler can mostly concentrate on to schedule tracking tasks of highly maneuvering targets to enhance the tracking performance.

Radar plan position indicator (PPI) displays taken from a simple scenario are shown in Figure 4.1(a) belongs one of less maneuvering targets and Figure 4.1(b) belongs one of highly maneuvering targets. These figures are given only to make clear why the classification of targets as maneuvering and non-maneuvering is required. Therefore it is not necessary to give the complete scenario with parameters at this point. The tracking task of each target is competing for radar time and there is not a decision method which classifies the target as maneuvering or non-maneuvering. Hence, the scheduler selects a target which has smaller task id than the others, when there is a target selection problem. Then confidence ellipses shown on the displays point out how well the tracker predicts positions of moving targets. Larger ellipses indicate worse predictions and smaller ellipses indicate better predictions. Therefore it is easily deduced that maneuvering targets cause worse predictions.

In this manner, a target classified as non-maneuvering, is indicated to be in Good state and a target classified as maneuvering, is indicated to be in Bad state. As mentioned before, the probability of being in Good state is defined to be equal to mode-probability of motion model-1 with $\mathbf{Q}^1$ provided by IMM estimator.

The decision making process for updating a target track requires to observe (measure) the quality of target track. The track is referred to as *good track* when trace of tracking error covariance is within the allowed values. Otherwise it is referred to as *bad track*. Then, the conditional observation probabilities are

- θ_0, the probability of obtaining a good track given that corresponding target is in Good state,
- θ_1, the probability of obtaining a good track given that corresponding target is in Bad state,

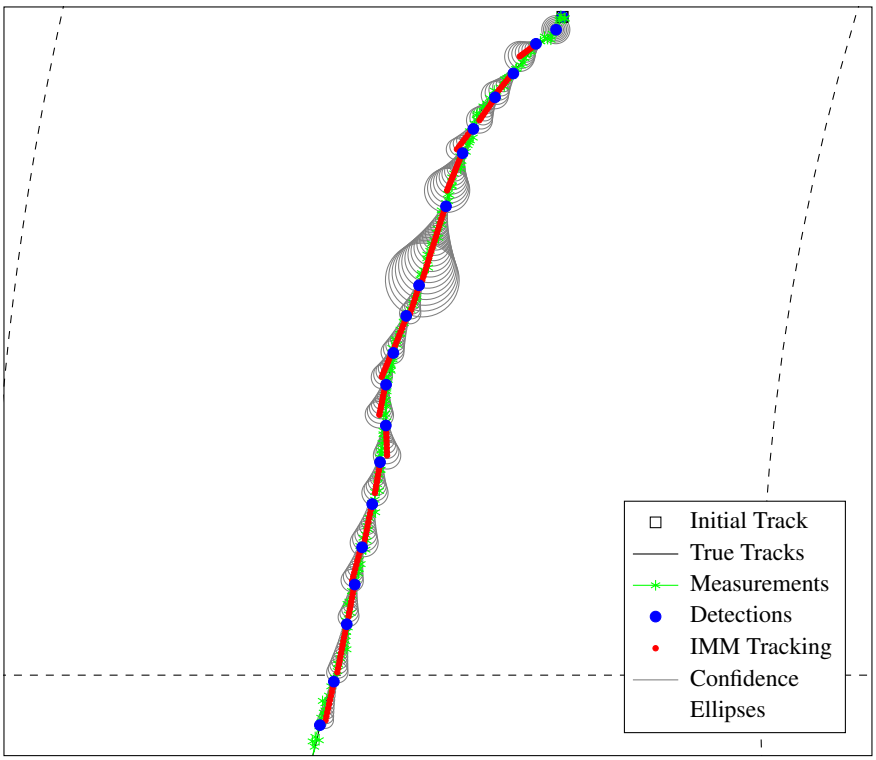

(a)

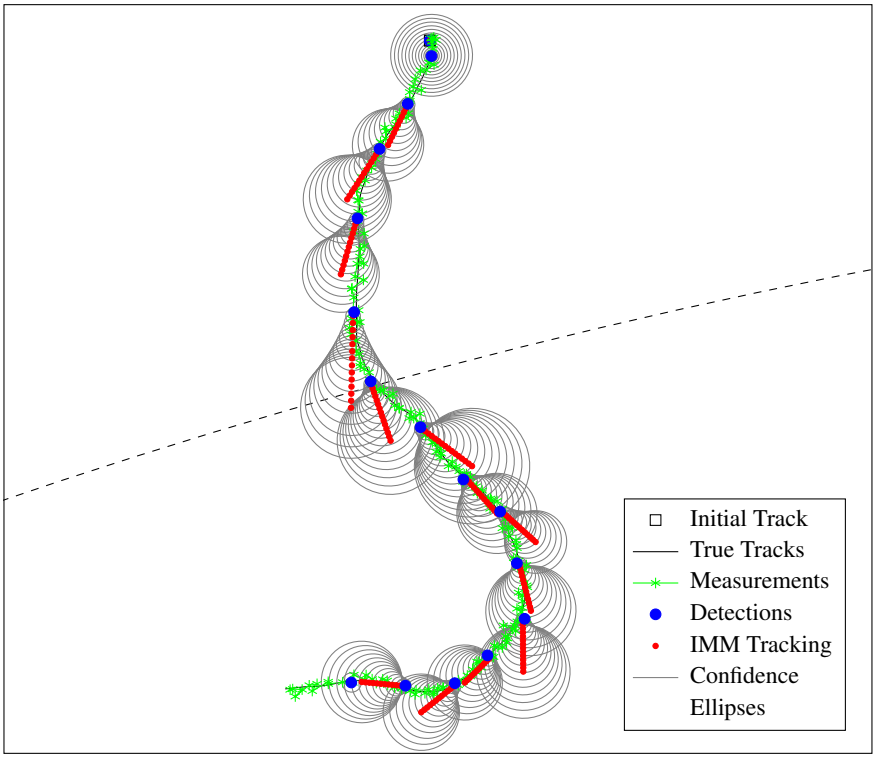

(b)

Figure 4.1: Tracking example of (a) non-maneuvering and (b) maneuvering targets.

- $1 - \theta_0$, the probability of obtaining a bad track given that corresponding target is in Good state,

- $1 - \theta_1$, the probability of obtaining a bad track given that corresponding target is in Bad state,

and it is assumed that $\theta_0 > \theta_1$ due to reliability on measurement process.

The state of a target is probabilistically evolving, such that if the target is in Good state at time k, it will be in Good state with probability r or it will change its state to Bad with probability $1 - r$ at time $k + 1$. Once the target enters Bad state, it is assumed to remain that state until its track is updated. The last sentence can be a bit confusing, since it claims that if a target start maneuvering, the target will continue maneuvering until a track update. In real world, the targets perform maneuvering in a random order so that they try to decrease the probability of being tracked.

If a target supposed to maneuver, its bearing (or azimuth) angle will start to change with higher deviation which cannot be tolerated by prediction. Seeing Figure 4.1(b), IMM tracking points are not compatible with the true tracks at the points where target performs maneuvering and prediction error grows up until a measurement is taken at detection points. Once a target enters to Bad state, it is assumed to stay there until radar takes a measurement. Thus, the case is summarized with the last statement.

Actions are UPD (update) and NUPD (not update) for the decision making process to update a target track. UPD action is similar to *replace the machine* action comes with a cost $\mathcal{K}$ that will be explained later. Again, UPD action may fail to guarantee that a target will be absolutely in Good state after applying the action. The target will be in Good state with probability q after taking the UPD action.

If NUPD action is taken, the transition of target states becomes a time-homogeneous Markov chain with Good state, a transient state, and Bad state, an absorbing state. Because NUPD action is similar to *continue with the same machine* action does nothing to change the process environment and the states only change due to evolving of the process.

In the following sections, the detailed description is presented for this scheme.

4.1.1 Problem Model

It is supposed that there are N_k targets at time k. Hence, there are N_k distinct Markov chains corresponding to each target, and the state transition probabilities of each target are independent.

Target n obeys a 2-state Markov chain with the following descriptions.

- State is $x_k^n \in \{1, 2\}$, where 1 denotes Good state and 2 denotes Bad state, with initial probability $P(x_0^n = i) = 0.5$ for $i = 1, 2$.
- Observation is $y_k^n \in \{gt, bt\}$, where gt denotes good track and bt denotes bad track.
- Action is $u_k^n \in \{0, 1\}$, where 0 denotes NUPD action and 1 denotes UPD action,

at time k for $n = 1, 2, \ldots, N_k$.

The transition probability matrices are

$$P(0) = \begin{bmatrix} r & 1-r \\ 0 & 1 \end{bmatrix} \text{ and } P(1) = \begin{bmatrix} q & 1-q \\ q & 1-q \end{bmatrix}, \tag{4.1}$$

where $r = P(x_{k+1}^n = 1 | x_k^n = 1, u_k^n = 0)$ and $q = P(x_{k+1}^n = 1 | x_k^n, u_k^n = 1)$ are the transition probabilities by taking NUPD and UPD actions respectively.

Markov chains are shown in Figure 4.2 for NUPD and UPD actions.

Taking NUPD action, state-1 represents a transient state and state-2 represents an absorbing state, shown in Figure 4.2(a) for $r \in (0, 1)$. Taking UPD action, both

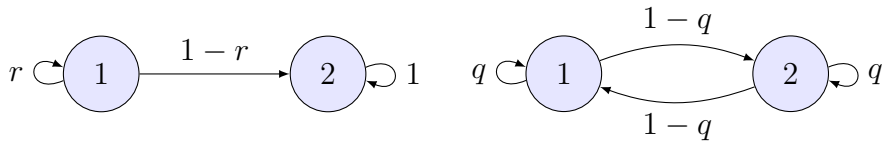

(a) $u_k^n = 0$ (b) $u_k^n = 1$

Figure 4.2: Markov chains for (a) NUPD and (b) UPD actions.

state-1 and state-2 become transient state, as shown in Figure 4.2(b), unless q is not assumed to be equal to 1 which claims the target is exactly in state-1 after UPD action.

Regarding to descriptions, the conditional observation probabilities previously stated are expressed as follows:

$$P(y_k^n = gt | x_k^n = 1) = \theta_0, \tag{4.2}$$

$$P(y_k^n = gt | x_k^n = 2) = \theta_1, \tag{4.3}$$

$$P(y_k^n = bt | x_k^n = 1) = 1 - \theta_0, \tag{4.4}$$

$$P(y_k^n = bt | x_k^n = 2) = 1 - \theta_1. \tag{4.5}$$

All of the variables essential to model the problem are briefly presented. In the next section, they are utilized to derive expressions for solving the problem.

4.1.2 Derivation of Required Expressions

It is important to remember that all derivations are originated to [57] and the idea is given in the same order as in referred work, while notations are changed and additional details are given to make explanation clearer.

Original notation is not sufficient to denote target id and time information. Hence a time term, k, and target id term, n, are inserted as subscript and superscript respectively wherever they are required. Functions which depend on observations are denoted with the observation term inserted as a subscript to a calligraphic letter.

Starting with the mostly used function, the probability of being in Good state is

$$\mu_k^n = P(x_k^n = 1), \tag{4.6}$$

where the symbol, μ is chosen to remind that probability of being in Good state is directly related to mode-probability provided by IMM estimator.

Then, the probability of observing good track is

$$P(y_k^n = gt) = \sum_{i=1}^{2} P(y_k^n = gt | x_k^n = i) P(x_k^n = i), \tag{4.7}$$

$$= \theta_0 \mu_k^n + \theta_1 (1 - \mu_k^n),$$

$$= (\theta_0 - \theta_1)\mu_k^n + \theta_1. \tag{4.8}$$

Similarly, the probability of observing bad track is

$$P(y_k^n = bt) = \sum_{i=1}^{2} P(y_k^n = bt | x_k^n = i) P(x_k^n = i), \tag{4.9}$$

$$= (1 - \theta_0)\mu_k^n + (1 - \theta_1)(1 - \mu_k^n),$$

$$= 1 - (\theta_0 - \theta_1)\mu_k^n - \theta_1, \tag{4.10}$$

$$= 1 - P(y_k^n = gt). \tag{4.11}$$

Hereafter, the observation probabilities expressed in (4.8) and (4.10) are defined as a functions of μ_k^n, since the only time-variant variable is μ_k^n while θ_0 and θ_1 are depicted as constants. The observation probabilities are

$$\mathcal{P}_{gt}(\mu_k^n) \triangleq P(y_k^n = gt), \tag{4.12}$$

$$= (\theta_0 - \theta_1)\mu_k^n + \theta_1, \tag{4.13}$$

$$\mathcal{P}_{bt}(\mu_k^n) \triangleq P(y_k^n = bt), \tag{4.14}$$

$$= 1 - (\theta_0 - \theta_1)\mu_k^n - \theta_1. \tag{4.15}$$

By applying Bayes' theorem, the posterior probabilities for Good state are given

$$P(x_k^n = 1 | y_k^n = gt) = \frac{P(y_k^n = gt | x_k^n = 1) P(x_k^n = 1)}{P(y_k^n = gt)}, \tag{4.16}$$

$$= \frac{\theta_0 \mu_k^n}{\mathcal{P}_{gt}(\mu_k^n)}, \tag{4.17}$$

$$P(x_k^n = 1 | y_k^n = bt) = \frac{P(y_k^n = bt | x_k^n = 1) P(x_k^n = 1)}{P(y_k^n = bt)}, \tag{4.18}$$

$$= \frac{(1 - \theta_0)\mu_k^n}{\mathcal{P}_{bt}(\mu_k^n)}. \tag{4.19}$$

The probability of being in Good state given that good track is observed and the probability of being in Good state given that bad track is observed are given in (4.17) and (4.19) respectively.

Using Markov property, it is assumed x_{k+1}^n is conditionally independent of y_k^n [59] so that the conditional probability of the next state is j given that gt is observed and NUPD action is taken in the current state is i, can be written as

$$P(x_{k+1}^n = j | x_k^n = i, y_k^n = gt, u_k^n = 0) = P(x_{k+1}^n = j | x_k^n = i, u_k^n = 0), \tag{4.20}$$

$$= P_{ij}(u_k^n), \tag{4.21}$$

where $i, j = 1, 2$.

The posterior probabilities of the current state at time k are expressed in (4.17) and (4.19). Furthermore, it is better to get information about the next state. By using these expressions and the law of total probability, the conditional probabilities of the next state are obtained. The probability of being in Good state at next time given that good track is observed and NUPD action is taken at current time is

$$P(x_{k+1}^n = 1 | y_k^n = gt, u_k^n = 0) = \sum_{i=1}^{2} P(x_{k+1}^n = 1, x_k^n = i | y_k^n = gt, u_k^n = 0), \tag{4.22}$$

$$= \sum_{i=1}^{2} P(x_{k+1}^n = 1 | x_k^n = i, y_k^n = gt, u_k^n = 0) \\ P(x_k^n = i | y_k^n = gt, u_k^n = 0),$$

$$= \sum_{i=1}^{2} P_{i1}(u_k^n) P(x_k^n = i | y_k^n = gt),$$

$$= r \cdot P(x_k^n = 1 | y_k^n = gt) \\ + 0 \cdot P(x_k^n = 2 | y_k^n = gt), \tag{4.23}$$

$$= \frac{r\theta_0 \mu_k^n}{\mathcal{P}_{gt}(\mu_k^n)}, \tag{4.24}$$

and the probability of being in Good state at next time given that bad track is observed and NUPD action is taken at current time is

$$P(x_{k+1}^n = 1|y_k^n = bt, u_k^n = 0) = \sum_{i=1}^{2} P(x_{k+1}^n = 1, x_k^n = i|y_k^n = bt, u_k^n = 0), \quad (4.25)$$

$$= \sum_{i=1}^{2} P(x_{k+1}^n = 1|x_k^n = i, y_k^n = bt, u_k^n = 0)$$
$$P(x_k^n = i|y_k^n = bt, u_k^n = 0),$$

$$= \sum_{i=1}^{2} P_{i1}(u_k^n) P(x_k^n = i|y_k^n = bt),$$

$$= r \cdot P(x_k^n = 1|y_k^n = bt)$$
$$+ 0 \cdot P(x_k^n = 2|y_k^n = bt), \quad (4.26)$$

$$= \frac{r(1-\theta_0)\mu_k^n}{\mathcal{P}_{bt}(\mu_k^n)}. \quad (4.27)$$

Similarly, the conditional probabilities given in (4.24) and (4.27) are defined as a functions of μ_k^n, since the only time-variant variable is μ_k^n while θ_0 and θ_1 are constants. The conditional probabilities are

$$\mathcal{H}_{gt}(\mu_k^n) \triangleq P(x_{k+1}^n = 1|y_k^n = gt, u_k^n = 0), \quad (4.28)$$

$$= \frac{r\theta_0\mu_k^n}{(\theta_0 - \theta_1)\mu_k^n + \theta_1}, \quad (4.29)$$

$$\mathcal{H}_{bt}(\mu_k^n) \triangleq P(x_{k+1}^n = 1|y_k^n = bt, u_k^n = 0), \quad (4.30)$$

$$= \frac{r(1-\theta_0)\mu_k^n}{1 - (\theta_0 - \theta_1)\mu_k^n - \theta_1}. \quad (4.31)$$

Lemma 1. *Both $\mathcal{H}_{gt}(\mu_k^n)$ and $\mathcal{H}_{bt}(\mu_k^n)$ are continuous and strictly increasing functions for $0 < \mu_k^n < 1$. Moreover, inverse functions $\mathcal{H}_{gt}^{-1}(\mu_k^n)$ of $\mathcal{H}_{gt}(\mu_k^n)$ and $\mathcal{H}_{bt}^{-1}(\mu_k^n)$ of $\mathcal{H}_{bt}(\mu_k^n)$ exist, and they are strictly increasing for $0 < \mu_k^n < r$.*

Lemma 2. *$\mathcal{H}_{gt}(\mu_k^n)$ is strictly concave and $\mathcal{H}_{bt}(\mu_k^n)$ is strictly convex for $0 < \mu_k^n < 1$.*

Lemma 1 and Lemma 2, proofs of whom can be found in Appendix B, are taken from [58]. According to Lemma 1, the inverse function $\mathcal{H}_{bt}^{-1}(\mu_k^n)$ is

$$\mathcal{H}_{bt}^{-1}(\mu_k^n) = \frac{(1-\theta_1)\mu_k^n}{(\theta_0 - \theta_1)\mu_k^n + (1-\theta_0)r} \quad (4.32)$$

for $0 < \mu_k^n < r$. Furthermore, existence of inverse leads to utilize function composition, such that

$$\mathcal{H}_{bt}\left(\mathcal{H}_{bt}^{-1}(\mu_k^n)\right) = \mu_k^n.$$

Then, a notation can be used

$$\mathcal{H}_{bt}^{\ell}(\mu_k^n) = \mathcal{H}_{bt}\left(\mathcal{H}_{bt}^{\ell-1}(\mu_k^n)\right) \text{ or } \mathcal{H}_{bt}^{-\ell}(\mu_k^n) = \mathcal{H}_{bt}^{-1}\left(\mathcal{H}_{bt}^{-\ell+1}(\mu_k^n)\right)$$

for $\ell \in \mathbb{Z}^+$ and it may be necessary to remind that

$$\mathcal{H}_{bt}^{0}(\mu_k^n) = \mathcal{H}_{bt}\left(\mathcal{H}_{bt}^{-1}(\mu_k^n)\right) = \mu_k^n.$$

The functions $\mathcal{H}_{gt}(\mu_k^n)$ and $\mathcal{H}_{bt}(\mu_k^n)$ depend on fixed parameters, r, θ_0 and θ_1 as well. The critical point for choosing the fixed parameters is to ensure the criteria, $r\theta_0 > \theta_1$, so that $\mathcal{H}_{gt}(\mu^*) = \mu^*$ does exist. The value of μ^* is computed as

$$\mu^* = \frac{r\theta_0 - \theta_1}{\theta_0 - \theta_1}. \tag{4.33}$$

The point, μ^*, divides the domain of μ_k^n into 2 sub-domains, $\mu^* < \mathcal{H}_{gt}(\mu_k^n) < \mu_k^n$ for $\mu_k^n > \mu^*$ and $\mathcal{H}_{gt}(\mu_k^n) > \mu_k^n$ for $0 < \mu_k^n < \mu^*$. If $r\theta_0 \leqslant \theta_1$, then $0 < \mathcal{H}_{gt}(\mu_k^n) < \mu_k^n$ for $0 < \mu_k^n \leqslant 1$, and hence, $\mathcal{H}_{gt}(\mu^*) = \mu^*$ does not exist.

Figure 4.3 illustrates both of these conditions for the functions $\mathcal{H}_{gt}(\mu_k^n)$ and $\mathcal{H}_{bt}(\mu_k^n)$. The first condition, $r\theta_0 > \theta_1$, is satisfied with $r = 0.8$, $\theta_0 = 0.9$ and $\theta_1 = 0.4$, as shown in Figure 4.3(a). The value of μ^* is computed as 0.64 by using (4.33). According to this value, it is concluded that if the probability of being in Good state is less than 0.64, then the probability of being in Good state at next time increases by observing good track at current time. Or vice versa, if the probability of being in Good state is greater than 0.64, then the probability of being in Good state at next time decreases by observing good track at current time. The second condition, $r\theta_0 < \theta_1$, is satisfied with $r = 0.6$, $\theta_0 = 0.6$ and $\theta_1 = 0.4$, as shown in Figure 4.3(b). Here, the linear function μ_k^n does not intersect $\mathcal{H}_{gt}(\mu_k^n)$ at any point for $\mu_k^n > 0$. Therefore the probability of being in Good state at next time always decreases by observing good track at current time. Then, observations become less valuable to give an idea about the probability of being in Good state.

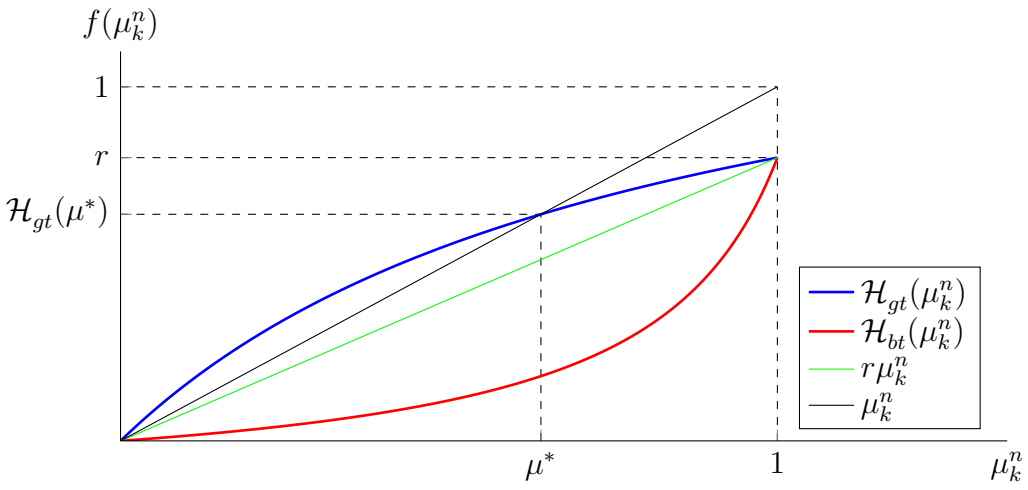

(a) $r\theta_0 > \theta_1$, where $r = 0.8$, $\theta_0 = 0.9$ and $\theta_1 = 0.4$.

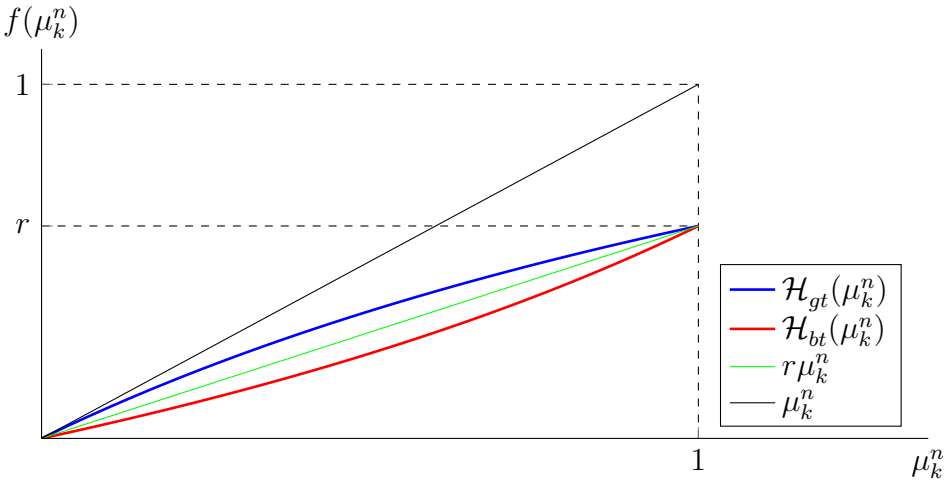

(b) $r\theta_0 < \theta_1$, where $r = 0.6$, $\theta_0 = 0.6$ and $\theta_1 = 0.4$.

Figure 4.3: $\mathcal{H}_{gt}(\mu_k^n)$ and $\mathcal{H}_{bt}(\mu_k^n)$ functions.

Flow diagram summarizes the descriptions explained up to now, as shown in Figure 4.4. The flow diagram has branches, that blue branches imply the observation probabilities, such that $\mathcal{P}_{gt}(\mu_k^n) = \sum_{i=1}^{2} P(y_k^n = gt|x_k^n = i)P(x_k^n = i)$ and black branches imply the conditional probabilities, such that $P(y_k^n = gt|x_k^n = 2) = \theta_1$, $\mathcal{H}_{gt}(\mu_k^n) = P(x_{k+1}^n = 1|y_k^n = gt, u_k^n = 0)$. Knowing the distribution of current state, i.e. $P(x_k^n = 1) = \mu_k^n$, observation probabilities can be computed via conditional observation probabilities.

Most of basic knowledge required for solving the problem has been given, and the next section describes the target-based cost parameter.

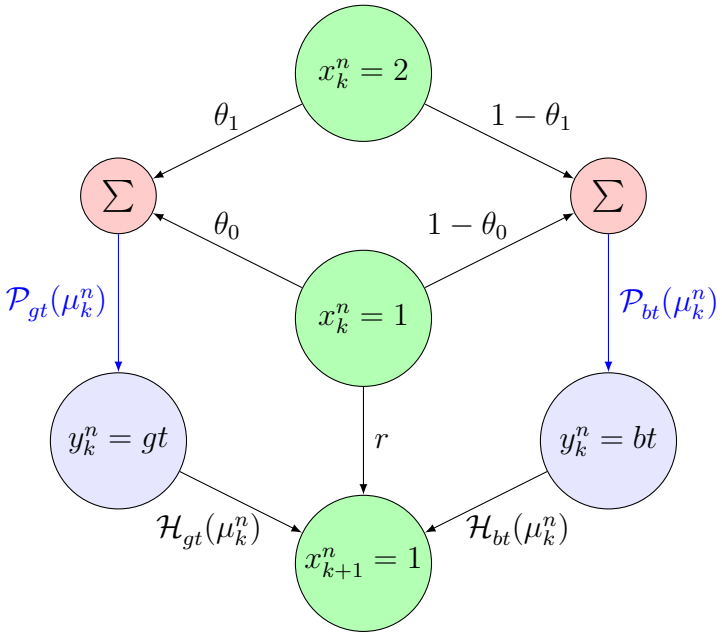

Figure 4.4: Flow diagram for $u_k^n = 0$.

4.1.3 Cost Parameter

The main concern for specifying the cost parameter is to differ the targets that really improve the overall tracking performance. The decisions, which are only made according to either track update time using a time dependent cost parameter or priority assignment using a priority dependent cost parameter, could not classify the targets as maneuvering or non-maneuvering. Then, the system may be too late to notice that a target needs a track update after each maneuver. As a result, tracking performance usually decreases. If there was a cost parameter to help the system to deal with that case, it would be very useful and widely used.

The same scenario previously shown in Figure 4.1 is revisited to uncover the importance of cost parameters. Maneuvers of targets in 2-D space is graphically shown in that figure with confidence ellipses which indicate the tracking performance and are directly related to tracking error covariance. Then, it is time to see the effect of maneuvering numerically via the plots shown in Figure 4.5.

Owing to non-maneuvering target shown in Figure 4.5(a) and maneuvering target shown in Figure 4.5(b), average of the trace of tracking error covariance is smaller

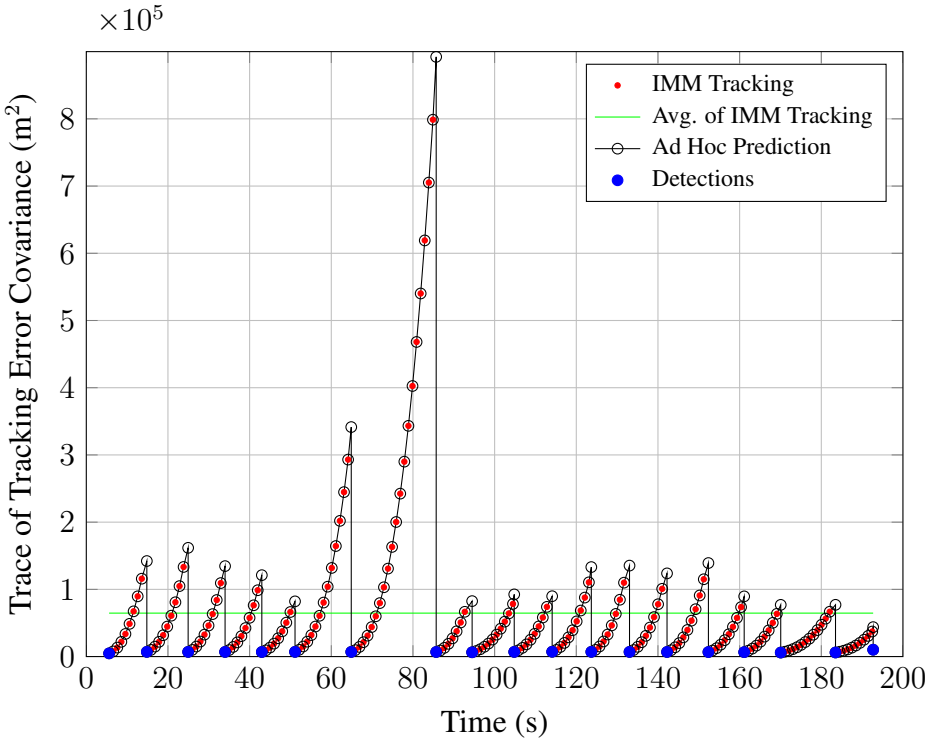

(a)

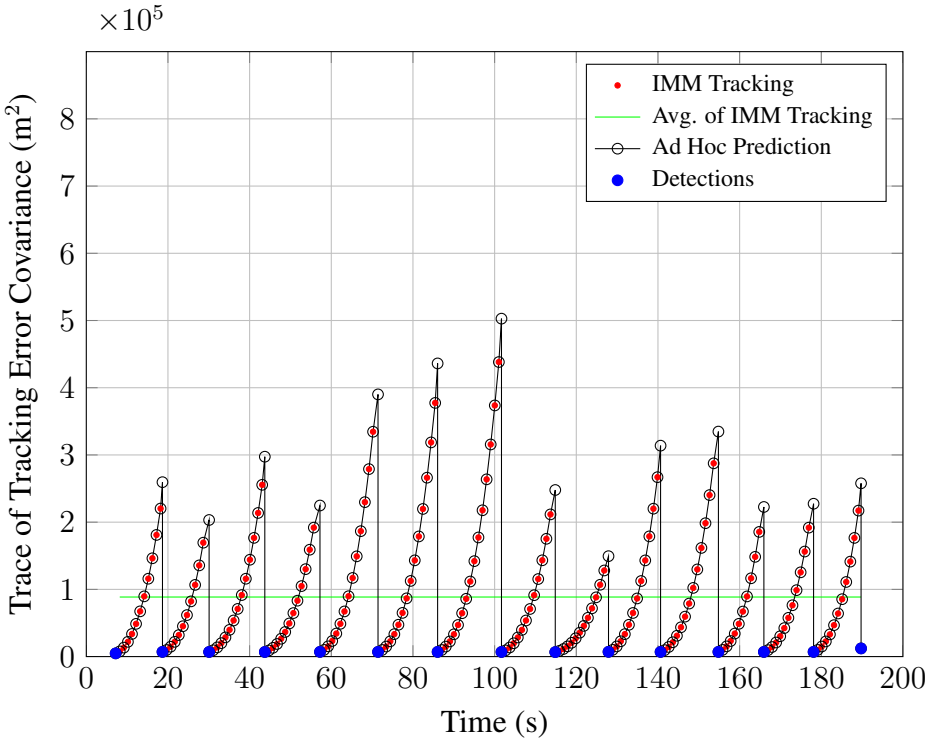

(b)

Figure 4.5: Tracking error covariance example for (a) non-maneuvering target and (b) maneuvering target.

for non-maneuvering target. Then, it is deduced that the overall tracking performance is better for non-maneuvering target, as it is expected.

It is shown in Figure 4.5(a), non-maneuvering target is almost precisely tracked except between $60 - 85$ s and the target gets the highest tracking error, $\sim 8 \times 10^5$ m^2, during that interval.

The number of red dots between blue and empty dots on the plots indicates the number of predictions. Tracking error is higher for prediction, since there is not any measurement provided. Especially between $60 - 85$ s, system has been probably overloaded and hence, the target has not been tracked for a while. Moreover, it is concluded that the target is probably less important than other targets. For the other intervals, red dots seem as being too squeezed. It means that the predictions are well-matched and the tracking errors are less.

The maneuvering target shown in Figure 4.5(b) is almost periodically updated and there is not an interval like that the non-maneuvering target. The maneuvering target gets the highest tracking error, $\sim 4.5 \times 10^5$ m^2, which is less than the highest value of non-maneuvering target.

The scenario given up to here, symbolizes the main problems for tracking. The reason of these problems is the limited radar resources and capabilities. Hence, the system can not perform all requested tasks and it selects the most appropriate one at each instant. To utilize resources effectively, the performing advantages of each task over the others must be provided to the system in an intelligent way. This can be done through the cost parameter. Thus, the cost parameter is preferable to contain both absolute and relative informations of each target.

Briefly, the main properties of the desired cost parameter are

- ✓ time dependent,
- ✓ maneuvering-based,
- ✓ target-based,
- ✓ combining all targets.

Considering all of them, the cost parameter, $\mathcal{K}_k^n$, is defined as

$$\mathcal{K}_k^n \triangleq \frac{\max\left\{m_k^{(0,\ell)} x^{\ell}_{\text{requesting},k}\right\}_{\ell=1,\,\ell\neq n}^{N_k}}{m_k^{(1,n)}} \cdot x^n_{\text{requesting},k}, \tag{4.34}$$

where $x^n_{\text{requesting},k} \in \{0,1\}$ indicates that if the target n requests a track update or not, $m_k^{(1,n)}$ denotes the estimated improvement on the tracking error covariance of the target n by taking UPD action $\left(u_k^n = 1\right)$ and $\max\left\{m_k^{(0,\ell)}\right\}_{\ell=1,\,\ell\neq n}^{N_k}$ denotes the maximum of estimated deterioration on the tracking error covariances of all targets which are not updated. Thus, the latter covers all targets except the target n. The improvement or deterioration issue is simply the change in the trace of the tracking error covariance. If the trace is thought to be decreased at time $k+1$, the improvement will be observed for tracking. Otherwise the deterioration occurs.

Figure 4.6 is given to visualize what is specified by $m_k^{(0,n)}$ and $m_k^{(1,n)}$ are

$$m_k^{(0,n)} = \left|\,\text{tr}\left(\hat{\mathbf{P}}^n_{k+1}\right) - \text{tr}\left(\mathbf{P}^n_{k+1}\right)\right|, \tag{4.35}$$

$$m_k^{(1,n)} = \left|\,\text{tr}\left(\mathbf{P}^n_{k}\right) - \text{tr}\left(\mathbf{P}^n_{k+1}\right)\right|, \tag{4.36}$$

where $\hat{\mathbf{P}}^n_{k+1}$ is predicted, in an ad hoc way, tracking error covariance at next time. $\hat{\mathbf{P}}^n_{k+1}$ is computed as the linear combination of current and previous tracking error covariances as follows:

$$\begin{aligned}\hat{\mathbf{P}}^n_{k+1} &= \mathbf{P}^n_k + \left(\mathbf{P}^n_k - \mathbf{P}^n_{k-1}\right), \\ &= 2\cdot\mathbf{P}^n_k - \mathbf{P}^n_{k-1}.\end{aligned} \tag{4.37}$$

It is known that system can use all of the available data related to each target and make predictions when there is not any measurement provided. Thus, track informations, not provided, have already been predicted at time $k-1$ for the current time k. In fact, prediction process is one of the jobs of tracker and it has a sampling interval, namely a period, T, i.e. $T = 1$ s. However, each target can request an update of track,

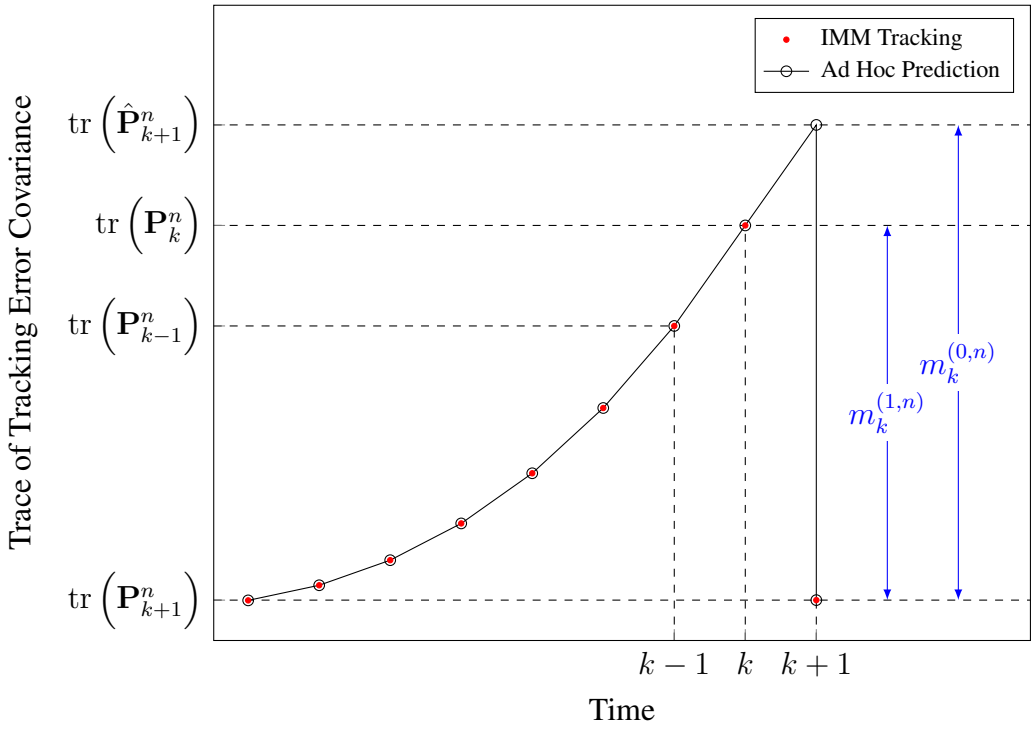

Figure 4.6: Description of parameters used for the cost value computation.

within T. Hence, the term, ad hoc prediction, is more preferable than prediction while describing (4.37).

It is almost clear how $m_k^{(0,n)}$ and $m_k^{(1,n)}$ are obtained by (4.35) and (4.36) respectively, but the parameter, $\mathbf{P}^n_{k+1}$, makes them a bit confusing to understand. The trace of tracking error covariance is increasing while time goes on until k, as shown in Figure 4.6. Then, it decreases to a value which is too close to a value at the beginning of the ad hoc prediction curve. This is the main clue to assign the value of $\mathbf{P}^n_{k+1}$. Owing to description of $m_k^{(1,n)}$, it is said that the trace of tracking error covariance improves after UPD action. Fortunately, UPD action comes with a measurement and hence, the trace of $\mathbf{P}^n_{k+1}$ is assumed to be equal to the trace of measurement noise covariance,

$$\mathrm{tr}\left(\mathbf{R}\right) = \sigma_x^2 + \sigma_y^2,$$

where σ_x and σ_y are standard deviations of measurement in x and y directions and they are known by the tracker.

The next section describes the infinite-horizon value functions.

4.1.4 Infinite-Horizon Value Functions

Problem will be solved for infinite-horizon case, since there is not a fixed period which resets the problem with fixed initial parameters. This is simply the result of problem modeling of multiple target tracking. Each target has a different motion characteristics and hence, target-based generalization of initial parameters will be too complex.

It is claimed in the previous paragraph that process always continues until the target of interest is out of range. Typically, the duration of scheduling is in the order of hundreds seconds, while the tracking task time is in order of milliseconds. This makes the time-variant solutions (finite-horizon solutions) become computationally intractable or unnecessarily comprehensive. The infinite-horizon optimization only refers the solution as a time-invariant solution and it is easier to optimize than its finite-horizon counterpart. The infinite-horizon case solution has the advantage of requiring less computation. It only computes a fixed threshold for the probability of being in Good state at infinite. Then, whenever the probability of being in Good state is less than the threshold, the optimal action is UPD action in order to avoid dropping the target.

The optimal action is determined via *the optimal value function*, $V^n(\cdot)$, according to the probability of being in Good state, μ_k^n,

$$V^n(\mu_k^n) = \max\left\{V_{nupd}^n(\mu_k^n), V_{upd}^n\right\}, \tag{4.38}$$

where $V_{nupd}^n(\mu_k^n)$ and V_{upd}^n are the infinite-horizon value functions for NUPD and UPD actions respectively as follows:

$$V_{nupd}^n(\mu_k^n) = \mu_k^n + \alpha \sum_{i\in\{gt,bt\}} \mathcal{P}_i(\mu_k^n) V^n\big(\mathcal{H}_i(\mu_k^n)\big), \tag{4.39}$$

$$= \mu_k^n + \alpha\Big[\mathcal{P}_{gt}(\mu_k^n) V^n\big(\mathcal{H}_{gt}(\mu_k^n)\big) + \mathcal{P}_{bt}(\mu_k^n) V^n\big(\mathcal{H}_{bt}(\mu_k^n)\big)\Big], \tag{4.40}$$

$$V_{upd}^n = -\mathcal{K}_k^n + V_{nupd}^n(q), \tag{4.41}$$

where α is a discount factor, satisfies $0 < \alpha < 1$.

The value functions (4.39) and (4.41) are explicitly depend on each other via $V^n(\mu_k^n)$ given in (4.38). Furthermore, $V_{nupd}^n(\mu_k^n)$, given in (4.40), is related to the optimal value function, $V^n(\cdot)$ through the functions $\mathcal{H}_{gt}(\mu_k^n)$ and $\mathcal{H}_{bt}(\mu_k^n)$, while $V^n(\cdot)$, given in (4.38), is already related to $V_{nupd}^n(\cdot)$. It is difficult to express $V_{nupd}^n(\mu_k^n)$ without any assumptions on $\mathcal{H}_{gt}(\mu_k^n)$ and $\mathcal{H}_{bt}(\mu_k^n)$.

It is previously said that both of $\mathcal{H}_{gt}(\mu_k^n)$ and $\mathcal{H}_{bt}(\mu_k^n)$ are examined within the interval, $0 < \mu_k^n < 1$, in Lemma 1. Thus, the properties of these functions are valid for $\mu_k^n = 0^+$ but not valid for $\mu_k^n = 0$. Though, it is impossible to define a range which includes all of the real numbers belong to the interval of $[0^+, 1^-]$ by a computer program due to the limited precision, while it is trivial to define an interval of $[0, 1]$. Considering the intervals, the first is a bit cumbersome and hence, the latter is more preferable for computer programming. If the latter is chosen, then problems may occur during a simulation by assigned values to parameters, θ_0, θ_1 and r. Especially, the function, $\mathcal{H}_{gt}(\mu_k^n)$, becomes $0/0$, an indeterminate form [51], at $\mu_k^n = 0$ for $\theta_1 = 0$. That is

$$\mathcal{H}_{gt}(0) \Big|_{\theta_1=0} = \frac{r\theta_0 \cdot 0}{(\theta_0 - \theta_1) \cdot 0 + \theta_1} \Big|_{\theta_1=0} = 0/0.$$

Choosing $\theta_1 = 0$ is a good idea which claims the probability of obtaining a good track given that corresponding target is in Bad state is 0. In this manner, it is only possible that a good track is obtained from a target which is in Good state. Moreover, the idea increases the reliability and validity of measurements. The value assignment of θ_1 can be done during the operation to decrease uncertainty about targets, when the system is overloaded. In this work, it is assumed that $\theta_1 = 0$ in order to simplify the scheme, and the functions described in Section 4.1.2 become

$$\begin{aligned} \mathcal{P}_{gt}(\mu_k^n) \Big|_{\theta_1=0} &= (\theta_0 - \theta_1)\mu_k^n + \theta_1 \Big|_{\theta_1=0}, \\ &= \theta_0 \mu_k^n, \qquad (4.42) \\ \mathcal{P}_{bt}(\mu_k^n) \Big|_{\theta_1=0} &= 1 - (\theta_0 - \theta_1)\mu_k^n - \theta_1 \Big|_{\theta_1=0}, \\ &= 1 - \theta_0 \mu_k^n, \qquad (4.43) \end{aligned}$$

$$\mathcal{H}_{gt}(\mu_k^n)\Big|_{\theta_1=0} = \frac{r\theta_0\mu_k^n}{(\theta_0-\theta_1)\mu_k^n+\theta_1}\Big|_{\theta_1=0},$$
$$= r, \tag{4.44}$$
$$\mathcal{H}_{bt}(\mu_k^n)\Big|_{\theta_1=0} = \frac{r(1-\theta_0)\mu_k^n}{1-(\theta_0-\theta_1)\mu_k^n-\theta_1}\Big|_{\theta_1=0},$$
$$= \frac{r(1-\theta_0)\mu_k^n}{1-\theta_0\mu_k^n}, \tag{4.45}$$
$$\mathcal{H}_{bt}^{-1}(\mu_k^n)\Big|_{\theta_1=0} = \frac{(1-\theta_1)\mu_k^n}{(\theta_0-\theta_1)\mu_k^n+(1-\theta_0)r}\Big|_{\theta_1=0},$$
$$= \frac{\mu_k^n}{\theta_0\mu_k^n+(1-\theta_0)r}. \tag{4.46}$$

Substituting (4.42), (4.43) and (4.44) in (4.40), infinite-horizon value function for NUPD action is expressed by

$$V_{nupd}^n(\mu_k^n) = \mu_k^n + \alpha\big[\theta_0\mu_k^n V^n(r) + (1-\theta_0\mu_k^n)V^n\big(\mathcal{H}_{bt}(\mu_k^n)\big)\big]. \tag{4.47}$$

Next, there is one more simplification required to handle (4.47) and (4.41). This simplification is related to q, the probability of transition to Good state by taking UPD action. There are two main assumptions for specifying q, such that

1. $q = 1$ means action is perfectly achieved (track is successfully updated) and
2. $q = r$, $(r \neq 1)$ means action may fail (mixed detection or sharp maneuvering).

For the rest of the work, the second assumption is considered to make the model more realistic. Then, (4.41) becomes

$$V_{upd}^n = -\mathcal{K}_k^n + V_{nupd}^n(r), \tag{4.48}$$

while $V_{nupd}^n(r)$ can be found as

$$V_{nupd}^n(r) = r + \alpha\big[\theta_0 r V^n(r) + (1-\theta_0 r)V^n\big(\mathcal{H}_{bt}(r)\big)\big]. \tag{4.49}$$

Both (4.47) and (4.49) require $V^n(r)$,

$$\begin{aligned} V^n(r) &= \max\left\{V^n_{nupd}(r), V^n_{upd}\right\}, \\ &= \max\left\{\mathcal{K}^n_k + V^n_{upd}, V^n_{upd}\right\}. \end{aligned} \tag{4.50}$$

It is true with certainty that $\mathcal{K}^n_k$, given in (4.34) cannot be negative, owing that it is a ratio of absolute differences. Then, (4.50) becomes

$$V^n(r) = \mathcal{K}^n_k + V^n_{upd}. \tag{4.51}$$

Using (4.51), the simplified value function of NUPD action, (4.47) becomes

$$V^n_{nupd}(\mu^n_k) = \mu^n_k + \alpha\big[\theta_0\mu^n_k\left(\mathcal{K}^n_k + V^n_{upd}\right) + (1-\theta_0\mu^n_k)V^n\big(\mathcal{H}_{bt}(\mu^n_k)\big)\big]. \tag{4.52}$$

In this section, the value functions for each action is obtained. In the next section, the computation of threshold value, that the update decision depends on, is examined.

4.1.5 The Threshold Value for Decision Making

The threshold value, μ^n_{th}, is the solution of $V^n_{nupd}(\mu^n_k) = V^n_{upd}$, where LHS and RHS are given in (4.52) and (4.48) respectively. According to μ^n_{th}, the decision policy is

$$u^n_k = \begin{cases} 0, & \mu^n_k \geqslant \mu^n_{th}, \\ 1, & \text{otherwise} \end{cases} \tag{4.53}$$

and the action will be not to update the track, if threshold is exceeded.

Up to here, only the formulas of infinite-horizon value functions have been given and the properties of these functions have not been sufficiently mentioned. Before obtaining the formula of μ^n_{th}, it is more convenient to describe the properties of value functions by assuming that μ^n_{th} is already known. Firstly, the effect of μ^n_{th} on $V^n_{nupd}(\mu^n_k)$ is

discussed within a proposition. Meanwhile, it can be better to remind that proofs for propositions, theorems, etc., are given again in this chapter after revising them owing to some typos noticed in [57].

Proposition 1. *For* $0 \leqslant \mu_k^n \leqslant r$*, the threshold,* μ_{th}^n*, generates all breakpoints of* $V_{nupd}^n(\mu_k^n)$ *in the manner that,* [57, Proposition 3]*,*

(i) $V_{nupd}^n(\mu_k^n)$ *has no breakpoints for* $0 \leqslant \mu_k^n < \mu_{th}^n$*,*

(ii) $V_{nupd}^n(\mu_k^n)$ *has breakpoints,* $B_1, B_2, \ldots,$ *satisfying* $\mu_{th}^n < B_1 < B_2 < \cdots < r$ *for* $\mu_{th}^n \leqslant \mu_k^n \leqslant r$*. Breakpoints are computed by inverse function of* $\mathcal{H}_{bt}(\cdot)$*, i.e.* $B_1 = \mathcal{H}_{bt}^{-1}(\mu_{th}^n)$*,* $B_2 = \mathcal{H}_{bt}^{-1}(B_1)$*.*

Proof. (i) If $\mu_k^n < \mu_{th}^n$, then $\mathcal{H}_{bt}(\mu_k^n) < \mu_k^n < \mu_{th}^n$ due to convexity explained in Lemma 2, see Figure 4.3. Thus, there is not breakpoint for this interval.

(ii) If $\mu_k^n < \mathcal{H}_{bt}^{-1}(\mu_{th}^n)$, then $\mathcal{H}_{bt}(\mu_k^n) < \mu_{th}^n$ by applying $\mathcal{H}_{bt}(\cdot)$ to both sides. The case of $\mathcal{H}_{bt}(\mu_k^n) < \mu_{th}^n$ leads the optimal action to be UPD, $V^n\big(\mathcal{H}_{bt}(\mu_k^n)\big) = V_{upd}^n$ for that interval. Then, the value function of NUPD action can be written as

$$V_{nupd}^n(\mu_k^n) = \mu_k^n + \alpha\big[\theta_0\mu_k^n(\mathcal{K}_k^n + V_{upd}^n) + (1 - \theta_0\mu_k^n)V_{upd}^n\big], \tag{4.54}$$

$$= \mu_k^n + \alpha\big[\theta_0\mu_k^n\mathcal{K}_k^n + V_{upd}^n\big],$$

$$= \mu_k^n(1 + \alpha\theta_0\mathcal{K}_k^n) + \alpha V_{upd}^n. \tag{4.55}$$

If $\mathcal{H}_{bt}^{-1}(\mu_{th}^n) < \mu_k^n < \mathcal{H}_{bt}^{-2}(\mu_{th}^n)$, then $\mu_{th}^n < \mathcal{H}_{bt}(\mu_k^n) < \mathcal{H}_{bt}^{-1}(\mu_{th}^n)$ by applying $\mathcal{H}_{bt}(\cdot)$ to both sides of inequalities. The case of $\mu_{th}^n < \mathcal{H}_{bt}(\mu_k^n)$ leads the optimal action to be NUPD, $V^n\big(\mathcal{H}_{bt}(\mu_k^n)\big) = V_{nupd}^n\big(\mathcal{H}_{bt}(\mu_k^n)\big)$ for that interval. Replacing μ_k^n with $\mathcal{H}_{bt}(\mu_k^n)$ in (4.55), $V_{nupd}^n\big(\mathcal{H}_{bt}(\mu_k^n)\big)$ can be obtained as

$$V_{nupd}^n\big(\mathcal{H}_{bt}(\mu_k^n)\big) = \mathcal{H}_{bt}(\mu_k^n)(1 + \alpha\theta_0\mathcal{K}_k^n) + \alpha V_{upd}^n. \tag{4.56}$$

Thus, $V^n\big(\mathcal{H}_{bt}(\mu_k^n)\big)$ known from (4.56) can be used to obtain value function of NUPD action in the following way,

$$V^n_{nupd}(\mu^n_k) = \mu^n_k + \alpha\big[\theta_0\mu^n_k\big(\mathcal{K}^n_k + V^n_{upd}\big) + (1-\theta_0\mu^n_k)V^n\big(\mathcal{H}_{bt}(\mu^n_k)\big)\big], \tag{4.57}$$

$$\begin{aligned}
&= \mu^n_k + \alpha\big[\theta_0\mu^n_k\big(\mathcal{K}^n_k + V^n_{upd}\big) + (1-\theta_0\mu^n_k) \\
&\qquad\qquad \big(\mathcal{H}_{bt}(\mu^n_k)(1+\alpha\theta_0\mathcal{K}^n_k) + \alpha V^n_{upd}\big)\big], \\
&= \mu^n_k + \alpha\big[\theta_0\mu^n_k\big(\mathcal{K}^n_k + V^n_{upd}\big) + \mathcal{H}_{bt}(\mu^n_k)(1+\alpha\theta_0\mathcal{K}^n_k) \\
&\qquad - \theta_0\mu^n_k\left(\mathcal{H}_{bt}(\mu^n_k)(1+\alpha\theta_0\mathcal{K}^n_k) + \alpha V^n_{upd}\right) + \alpha V^n_{upd}\big], \\
&= \mu^n_k + \alpha\big[\theta_0\mu^n_k\left(\mathcal{K}^n_k + V^n_{upd}(1-\alpha) - \mathcal{H}_{bt}(\mu^n_k)(1+\alpha\theta_0\mathcal{K}^n_k)\right) \\
&\qquad\qquad + \mathcal{H}_{bt}(\mu^n_k)(1+\alpha\theta_0\mathcal{K}^n_k) + \alpha V^n_{upd}\big].
\end{aligned} \tag{4.58}$$

The linear equations (4.55) and (4.58) have different value at $\mu^n_k = 0$, such that the former has αV^n_{upd} and the latter has $\alpha^2 V^n_{upd}$. Thus, $B_1 = \mathcal{H}^{-1}_{bt}(\mu^n_{th})$ is a breakpoint, as shown in Figure 4.7. The other breakpoints, $B_2, B_3, \ldots$, can be shown in a similar way. □

Proposition 1 claims that the knowledge of μ^n_k is sufficient to obtain breakpoints and intersections of linear segments, of $V^n_{nupd}(\mu^n_k)$. Moreover, $V^n_{nupd}(\mu^n_k)$ can be obtained

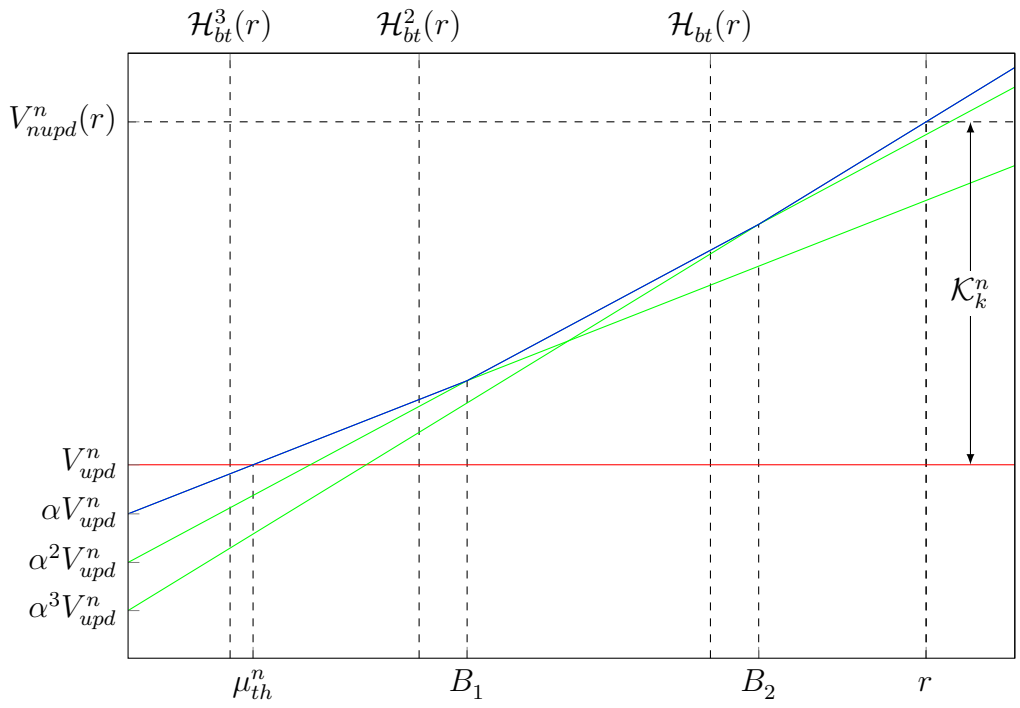

Figure 4.7: The value function of NUPD action for $M = 3$.

explicitly by knowing both V^n_{upd} and μ^n_{th}. It is interesting to note that if $V^n_{nupd}(r)$ is known, (4.48) can be used to find V^n_{upd}. However, if μ^n_{th} is known, $V^n_{nupd}(\mu^n_k)$ for $0 < \mu^n_k \leqslant r$ can be found from V^n_{upd}. Hence, in a system with limited memory, storing only μ^n_{th} and V^n_{upd} can be more efficient than storing $V^n_{nupd}(\mu^n_k)$ for $0 < \mu^n_k \leqslant r$.

The properties of $V^n_{nupd}(\mu^n_k)$ deduced from Proposition 1, can be generalized by a theorem.

Theorem 1. *The infinite-horizon value functions for NUPD action, $V^n_{nupd}(\mu^n_k)$, is a piecewise-linear convex function for $\theta_1 = 0$,* [57, Theorem 2].

Proof. For $\theta_1 = 0$, the infinite-horizon value functions for NUPD action, $V^n_{nupd}(\mu^n_k)$, is given in (4.52) and $V^n\big(\mathcal{H}_{bt}(\mu^n_k)\big)$, in that expression, is obtained as

$$V^n\big(\mathcal{H}_{bt}(\mu^n_k)\big) = \max\left\{V^n_{nupd}\big(\mathcal{H}_{bt}(\mu^n_k)\big), V^n_{upd}\right\} \tag{4.59}$$

by using (4.38). According to (4.38), $V^n(\cdot)$ is composed of upper part of functions that V^n_{upd} is a constant function and $V^n_{nupd}(\cdot)$ consists of the linear segments shown in Proposition 1. Then, $V^n(\cdot)$ is a piecewise-linear convex function. Hence, $V^n_{nupd}(\mu^n_k)$ is also a piecewise-linear convex function. Further details can be found in [60]. □

Before continuing discussions about the threshold value, it may be better to mention that there is a different statement on the proof of Theorem 1. It is noted in [57] that, to prove $V^n_{nupd}(\mu^n_k)$ to be piecewise-linear, it is required to show the finiteness of the number of breakpoints. To do so, it is sufficient to show that the length of the intervals, $(B_0 = \mu^n_{th}, B_1), (B_1, B_2), \ldots$, is increasing. To the best our understanding, the length of interval depends on the starting point,

$$B_{i+1} - B_i = \mathcal{H}^{-1}_{bt}(B_i) - B_i, \tag{4.60}$$

$$= \frac{B_i}{\theta_0 B_i + (1-\theta_0)r} - B_i, \tag{4.61}$$

and the first derivative of (4.61) is always positive with respect to B_i, then it can be said that the length of interval is increasing.

$$\mathcal{D}(B_i) \triangleq \frac{B_i}{\theta_0 B_i + (1-\theta_0)r} - B_i, \tag{4.62}$$

$$\mathcal{D}'(B_i) = \frac{\mathrm{d}\mathcal{D}(B_i)}{\mathrm{d}B_i}, \tag{4.63}$$

$$= \frac{(1-\theta_0)r}{\left[\theta_0 B_i + (1-\theta_0)r\right]^2} - 1. \tag{4.64}$$

The derivative of the function given in (4.64), is not always positive. Hence, it cannot be said that the length of interval is increasing.

When Figure 4.7 is examined again, to obtain segments of $V^n_{nupd}(\mu^n_k)$, breakpoints, B_1 and B_2, are computed by $\mathcal{H}^{-1}_{bt}(\mu^n_{th})$ and $\mathcal{H}^{-2}_{bt}(\mu^n_{th})$ respectively. In fact, μ^n_{th}, is not a breakpoint of $V^n_{nupd}(\mu^n_k)$, while it is a breakpoint of $V^n(\mu^n_k)$ according to (4.38) for $\mu^n_{th} > 0$. Hence, μ^n_{th} can also behave like a breakpoint. Then, $\mathcal{H}^3_{bt}(r)$, $\mathcal{H}^2_{bt}(r)$ and $\mathcal{H}_{bt}(r)$ come right before μ^n_{th}, B_1 and B_2 respectively. These points depend on r which has a presumed value, while breakpoints are directly related to μ^n_{th} which depends on the basic parameters, α, θ_0, r, $\mathcal{K}^n_k$. Thus, it is simpler to compute these points than breakpoints which require the μ^n_{th}. One can try to compute other points, $\mathcal{H}^4_{bt}(r),\ \mathcal{H}^5_{bt}(r), \ldots$, until they become sufficiently close to zero. Thus, there is no limit for the number of these points.

The number of segments of $V^n_{nupd}(\mu^n_k)$ can be given with the following corollary.

Corollary 1. *Assuming that M is the number of segments of $V^n_{nupd}(\mu^n_k)$, $0 \leqslant \mu^n_k \leqslant r$, there are $M-1$ breakpoints from Proposition 1. Then, μ^n_{th} satisfies the condition,* [57, Corollary 1]*,*

$$r > \mathcal{H}_{bt}(r) > \mathcal{H}^2_{bt}(r) > \cdots > \mathcal{H}^{M-2}_{bt}(r) > \mathcal{H}^{M-1}_{bt}(r) > \mu^n_{th} > \mathcal{H}^M_{bt}(r).$$

Corollary 1 depicts $\mathcal{H}^M_{bt}(r) < \mu^n_{th}$ which can be used to determine the number of segments, M, without explicitly finding breakpoints of $V^n_{nupd}(\mu^n_k)$. A simple function to realize this idea is given in Algorithm 4.1.

Moreover, it is deduced that

$$\mu^n_k > \mathcal{H}^{M-1}_{bt}(r) \wedge \mathcal{H}^{M-1}_{bt}(r) > \mu^n_{th} \implies \mu^n_k > \mu^n_{th},$$

$$\therefore V^n_{nupd}(\mu^n_k) > V^n_{upd} \implies V^n(\mu^n_k) = V^n_{nupd}(\mu^n_k).$$

Algorithm 4.1 Number of segments.

function NOFSEGMENT$\big(\alpha,\ \theta_0,\ r,\ \mathcal{K}_k^n\big)$
  $M = 1$
  compute $\mathcal{H}_{bt}^{M}(r)$
  compute μ_{th}^{n}
  while $\mathcal{H}_{bt}^{M}(r) \geqslant \mu_{th}^{n}$ **do**
    $M{+}{+}$
    compute $\mathcal{H}_{bt}^{M}(r)$
    compute μ_{th}^{n}
  end while
  return M
end

from Corollary 1. Hence, the optimal value function becomes

$$V^n(\mu_k^n) = \mu_k^n + \alpha\big[\theta_0\mu_k^n\left(\mathcal{K}_k^n + V_{upd}^n\right) + (1-\theta_0\mu_k^n)V^n\big(\mathcal{H}_{bt}(\mu_k^n)\big)\big], \tag{4.65}$$

for $\mu_k^n > \mathcal{H}_{bt}^{M-1}(r)$.

In the beginning of this section, it is said that μ_{th}^n is the solution of $V_{nupd}^n(\mu_k^n) = V_{upd}^n$ so that $V_{nupd}^n(\mu_{th}^n) = V_{upd}^n$. It is also added that μ_{th}^n and V_{upd}^n are sufficient to determine $V_{nupd}^n(\mu_k^n)$ by Proposition 1. Summing them, it is more confident to think that μ_{th}^n and V_{upd}^n are dependent. The relation between them is clarified with the following proposition.

Proposition 2. *The threshold, μ_{th}^n, can be computed as*

$$\mu_{th}^n = \frac{1-\alpha}{1+\alpha\theta_0\mathcal{K}_k^n}V_{upd}^n, \tag{4.66}$$

if V_{upd}^n is known, [57, Proposition 4].

Proof. The threshold value, μ_{th}^n, satisfies $V_{nupd}^n(\mu_k^n) = V_{upd}^n$ for $\mu_k^n = \mu_{th}^n$. By using (4.59), $V^n\big(\mathcal{H}_{bt}(\mu_{th}^n)\big) = V_{upd}^n$ owing to $\mathcal{H}_{bt}(\mu_{th}^n) < \mu_{th}^n$, as shown in Figure 4.3(a). It

is known $r > \mu_{th}^n$ and $V^n(r) = V_{nupd}^n(r) = \mathcal{K}_k^n + V_{upd}^n$. Combining all of them, V_{upd}^n becomes

$$\begin{aligned} V_{upd}^n &= \mu_{th}^n + \alpha\big[\theta_0\mu_{th}^n V^n(r) + (1-\theta_0\mu_{th}^n)V_{upd}^n\big], \qquad (4.67)\\ &= \mu_{th}^n + \alpha\big[\theta_0\mu_{th}^n\big(\mathcal{K}_k^n + V_{upd}^n\big) + (1-\theta_0\mu_{th}^n)V_{upd}^n\big],\\ &= \mu_{th}^n + \alpha\big[\theta_0\mu_{th}^n\mathcal{K}_k^n + V_{upd}^n\big],\\ &= \mu_{th}^n\big(1+\alpha\theta_0\mathcal{K}_k^n\big) + \alpha V_{upd}^n,\\ &= \mu_{th}^n\left(\frac{1+\alpha\theta_0\mathcal{K}_k^n}{1-\alpha}\right). \qquad (4.68) \end{aligned}$$

The relation, $\mu_{th}^n \propto V_{upd}^n$, is given in (4.68), and (4.66) can be obtained simply with this relation. □

It is suggested within Proposition 2 that μ_{th}^n is directly obtained from V_{upd}^n. Indeed, V_{upd}^n can be thought as the base point of all functions. Hence, the expression of V_{upd}^n, which depends only on the basic parameters, is given in the following theorem.

Theorem 2. *Supposing that $V_{nupd}^n(\mu_k^n)$ consists of M segments, V_{upd}^n can be computed by,* [57, Theorem 3 and 4]*,*

$$V_{upd}^n \triangleq \frac{\mathcal{A}_M^n(r)(1+\alpha\theta_0\mathcal{K}_k^n) - \mathcal{K}_k^n}{1-\alpha\theta_0\mathcal{A}_M^n(r) - \mathcal{B}_M^n(r)}, \qquad (4.69)$$

where $\mathcal{A}_M^n(r)$ is defined as

$$\mathcal{A}_M^n(r) \triangleq \begin{cases} r, & M = 1,\\ r + \sum_{i=1}^{M-1}\alpha^i\mathcal{H}_{bt}^i(r)\prod_{j=0}^{i-1}\big(1-\theta_0\mathcal{H}_{bt}^j(r)\big), & M \geqslant 2 \end{cases} \qquad (4.70)$$

and $\mathcal{B}_M^n(r)$ is defined as

$$\mathcal{B}_M^n(r) \triangleq \prod_{i=0}^{M-1}\alpha\big(1-\theta_0\mathcal{H}_{bt}^i(r)\big), \qquad (4.71)$$

for $M \geqslant 1$.

Proof. To compute V^n_{upd}, it is necessary and sufficient to solve $M+1$ distinct equations as follows:

$$V^n(r) = r + \alpha\big[\theta_0 r V^n(r) + (1-\theta_0 r)V^n\big(\mathcal{H}_{bt}(r)\big)\big], \tag{4.72}$$

$$V^n\big(\mathcal{H}_{bt}(r)\big) = \mathcal{H}_{bt}(r) + \alpha\big[\theta_0 \mathcal{H}_{bt}(r)V^n(r) + \big(1-\theta_0\mathcal{H}_{bt}(r)\big)V^n\big(\mathcal{H}^2_{bt}(r)\big)\big], \tag{4.73}$$

$$V^n\big(\mathcal{H}^2_{bt}(r)\big) = \mathcal{H}^2_{bt}(r) + \alpha\big[\theta_0 \mathcal{H}^2_{bt}(r)V^n(r) + \big(1-\theta_0\mathcal{H}^2_{bt}(r)\big)V^n\big(\mathcal{H}^3_{bt}(r)\big)\big], \tag{4.74}$$

$$\vdots$$

$$V^n\big(\mathcal{H}^{M-2}_{bt}(r)\big) = \mathcal{H}^{M-2}_{bt}(r) + \alpha\big[\theta_0 \mathcal{H}^{M-2}_{bt}(r)V^n(r) + \big(1-\theta_0\mathcal{H}^{M-2}_{bt}(r)\big)V^n\big(\mathcal{H}^{M-1}_{bt}(r)\big)\big], \tag{4.75}$$

$$V^n\big(\mathcal{H}^{M-1}_{bt}(r)\big) = \mathcal{H}^{M-1}_{bt}(r) + \alpha\big[\theta_0 \mathcal{H}^{M-1}_{bt}(r)V^n(r) + \big(1-\theta_0\mathcal{H}^{M-1}_{bt}(r)\big)V^n_{upd}\big]. \tag{4.76}$$

From (4.72) to (4.76), M equations, are obtained directly using (4.65). In (4.76), the last term becomes V^n_{upd}, while it can be written as $V^n\big(\mathcal{H}^M_{bt}(r)\big)$. This is concluded from Corollary 1 claims that

$$\mathcal{H}^M_{bt}(r) < \mu^n_{th} \implies V^n_{nupd}\big(\mathcal{H}^M_{bt}(r)\big) < V^n_{upd},$$
$$\therefore V^n\big(\mathcal{H}^M_{bt}(r)\big) = V^n_{upd}.$$

Substituting (4.73) into (4.72), the expression is obtained as

$$V^n(r) = r + \alpha\big[\theta_0 r V^n(r) + (1-\theta_0 r) \big(\mathcal{H}_{bt}(r) + \alpha\big[\theta_0\mathcal{H}_{bt}(r)V^n(r) + \big(1-\theta_0\mathcal{H}_{bt}(r)\big)V^n\big(\mathcal{H}^2_{bt}(r)\big)\big)\big]. \tag{4.77}$$

Then, (4.77) can be converted into a more compact form,

$$V^n(r) = (r + \alpha(1-\theta_0 r)\mathcal{H}_{bt}(r)) + \alpha\theta_0\,(r + \alpha(1-\theta_0 r)\mathcal{H}_{bt}(r))\,V^n(r) + \alpha^2(1-\theta_0 r)\big(1-\theta_0\mathcal{H}_{bt}(r)\big)V^n\big(\mathcal{H}^2_{bt}(r)\big). \tag{4.78}$$

Substituting (4.74) into (4.78), the expression is obtained as

$$V^n(r) = \big(r + \alpha(1-\theta_0 r)\mathcal{H}_{bt}(r) + \alpha^2(1-\theta_0 r)\big(1-\theta_0\mathcal{H}_{bt}(r)\big)\mathcal{H}^2_{bt}(r)\big) + \alpha\theta_0\left(r + \alpha(1-\theta_0 r)\mathcal{H}_{bt}(r) + \alpha^2(1-\theta_0 r)\big(1-\theta_0\mathcal{H}_{bt}(r)\big)\mathcal{H}^2_{bt}(r)\right) V^n(r) + \alpha^3(1-\theta_0 r)\big(1-\theta_0\mathcal{H}_{bt}(r)\big)\big(1-\theta_0\mathcal{H}^2_{bt}(r)\big)V^n\big(\mathcal{H}^3_{bt}(r)\big). \quad (4.79)$$

Continuing in this way, (4.72) becomes

$$V^n(r) = \mathcal{A}^n_M(r) + \alpha\theta_0\mathcal{A}^n_M(r)V^n(r) + \mathcal{B}^n_M(r)V^n_{upd}, \quad (4.80)$$

where $\mathcal{A}^n_M(r)$ is

$$\begin{aligned}\mathcal{A}^n_M(r) &= r + \alpha\big(1-\theta_0 r\big)\mathcal{H}_{bt}(r) \\ &\quad + \alpha^2\big(1-\theta_0 r\big)\big(1-\theta_0\mathcal{H}_{bt}(r)\big)\mathcal{H}^2_{bt}(r) \\ &\quad \vdots \\ &\quad + \alpha^{M-1}\big(1-\theta_0 r\big)\big(1-\theta_0\mathcal{H}_{bt}(r)\big)\big(1-\theta_0\mathcal{H}^2_{bt}(r)\big) \\ &\qquad\qquad \cdots\big(1-\theta_0\mathcal{H}^{M-2}_{bt}(r)\big)\mathcal{H}^{M-1}_{bt}(r), \\ &= r + \sum_{i=1}^{M-1}\alpha^i\mathcal{H}^i_{bt}(r)\prod_{j=0}^{i-1}\big(1-\theta_0\mathcal{H}^j_{bt}(r)\big), \end{aligned} \quad (4.81)$$

and $\mathcal{B}^n_M(r)$ is

$$\begin{aligned}\mathcal{B}^n_M(r) &= \alpha^M\big(1-\theta_0 r\big)\big(1-\theta_0\mathcal{H}_{bt}(r)\big)\big(1-\theta_0\mathcal{H}^2_{bt}(r)\big)\cdots\big(1-\theta_0\mathcal{H}^{M-1}_{bt}(r)\big), \\ &= \prod_{i=0}^{M-1}\alpha\big(1-\theta_0\mathcal{H}^i_{bt}(r)\big). \end{aligned} \quad (4.82)$$

If $M = 1$, then (4.76) becomes

$$V^n\big(\mathcal{H}^0_{bt}(r)\big) = \mathcal{H}^0_{bt}(r) + \alpha\big[\theta_0\mathcal{H}^0_{bt}(r)V^n(r) + \big(1-\theta_0\mathcal{H}^0_{bt}(r)\big)V^n_{upd}\big], \quad (4.83)$$

where

$$\mathcal{H}_{bt}^{0}(r) = \mathcal{H}_{bt}\left(\mathcal{H}_{bt}^{-1}(r)\right) = r \implies \mathcal{A}_{1}^{n}(r) = r.$$

Here, M of $M+1$ equations are presented and the other required equation is (4.51) to find V_{upd}^{n}. Substituting (4.51) into (4.80), the expression is obtained as

$$\mathcal{K}_{k}^{n} + V_{upd}^{n} = \mathcal{A}_{M}^{n}(r) + \alpha\theta_{0}\mathcal{A}_{M}^{n}(r)\left(\mathcal{K}_{k}^{n} + V_{upd}^{n}\right) + \mathcal{B}_{M}^{n}(r)V_{upd}^{n}. \tag{4.84}$$

By using (4.84), (4.69) can be obtained simply. □

The way for obtaining the value V_{upd}^{n} is given by Theorem 2. After carefully examining (4.69), it is obvious to say that V_{upd}^{n} can be negative with respect to $\mathcal{K}_{k}^{n}$ value. If $\mathcal{K}_{k}^{n}$ is high enough, then V_{upd}^{n} is negative and hence, μ_{th}^{n} also becomes negative according to (4.66). Therefore NUPD action becomes always optimal for the negative threshold value, since μ_{k}^{n} is always positive. This makes computations for decision making process unnecessary. Because it is explicitly inferred from $\mathcal{K}_{k}^{n}$, whether μ_{th}^{n} is negative or not. The upper bound of $\mathcal{K}_{k}^{n}$, which guarantees that μ_{th}^{n} is positive, is discussed in the following proposition.

Proposition 3. *If $\mathcal{K}_{k}^{n} > r/(1-\alpha r)$, then the decision policy becomes a degenerate policy and the optimal action is always NUPD,* [61, Proposition 2].

Proof. To begin the proof, the infinite-horizon value functions given in (4.47) and (4.48) are converted to the finite-horizon case,

$$V_{nupd}^{n,t}(\mu_{k}^{n}) = \mu_{k}^{n} + \alpha\left[\theta_{0}\mu_{k}^{n}V^{n,t-1}(r) + (1-\theta_{0}\mu_{k}^{n})V^{n,t-1}\left(\mathcal{H}_{bt}(\mu_{k}^{n})\right)\right], \tag{4.85}$$

$$V_{upd}^{n,t} = -\mathcal{K}_{k}^{n} + V_{nupd}^{n,t}(r), \tag{4.86}$$

for $t \geqslant 1$.

Assumed initial condition is $V^{n,0}(\mu_{k}^{n}) = 0$, i.e. there is not any value or utility at the initial point for each target. Then, starting from horizon-1 and always choosing

NUPD as an optimal action until horizon-t, value functions given in (4.85) and (4.86) are employed as

$$
\begin{aligned}
V^{n,1}_{nupd}(\mu^n_k) &= \mu^n_k, \\
V^{n,1}_{upd} &= -\mathcal{K}^n_k + r, \\
V^{n,1}(\mu^n_k) &= \mu^n_k, \\
V^{n,2}_{nupd}(\mu^n_k) &= \mu^n_k + \alpha\big[\theta_0\mu^n_k V^{n,1}(r) + (1-\theta_0\mu^n_k)V^{n,1}\big(\mathcal{H}_{bt}(\mu^n_k)\big)\big] \\
&= \mu^n_k + \alpha\big[\theta_0\mu^n_k r + (1-\theta_0\mu^n_k)\mathcal{H}_{bt}(\mu^n_k)\big] \\
&= \mu^n_k + \alpha\left[\theta_0\mu^n_k r + \cancel{(1-\theta_0\mu^n_k)}\cdot\frac{r(1-\theta_0)\mu^n_k}{\cancel{1-\theta_0\mu^n_k}}\right], \\
&= \mu^n_k + \cancel{\alpha\theta_0\mu^n_k r} + \alpha r\mu^n_k - \cancel{\alpha r\theta_0\mu^n_k}, \\
&= \mu^n_k(1+\alpha r), \\
V^{n,2}_{upd} &= -\mathcal{K}^n_k + r(1+\alpha r), \\
V^{n,2}(\mu^n_k) &= \mu^n_k(1+\alpha r), \\
V^{n,3}_{nupd}(\mu^n_k) &= \mu^n_k + \alpha\big[\theta_0\mu^n_k V^{n,2}(r) + (1-\theta_0\mu^n_k)V^{n,2}\big(\mathcal{H}_{bt}(\mu^n_k)\big)\big] \\
&= \mu^n_k + \alpha(1+\alpha r)\big[\theta_0\mu^n_k r + (1-\theta_0\mu^n_k)\mathcal{H}_{bt}(\mu^n_k)\big] \\
&= \mu^n_k + \alpha(1+\alpha r)r\mu^n_k, \\
&= \mu^n_k\left(1+\alpha r+\alpha^2 r^2\right), \\
V^{n,3}_{upd} &= -\mathcal{K}^n_k + r\left(1+\alpha r+\alpha^2 r^2\right), \\
V^{n,3}(\mu^n_k) &= \mu^n_k\left(1+\alpha r+\alpha^2 r^2\right), \\
&\vdots \\
V^{n,t}_{nupd}(\mu^n_k) &= \mu^n_k\sum_{\ell=0}^{t-1}\alpha^\ell r^\ell, \qquad (4.87) \\
V^{n,t}_{upd} &= -\mathcal{K}^n_k + r\sum_{\ell=0}^{t-1}\alpha^\ell r^\ell, \qquad (4.88) \\
V^{n,t}(\mu^n_k) &= \max\left\{V^{n,t}_{nupd}(\mu^n_k), V^{n,t}_{upd}\right\}. \qquad (4.89)
\end{aligned}
$$

As $t\to\infty$, (4.88) becomes,

$$
V^{n,t}_{upd} = -\mathcal{K}^n_k + r\sum_{\ell=0}^{t-1}\alpha^\ell r^\ell \underset{t\to\infty}{=} -\mathcal{K}^n_k + \frac{r}{1-\alpha r}.
$$

$V_{nupd}^{n,t}(\mu_k^n)$ given in (4.87), is always positive. If $\mathcal{K}_k^n > r/(1-\alpha r)$, then $V_{upd}^{n,t}$ given in (4.88), is negative and the optimal action is again NUPD, $V^{n,t}(\mu_k^n) = V_{nupd}^{n,t}(\mu_k^n)$, at horizon-$t$ for $t \to \infty$. Hence, the decision policy becomes a degenerate policy and the optimal action is always NUPD. □

Fortunately, the solution is completed by substituting (4.69) into (4.66). The threshold value is determined by

$$\mu_{th}^n = \begin{cases} 0, & \mathcal{K}_k^n > \dfrac{r}{1-\alpha r}, \\ \dfrac{1-\alpha}{1+\alpha\theta_0\mathcal{K}_k^n}\left(\dfrac{\mathcal{A}_M^n(r)(1+\alpha\theta_0\mathcal{K}_k^n)-\mathcal{K}_k^n}{1-\alpha\theta_0\mathcal{A}_M^n(r)-\mathcal{B}_M^n(r)}\right), & \text{otherwise} \end{cases} \tag{4.90}$$

and the way of computing μ_{th}^n is given with Algorithm 4.2.

Algorithm 4.2 The threshold value computation.

function THRESHOLD$\big(\alpha,\ \theta_0,\ r,\ \mathcal{K}_k^n\big)$
  if $\mathcal{K}_k^n > r/(1-\alpha r)$ **then**
    $\mu_{th}^n = 0$
  else
    $M = 1$
    compute $\mathcal{H}_{bt}^M(r)$, $\mathcal{A}_M^n(r)$ and $\mathcal{B}_M^n(r)$
    compute V_{upd}^n
    compute μ_{th}^n
    while $\mathcal{H}_{bt}^M(r) \geqslant \mu_{th}^n$ **do**
      $M{+}{+}$
      compute $\mathcal{H}_{bt}^M(r)$, $\mathcal{A}_M^n(r)$ and $\mathcal{B}_M^n(r)$
      compute V_{upd}^n
      compute μ_{th}^n
    end while
  end if
  return μ_{th}^n
end

Assuming $\alpha = 0.99$, the other basic parameters, θ_0, r and $\mathcal{K}_k^n$ are changed to obtain distinct infinite-horizon value functions. Then obtained thresholds and the numbers of segments are given in Table 4.1. Furthermore, Figure 4.8 shows these functions, when $\theta_0 = 0.60$ and $r = 0.90$.

The comments for the data given in Table 4.1 can be given as follows:

- The higher r makes μ_{th}^n higher, since $\mathcal{A}_M^n(r)$ increases with r, and V_{nupd}^n also increases. This statement is inferred from Theorem 2.
- The higher $\mathcal{K}_k^n$ makes μ_{th}^n smaller, as mentioned in Proposition 3. That is

$$\mathcal{K}_k^n < r/(1-\alpha r) \wedge \mathcal{K}_k^n \to r/(1-\alpha r) \implies \mu_{th}^n \to 0.$$

- M depends on both θ_0 and $\mathcal{K}_k^n$, as depicted more clearly in Table 4.1(c).

Table4.1: Comparison of the threshold value and number of segments for $\alpha = 0.99$ and (a) $\mathcal{K}_k^n = 0.3$, (b) $\mathcal{K}_k^n = 1.2$, (c) $\mathcal{K}_k^n = 2.8$.

(a)

	$r = 0.90$			$r = 0.95$		
	$\theta_0 = 0.60$	$\theta_0 = 0.75$	$\theta_0 = 0.90$	$\theta_0 = 0.60$	$\theta_0 = 0.75$	$\theta_0 = 0.90$
μ_{th}^n	0.6454	0.6547	0.6633	0.6954	0.7047	0.7133
M	1	1	1	1	1	1

(b)

	$r = 0.90$			$r = 0.95$		
	$\theta_0 = 0.60$	$\theta_0 = 0.75$	$\theta_0 = 0.90$	$\theta_0 = 0.60$	$\theta_0 = 0.75$	$\theta_0 = 0.90$
μ_{th}^n	0.3574	0.3525	0.3369	0.4256	0.4194	0.4017
M	2	2	2	2	2	2

(c)

	$r = 0.90$			$r = 0.95$		
	$\theta_0 = 0.60$	$\theta_0 = 0.75$	$\theta_0 = 0.90$	$\theta_0 = 0.60$	$\theta_0 = 0.75$	$\theta_0 = 0.90$
μ_{th}^n	0.1654	0.1581	0.1507	0.2388	0.2260	0.2083
M	3	3	2	3	3	2

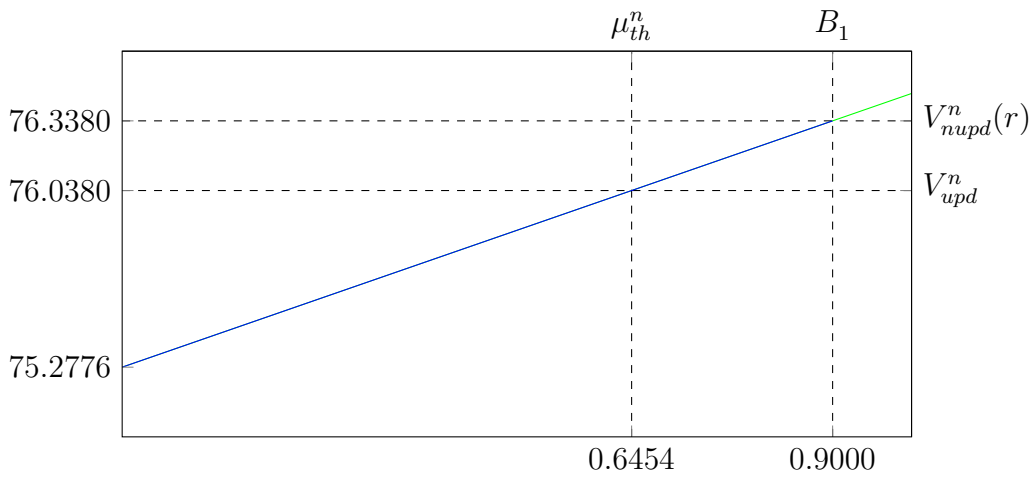

(a)

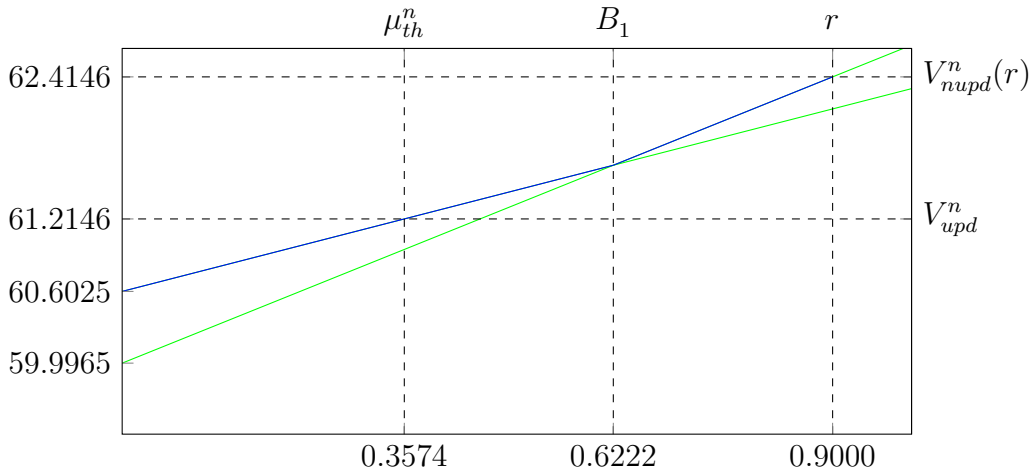

(b)

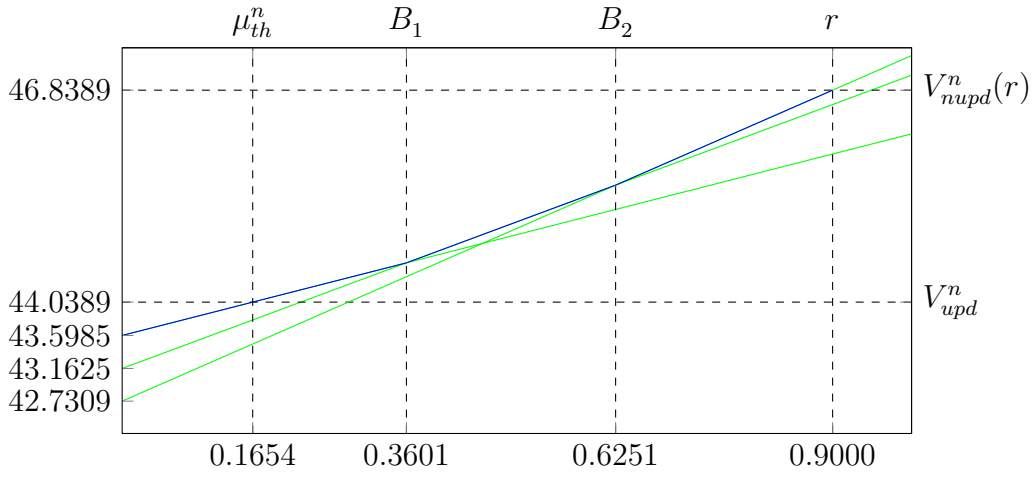

(c)

Figure 4.8: Sample infinite-horizon value functions of NUPD action with $\alpha = 0.99$, $\theta_0 = 0.60$, $r = 0.90$ and (a) $\mathcal{K}^n_k = 0.3$, (b) $\mathcal{K}^n_k = 1.2$, (c) $\mathcal{K}^n_k = 2.8$.

The decision making process does not only consider that the track update of a target is actually required whether or not. The main aim for using this method is to choose the best target at each scheduling instant for track update. The next section describes how the best target is chosen via this method.

4.1.6 Choosing the Best Target

The best target which mostly deserves the track update must be among the targets that have a cost value $\mathcal{K}_k^n$, given in (4.34), is greater than zero. Because other targets which have a cost parameter equal to zero do not request a track update at time k such that

$$\begin{aligned} \text{the target } n \text{ does not request a track update} &\implies x^n_{\text{requesting},k} = 0 \implies \mathcal{K}_k^n = 0, \\ \text{the target } n \text{ requests a track update} &\implies x^n_{\text{requesting},k} = 1 \implies \mathcal{K}_k^n > 0. \end{aligned}$$

It is known that the target n has its own threshold value, μ_{th}^n, and the probability of being in Good state, μ_k^n, which summarizes the available information about that target. Here, μ_k^n indicates the absolute information that is directly related to the target, while μ_{th}^n indicates the relative information about the target among the other targets due to the definition of cost parameter. Thus, both absolute and relative informations about each of targets are provided, and these informations are thought to be sufficient for choosing the best target.

According to previous section, it is obvious that higher $\mathcal{K}_k^n$ makes μ_{th}^n smaller. The definition of $\mathcal{K}_k^n$ given in (4.34) claims that if there is a target which is maneuvering, its trace of error covariance continues to increase until the next track update. From the given example in Figure 4.1, it is deduced that the increment in the trace of error covariance is faster for a highly maneuvering target than a less maneuvering target. It is important to see this case which makes $\mathcal{K}_k^n$ less for a highly maneuvering target than a less maneuvering target.

Supposing that there are only two targets, such as target 1 and target 2, and they request track update at time k, the case can be expressed as

$$x^1_{\text{requesting},k} = x^2_{\text{requesting},k} = 1,$$

and the cost parameters are determined as

$$\mathcal{K}_k^1 = \frac{m_k^{(0,2)}}{m_k^{(1,1)}}, \quad \mathcal{K}_k^2 = \frac{m_k^{(0,1)}}{m_k^{(1,2)}}$$

respectively by using (4.34).

If both targets have track update scheduled at next time, $k+1$, it will be true that

$$\mathrm{tr}\left(\mathbf{P}_{k+1}^1\right) = \mathrm{tr}\left(\mathbf{P}_{k+1}^2\right) \tag{4.91}$$

due to tracking process. Moreover, it is assumed that target 1 is less maneuvering, and target 2 is highly maneuvering. Hence, the statement about the increment in the trace of error covariance,

$$\mathrm{tr}\left(\mathbf{P}_k^1 - \mathbf{P}_{k-1}^1\right) < \mathrm{tr}\left(\mathbf{P}_k^2 - \mathbf{P}_{k-1}^2\right),$$

implies that

$$\mathrm{tr}\left(\mathbf{P}_k^1\right) < \mathrm{tr}\left(\mathbf{P}_k^2\right) \tag{4.92}$$

and it is clear to denote that

$$\mathrm{tr}\left(\hat{\mathbf{P}}_{k+1}^1\right) < \mathrm{tr}\left(\hat{\mathbf{P}}_{k+1}^2\right) \tag{4.93}$$

by using (4.37).

From (4.36), the estimated improvements on the tracking error covariance of target 1 and target 2 by taking UPD action, are given as

$$m_k^{(1,1)} = \left|\mathrm{tr}\left(\mathbf{P}_k^1\right) - \mathrm{tr}\left(\mathbf{P}_{k+1}^1\right)\right|, \quad m_k^{(1,2)} = \left|\mathrm{tr}\left(\mathbf{P}_k^2\right) - \mathrm{tr}\left(\mathbf{P}_{k+1}^2\right)\right|$$

respectively. Then, it is deduced that

$$m_k^{(1,1)} < m_k^{(1,2)} \tag{4.94}$$

by jointly combining (4.91) and (4.92).

From (4.35), the estimated changes on the tracking error covariance of target 1 and target 2 by taking NUPD action, are given as

$$m_k^{(0,1)} = \left| \operatorname{tr}\left(\hat{\mathbf{P}}_{k+1}^1\right) - \operatorname{tr}\left(\mathbf{P}_{k+1}^1\right) \right|, \quad m_k^{(0,2)} = \left| \operatorname{tr}\left(\hat{\mathbf{P}}_{k+1}^2\right) - \operatorname{tr}\left(\mathbf{P}_{k+1}^2\right) \right|$$

respectively. Then, it is deduced that

$$m_k^{(0,1)} < m_k^{(0,2)} \tag{4.95}$$

by jointly combining (4.91) and (4.93).

Lastly, it is seen that

$$\mathcal{K}_k^1 > \mathcal{K}_k^2$$

by using (4.94) and (4.95).

The main contribution of this statement is that

$$\mathcal{K}_k^1 > \mathcal{K}_k^2 \implies \mu_{th}^1 < \mu_{th}^2 \tag{4.96}$$

owing to the common parameters, α, θ_0, r.

It is known that μ_k^n also specifies the probability of non-maneuvering which is directly proportional to the probability of being in Good state. Hence, it is obvious that

$$\mu_k^1 > \mu_k^2 \tag{4.97}$$

and it is also noticed that

$$\mu_k^1 - \mu_{th}^1 > \mu_k^2 - \mu_{th}^2$$

by jointly combining (4.96) and (4.97). This inequality compares the objective criterion for each target, and ideally helps choose the best target for track update. Because the utilized objective criterion, i.e. $\mu_k^n - \mu_{th}^n$ for target n, combines both absolute and relative informations about each of targets.

Method described for two targets can be extended by induction. When there are more than two targets which request track update for the same instant, all targets can be

sorted with respect to their probability of maneuvering, through the same way. Then, the best target is assigned as a target that has the minimum objective criterion among the targets which request track update, in the following way,

$$i = \underset{n\in\{1,2,\ldots,N_k\}}{\operatorname{argmin}} \{\mu_k^n - \mu_{th}^n\}. \quad \text{subject to } x^n_{\text{requesting},k} = 1; \quad \mu_k^n < \mu_{th}^n \tag{4.98}$$

The constraint given as $\mu_k^n < \mu_{th}^n$ in (4.98) confirms that the optimal action is UPD for the target n. This confirmation sometimes causes that the solution does not exist, namely $i = \emptyset$, when the constraint, $\mu_k^n < \mu_{th}^n$, is not satisfied by all of the candidate targets for target selection. Because μ_{th}^n depends on common parameters, α, θ_0, r, and the cost parameter, $\mathcal{K}_k^n$, which is determined by combining all of the candidate targets for target selection. Hence, it is not guaranteed that $\mu_k^n < \mu_{th}^n$ is always valid even if the target n requests a track update. If i is undefined after using (4.98), the best target can be assigned in the following way

$$i = \underset{n\in\{1,2,\ldots,N_k\}}{\operatorname{argmin}} \{n\}. \quad \text{subject to } x^n_{\text{requesting},k} = 1 \tag{4.99}$$

The method which combines (4.98) and (4.99) is called as the method of decision policy (DecP). Here, (4.98) is always employed, and (4.99) can also be employed if it is required. The DecP is utilized for the scenario shown in Figure 4.1, and PPI displays are shown in Figure 4.9. Non-maneuvering target is tracked more precisely, since the average of tracking error decreases from $\sim 6.5 \times 10^4$ m^2, as shown in Figure 4.5(a), to $\sim 4.6 \times 10^4$ m^2, as shown in Figure 4.10(a). Maneuvering target is also tracked more precisely, since the average of tracking error decreases from $\sim 8.9 \times 10^4$ m^2, as shown in Figure 4.5(b) to $\sim 6.9 \times 10^4$ m^2, as shown in Figure 4.10(b). The highest tracking error of maneuvering target is $\sim 2.5 \times 10^5$ m^2 and it is higher than the highest value of non-maneuvering target $\sim 2.3 \times 10^5$ m^2 obtained between $60 - 70$ s, as shown in Figure 4.10(a).

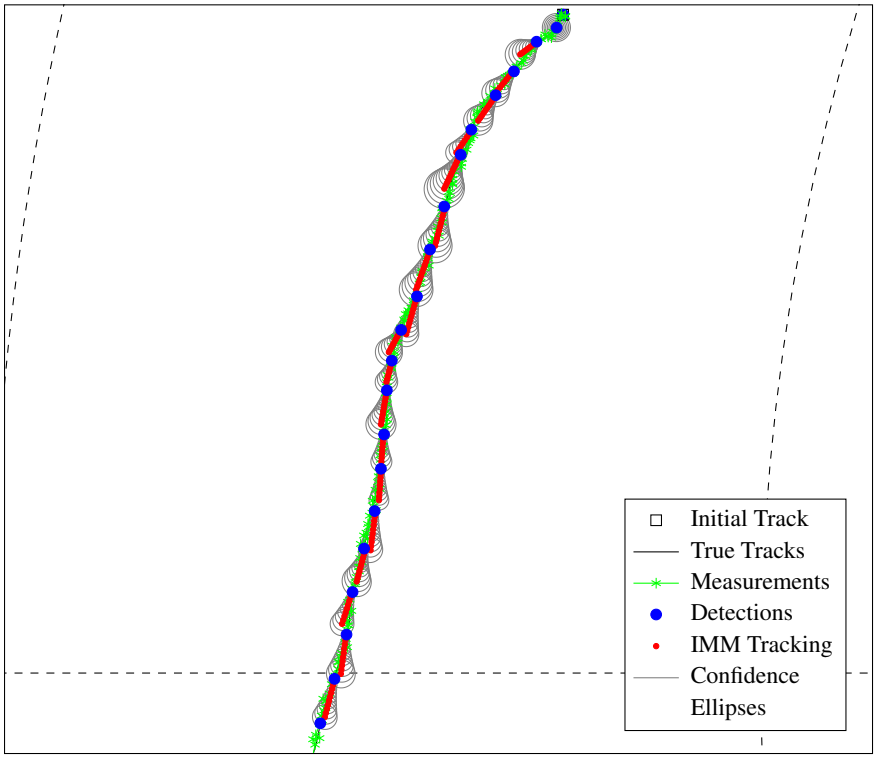

(a)

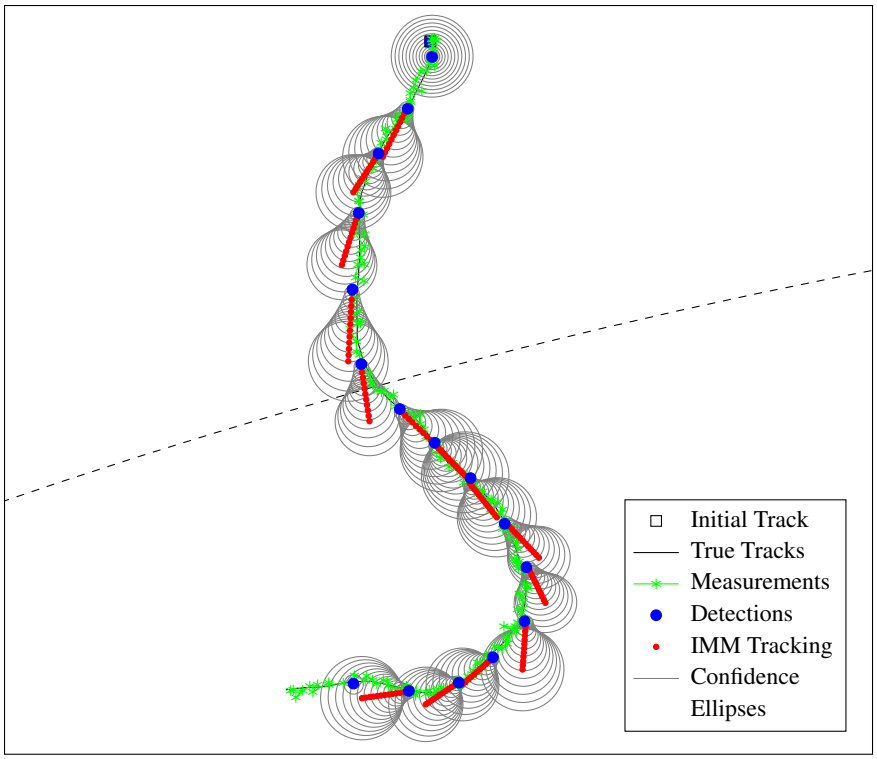

(b)

Figure 4.9: Tracking example of (a) non-maneuvering and (b) maneuvering targets by using the method of decision policy.

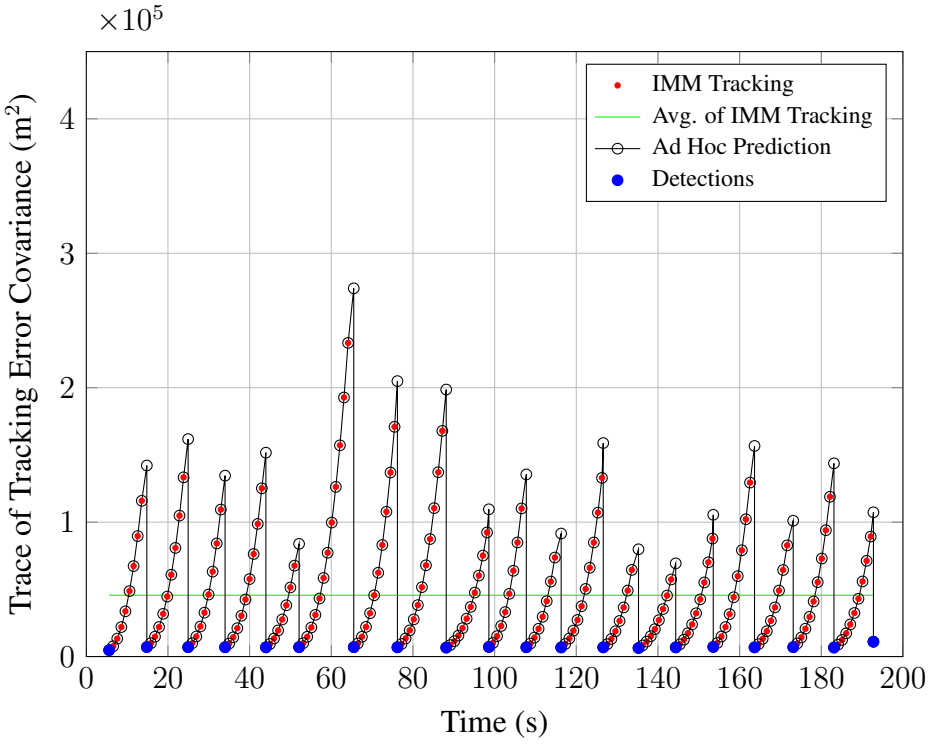

(a)

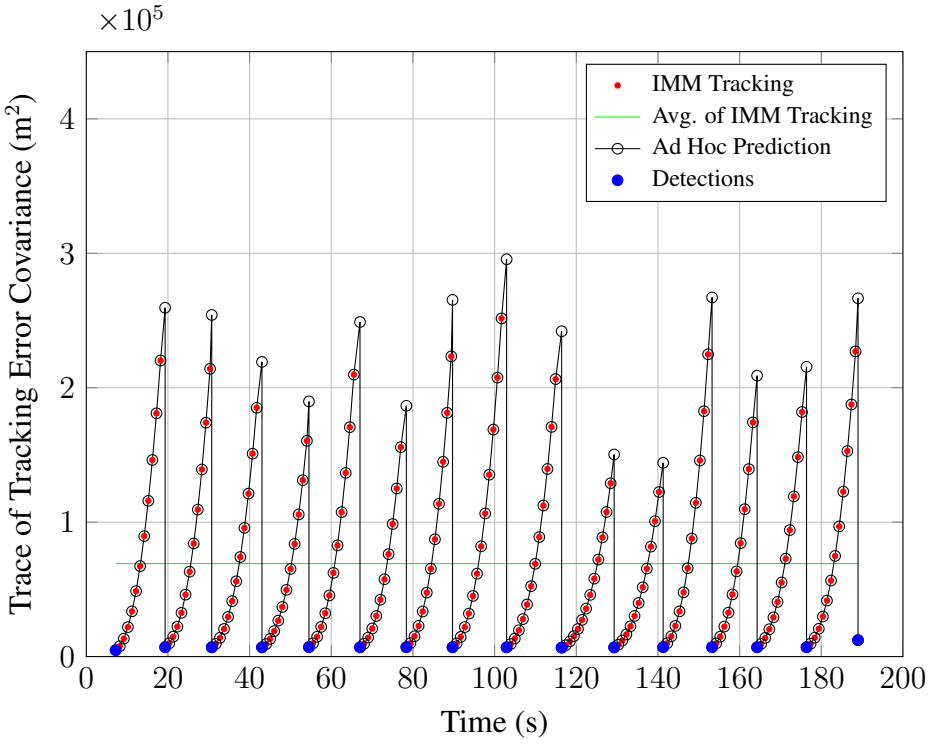

(b)

Figure 4.10: Tracking error covariance example using the method of decision policy for (a) non-maneuvering target and (b) maneuvering target.

The numbers given in the previous paragraph shows that the described method is more preferable in this run. However, it is important to remind that DecP does not guarantee a better operation at every run. After choosing one of the targets, dynamics (position, velocity) of target environment change and the other targets will wait more for the track update. Hence, it is not guaranteed to have a better overall performance. In Chapter 5, additional numerical experiments are given to utilize DecP which is compared with other methods.

Indeed, the approach given in (4.99) is utilized, when there is not a specific method for decision making process. For example, assuming that target 3, target 9 and target 14 have the same TB value, t_{TB}, which is higher than other t_{TB}'s at time k, a TB technique based scheduler verifies that target 9 and target 14 have the same priority level which is higher than the priority level of target 3. Then, the scheduler assigns $x_{\text{requesting},k}$ as 1 for target 9 and target 14, and 0 for other targets. Without utilizing DecP, the scheduler selects target 9 to schedule a tracking task. This case is originated to the service policy; first-come, first-served (FCFS) [62], since the scheduler analyzes targets starting from the target which has the smallest task id, n. Then, the method is called as the method of choosing first target in the update list (CfTUL). The PPI displays shown in Figure 4.1 and the numerical results shown in Figure 4.5 are obtained by using CfTUL as a decision method which exploits the help of (4.99) whenever it is required.

In the following two sections, two different methods which provide other approaches to the same problem are given.

4.2 Method of Minimizing the Tracking Error

In the previous section, it is stated that increment in the trace of error covariance is faster for a highly maneuvering target than a less maneuvering target. Hence, it is thought that the highly maneuvering target increases the average of tracking error faster. Thus, the best target is assigned as a target, the trace of error covariance of whom is the highest one among the targets which request track update, in the following way,

$$i = \underset{n\in\{1,2,\ldots,N_k\}}{\operatorname{argmax}} \left\{ \operatorname{tr}\left(\mathbf{P}_k^n\right) \right\}. \tag{4.100}$$
$$\text{subject to } x^n_{\text{requesting},k} = 1$$

This method is called as the method of minimizing the tracking error (MinTE) and compared with other methods in Chapter 5 which gives the numerical experiments.

4.3 Method of Pursuing the Most Maneuvering

Generally speaking, it is not always valid that the trace of error covariance of a highly maneuvering target is higher than the target which is less maneuvering. An example that supports this statement is previously given in Figure 4.5. The method to minimize the tracking error, described in the previous section, is extended to a novel method by exploiting μ_k^n.

If the probability of non-maneuvering is directly proportional to μ_k^n, then the probability of maneuvering is proportional to $1-\mu_k^n$. Thus, the target can be chosen to update its track via the multiplication of the trace of error covariance and the probability of maneuvering, in the following way,

$$i = \underset{n\in\{1,2,\ldots,N_k\}}{\operatorname{argmax}} \left\{ (1-\mu_k^n+\epsilon) \operatorname{tr}\left(\mathbf{P}_k^n\right) \right\}, \tag{4.101}$$
$$\text{subject to } x^n_{\text{requesting},k} = 1$$

where $\epsilon > 0$ is added to avoid multiplication by zero.

This method is called as the method of pursuing the most maneuvering (PurMM) and compared with other methods in Chapter 5 which gives the numerical experiments.

4.4 Summary

In this chapter, the decision process to choose a target among the targets which require track update concurrently is studied. The method of decision policy based on [57] is

presented analytically for the solution of the problem.

In the final parts of this chapter, two other methods; the method of minimizing the tracking error and the method of pursuing the most maneuvering are proposed as some other ad hoc methods to the problem. These methods are simpler to implement and makes more intuitive sense.

CHAPTER 5

EXPERIMENTAL RESULTS

In this chapter, the experimental results for the comparisons of proposed schedulers (described in Chapter 3) with different decision methods (described in Chapter 4) are given. The simulation environment which supports the described techniques, is written in MATLAB and its operation is briefly presented in Appendix C. The same scenarios and parameters are chosen to make a fair comparison between different methods, unless it is noted otherwise.

For all simulations, the assumptions are as follows:

- Surveillance task is not fragmented and interleaved.
- Surveillance task is periodic and forced to be scheduled whenever it is requested by using dynamic task prioritization.
- Dynamic task prioritization is utilized.
- The scheduler is forced to schedule the surveillance task, before detecting a target or dropping the previously tracked target.

The latter is assumed to make the radar system more realistic, since the surveillance task is scheduled to detect a new target or check one of the existing targets is dropped. In simulations, all target trajectories are generated before the scheduling. The trajectories show the information where each target is at given time. The trajectory information is not known by radar system. The surveillance tasks are scheduled whenever a scheduling technique declares a target drop.

The scenario where $N = 15$ targets are present in the duration of $t_{max} = 500$ s, as shown in Figure 3.10 is considered. A comparison of the proposed scheduling techniques described in Section 3.2, is given in Table 5.1 and the distribution of scheduled tasks are shown in Figure 5.1. Here, the main goal is to see the occupancy and task interleaving capability of the scheduler by using CfTUL as the decision method, and disabling the adaptive update-rate and multi-frequency band usage techniques. In Table 5.1(a), all types of MTATBS and KS are compared when interleaving technique is not applied. The occupancy values are approximately 100% for all of techniques. There is a trade off between the number of surveillance and tracking tasks, since task time of the surveillance is 2 s that is almost 2 times of the task time of a tracking task. Owing to maximization of the instantaneous value, KS schedules mostly tracking tasks and rarely surveillance tasks. All types of MTATBS give similar results. The number of probable drops is related to the lateness of tasks. The MTATBS-Type 1 and MTATBS-Type 3 that the latter is the modified version of the former, are more successful for this scenario and KS has the highest number of probable drops owing to the simpler approach utilized for the micro scheduler.

The cost value depends on the algorithm of scheduler and becomes higher, if there are tasks which are not properly scheduled. Thus, the updating method of t_{TB} for MTATBS-Type 1 and MTATBS-Type 2, and the surveillance task for KS increase their cost. The criterion, average of errors, can be thought to be decreased by increasing the number of tracking tasks. However, this is not always true. Because the average of errors for a target is to be decreased, when the target is precisely tracked. Thus, average of errors which combines all of targets, is not proportional to the number of tracking tasks, as shown the table.

In Table 5.1(b), all types of MTATBS are compared when task interleaving technique is applied. Here, the cost, the number of probable drops and the occupancy rates are smaller than the previous case. Hence, the radar seems to be underloaded. The number of tracking tasks are higher due to task interleaving, while the number of surveillance tasks which cannot be interleaved, does not significantly change. The comment about the average of error still holds. The MTATBS-Type 2 has the highest value for both the number tracking tasks and the average of errors.

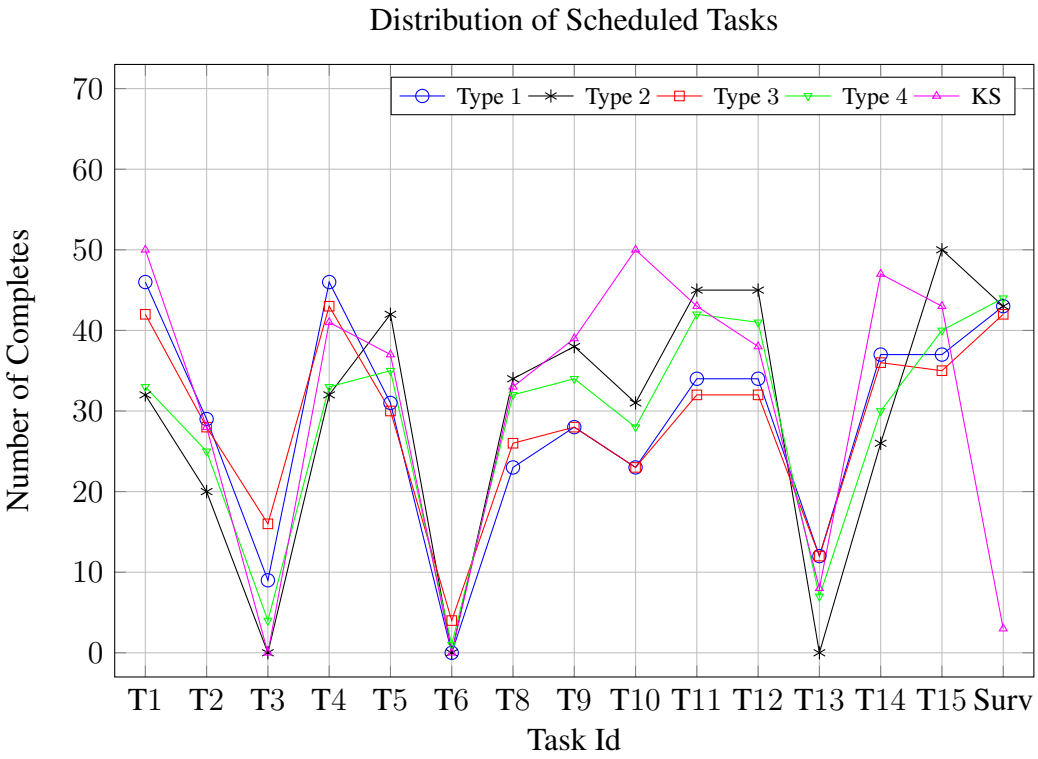

(a) Task interleaving technique is disabled.

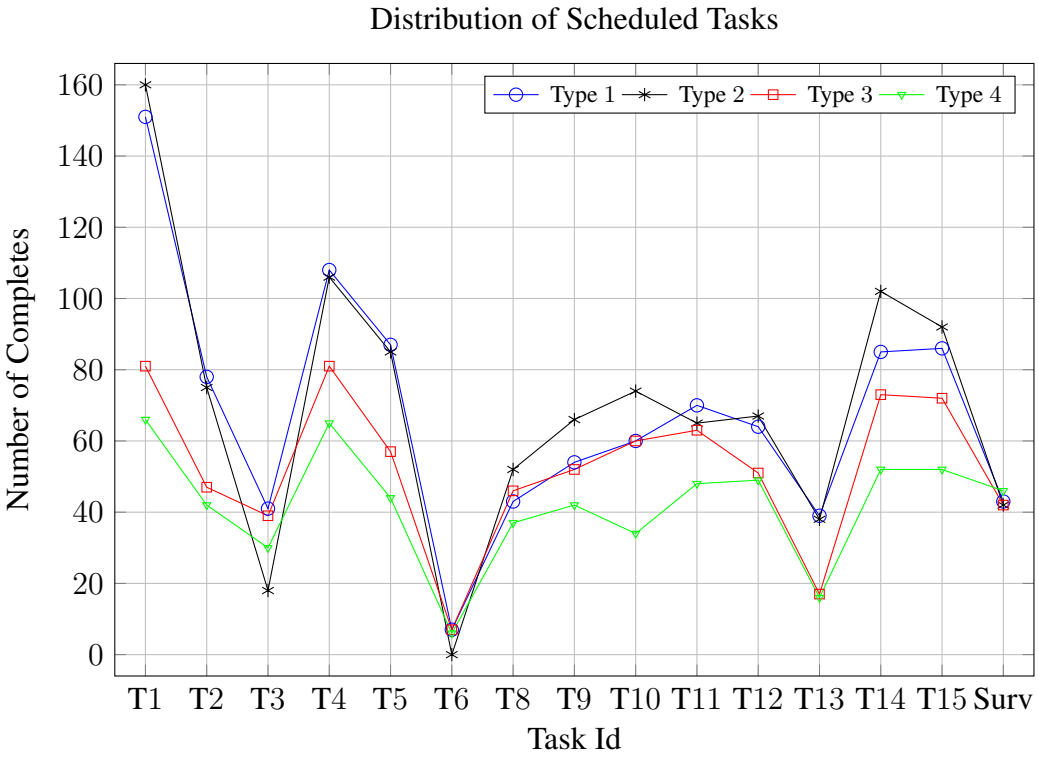

(b) Task interleaving technique is enabled.

Figure 5.1: Comparison of techniques within the distribution of scheduled tasks.

Table5.1: Comparison of scheduling techniques when task interleaving technique is (a) disabled and (b) enabled by using CfTUL as the decision method, and disabling adaptive update-rate and multi-frequency band usage techniques.

(a)

	Type 1	Type 2	Type 3	Type 4	KS
# of tracking tasks	389	395	387	385	**457**
# of surveillances	43	43	42	**44**	3
# of prob. drops	**15**	39	19	37	66
Occupancy (%)	**100.00**	**100.00**	99.52	98.90	99.60
Cost (s^2)	3.94×10^{7}	9.74×10^{6}	2.20×10^{4}	$\mathbf{1.68\times10^{4}}$	2.16×10^{5}
Avg. of errors (m^2)	1.70×10^{5}	1.53×10^{5}	1.46×10^{5}	1.56×10^{5}	$\mathbf{1.45\times10^{5}}$

(b)

	Type 1	Type 2	Type 3	Type 4
# of tracking tasks	973	**1000**	746	583
# of surveillances	43	42	42	**46**
# of prob. drops	15	28	13	**1**
Occupancy (%)	59.33	**60.24**	48.93	43.05
Cost (s^2)	9.68×10^{3}	2.61×10^{4}	0.52×10^{3}	$\mathbf{0.49\times10^{3}}$
Avg. of errors (m^2)	$\mathbf{3.38\times10^{4}}$	1.08×10^{5}	4.51×10^{4}	5.83×10^{4}

The effects of the multi-frequency band usage on scheduling is shown in Table 5.2 for the same scenario shown in Figure 3.10. Here, the main goal is to see the occupancies provided by the schedulers when task interleaving technique is applied by jointly using the multi-frequency band usage technique. In Table 5.2(a) and Table 5.2(b), the number of available frequency bands is set as 2 and 7, respectively. The higher number of frequency bands increases the scheduling performance; higher number of scheduled tasks, smaller cost, smaller number of probable drops, higher occupancy, smaller average of errors due to increment in the utilization of the radar timeline.

Up to here, the simulations are run on a specific scenario. From now on, the comparisons are made on the average of the scheduler performance by running them on the identical scenario with randomly generated targets for 100 times. That is at every run, $N = 15$ and $N = 25$ targets are moving for the duration of $t_{max} = 200$ s.

Table5.2: Effects of multi-frequency band usage technique on scheduling when the number of frequency bands is (a) 2 and (b) 7.

(a)

	Type 1	Type 2	Type 3	Type 4
# of tracking tasks	921	759	**934**	860
# of surveillances	36	36	**37**	36
# of prob. drops	83	**54**	70	103
Occupancy (%)	55.41	46.96	**56.41**	51.94
Cost (s^2)	3.21×10^6	3.59×10^6	$\mathbf{3.85\times10^3}$	3.11×10^5
Avg. of errors (m^2)	3.76×10^4	3.60×10^4	$\mathbf{3.15\times10^4}$	1.82×10^5

(b)

	Type 1	Type 2	Type 3	Type 4
# of tracking tasks	1447	**1492**	1307	1335
# of surveillances	**42**	41	40	40
# of prob. drops	17	30	24	**16**
Occupancy (%)	81.09	**82.67**	74.06	75.18
Cost (s^2)	3.13×10^5	5.44×10^4	$\mathbf{0.44\times10^3}$	0.55×10^3
Avg. of errors (m^2)	$\mathbf{1.55\times10^4}$	2.15×10^4	1.71×10^4	1.67×10^4

The distribution of scheduler rankings with respect to average of errors is given at the end of each table. This ranking given in the tables will denote that average and the scenario based performance are not proportional which holds the comment about the average of tracking error.

In Table 5.3, all types of MTATBS and KS are compared when task interleaving technique is not applied. Here, the main goal is to see the statistics (the average of errors and the number of probable drops) of the scheduler by using CfTUL as the decision method, and disabling the adaptive update-rate technique. These optional techniques are disabled to see core performance of the schedulers. Moreover, all types of MTATBS are ranked within each other, as shown in parenthesis.

Table5.3: Comparison of scheduling techniques for (a) $N = 15$ and (b) $N = 25$ targets by disabling task interleaving and adaptive update-rate techniques, within the duration of $t_{max} = 200$ s.

(a)

	Average of statistics after 100 simulations				
	Type 1	Type 2	Type 3	Type 4	KS
# of tracking tasks	148.16	153.02	148.17	151.12	**177.34**
# of surveillances	18.54	**18.59**	18.35	18.45	2.71
# of prob. drops	32.07	10.61	29.53	17.43	**9.96**
Occupancy (%)	**100.00**	**100.00**	99.85	99.76	99.59
Cost (s^2)	1.46×10^6	8.32×10^5	$\mathbf{1.14\times10^4}$	1.10×10^5	2.16×10^4
Avg. of errors (m^2)	3.35×10^5	2.54×10^5	2.37×10^5	3.28×10^5	$\mathbf{1.77\times10^5}$
	Distributions of rankings with respect to avg. of errors				
Best	2(5)	**46**(**59**)	3(21)	7(15)	42
Runner-up	5(14)	13(10)	29(**59**)	11(17)	**42**
Honorable Mention	14(**40**)	12(13)	**50**(20)	16(27)	8
Last	38(**41**)	18(18)	0(0)	**39**(**41**)	5

(b)

	Average of statistics after 100 simulations				
	Type 1	Type 2	Type 3	Type 4	KS
# of tracking tasks	132.51	140.12	132.33	139.08	**183.91**
# of surveillances	26.90	**27.15**	26.98	27.09	0.50
# of prob. drops	100.80	16.33	103.99	25.55	**13.13**
Occupancy (%)	**100.00**	**100.00**	**100.00**	**100.00**	**100.00**
Cost (s^2)	5.38×10^6	2.85×10^6	1.96×10^5	1.39×10^6	$\mathbf{3.55\times10^4}$
Avg. of errors (m^2)	1.44×10^6	$\mathbf{4.09\times10^5}$	1.22×10^6	6.02×10^5	8.44×10^5
	Distributions of rankings with respect to avg. of errors				
Best	0(0)	**66**(**68**)	0(0)	30(32)	4
Runner-up	1(2)	25(26)	4(15)	**39**(**57**)	31
Honorable Mention	5(25)	3(2)	33(**70**)	21(3)	**38**
Last	**55**(**73**)	3(4)	14(15)	7(8)	21

In Table 5.3(a) and Table 5.3(b), the number of targets is set as 15 which refers full-load, and 25 which refers overload, respectively. In full-load case, KS has the smallest number probable drops and average of errors. According to ranking distribution, KS competes with MTATBS-Type 2. However, MTATBS-Type 3 has the smallest average of errors within all types of MTATBS. The reason of this can be seen from the distribution of rankings that MTATBS-Type 3 has not provided the worst result. When the number of probable drops is taken into account, MTATBS-Type 2 and MTATBS-Type 4 show better performance, while KS is the best. These types of MTATBS schedules only more important tasks. Thus, one or more targets which are less important, may not be included in scheduling process and the other targets are properly scheduled. In over-load case, MTATBS-Type 2 shows better performance. It has the smallest average of errors and shows the best performance for 66 times out of 100. The number of probable drops is also better for this scheduler, while MTATBS-Type 1 and MTATBS-Type 3 which try to schedule all of the targets, show worse performance. Owing to the results given Table 5.3, MTATBS-Type 2 which outperforms the others for both of the cases, seems as a good choice.

In Table 5.4, all types of MTATBS are compared when task interleaving technique is applied without multi-frequency band usage technique. In Table 5.4(a), MTATBS-Type 1 and MTATBS-Type 2 show better performance than the others. The former has the best values for both the average of errors and the number of probable drops. The MTATBS-Type 3 and MTATBS-Type 4 show similar performance. The number of tracking tasks and hence, the occupancy values of them are smaller owing that they differ from the others by setting t_{TB} as the negative of the task update time after scheduling the task. The occupancies change between 50% and 55%, since the full-load case turns into under-load case, after employing the task interleaving.

In Table 5.4(b), MTATBS-Type 1 has the smallest average of errors, while MTATBS-Type 2 has the smallest number of probable drops. The MTATBS-Type 2 has both the highest number of tracking tasks and the highest average of errors that the similar case is previously emphasized in Table 5.1(b). The MTATBS-Type 3 and MTATBS-Type 4 show similar performance which can be said to be better than the performance of MTATBS-Type 2.

Table5.4: Comparison of scheduling techniques for (a) $N = 15$ and (b) $N = 25$ targets by enabling task interleaving technique, and disabling adaptive update-rate and multi-frequency band usage techniques, within the duration of $t_{max} = 200$ s.

(a)

	Average of statistics after 100 simulations			
	Type 1	Type 2	Type 3	Type 4
# of tracking tasks	322.15	**323.54**	287.83	288.26
# of surveillances	**19.19**	19.09	19.11	19.10
# of prob. drops	**3.18**	3.90	3.65	4.22
Occupancy (%)	54.62	**54.66**	50.75	50.75
Cost (s^2)	5.91×10^2	5.74×10^2	4.07×10^2	$\mathbf{3.33\times10^2}$
Avg. of errors (m^2)	$\mathbf{4.92\times10^4}$	5.02×10^4	5.63×10^4	5.66×10^4
	Distributions of rankings with respect to avg. of errors			
Best	**47**	38	5	10
Runner-up	**37**	35	13	15
Honorable Mention	13	19	**41**	27
Last	3	8	41	**48**

(b)

	Average of statistics after 100 simulations			
	Type 1	Type 2	Type 3	Type 4
# of tracking tasks	491.87	**519.55**	443.72	455.30
# of surveillances	25.86	25.91	25.98	**26.12**
# of prob. drops	24.70	**23.20**	24.66	23.98
Occupancy (%)	80.11	**82.61**	74.89	75.94
Cost (s^2)	9.24×10^4	7.05×10^4	$\mathbf{5.56\times10^3}$	7.25×10^3
Avg. of errors (m^2)	$\mathbf{8.61\times10^4}$	1.41×10^5	8.96×10^4	8.90×10^4
	Distributions of rankings with respect to avg. of errors			
Best	**54**	16	13	17
Runner-up	24	11	**41**	24
Honorable Mention	19	5	31	**45**
Last	3	**68**	15	14

Owing to the results given Table 5.4, MTATBS-Type 1 which outperforms the others for both of the cases, seems as a good choice. Although, MTATBS-Type 1 and MTATBS-Type 2 are the leading schedulers, they are not suggested to employ on a real system. Because it is said that the consecutive updates consume vast radar time resources, in Section 3.2.1.5, and both of these schedulers exploit the consecutive updates. Then, MTATBS-Type 3 and MTATBS-Type 4 are preferable that the former tries to schedule all tasks and the latter schedules only more important tasks. If the results given in Table 5.3 and Table 5.4, are revised, it is seen that MTATBS-Type 4 shows better performance for over-load case. Hence, MTATBS-Type 4 is chosen as the base scheduler for the following comparisons.

In Table 5.5 and Table 5.6, the decision methods are compared when there are $N = 15$ and $N = 25$ targets, respectively. Here, the main goal is to see the statistics, the average of errors and the number of probable drops, of MTATBS-Type 4 by using each of the decision methods, and applying the adaptive update-rate and multi-frequency band usage techniques. Furthermore, the effect of multi-frequency band usage technique on the tracking performance is compared by setting the number of frequency bands as 2 that the results are given in Table 5.5(a) and Table 5.6(a), and 7 that the results are given in Table 5.5(b) and Table 5.6(b). The proposed methods, DeCP, MinTE and PurMM are compared with CfTUL which is assigned as the reference method. Then, DecP is the unique method which has the smaller number of probable drops and the smaller average of errors than CfTUL owing to the results given in these tables. Indeed, there is not a significant difference between the results of the proposed methods. All of them are usually better than CfTUL that is concluded from the distribution of rankings. The PurMM has the smallest average of errors, and MinTE shows more frequently the best performance than the others when there are 25 targets, as shown in Table 5.6.

Table5.5: Comparison of the decision methods by enabling adaptive update-rate technique and the number of frequency bands is (a) 2 and (b) 7 by scheduling $N = 15$ targets with MTATBS-Type4 within the duration of $t_{max} = 200$ s.

(a)

	Average of statistics after 100 simulations			
	CfTUL	DecP	MinTE	PurMM
# of tracking tasks	**296.94**	296.05	294.24	**296.94**
# of surveillances	17.55	**17.68**	17.54	17.57
# of prob. drops	24.98	**24.05**	24.54	24.68
Occupancy (%)	49.81	**49.83**	49.46	49.82
Cost (s^2)	1.77×10^4	2.12×10^4	$\mathbf{1.68\times10^4}$	1.99×10^4
Avg. of errors (m^2)	1.97×10^5	$\mathbf{1.82\times10^5}$	1.95×10^5	2.06×10^5
	Distributions of rankings with respect to avg. of errors			
Best	**27**	26	25	22
Runner-up	17	27	25	**31**
Honorable Mention	20	**29**	28	23
Last	**36**	18	22	24

(b)

	Average of statistics after 100 simulations			
	CfTUL	DecP	MinTE	PurMM
# of tracking tasks	365.36	366.98	364.83	**367.98**
# of surveillances	**19.25**	19.15	**19.25**	19.12
# of prob. drops	14.72	**14.10**	14.92	14.29
Occupancy (%)	59.35	59.46	59.31	**59.52**
Cost (s^2)	0.44×10^3	$\mathbf{0.40\times10^3}$	0.41×10^3	0.47×10^3
Avg. of errors (m^2)	7.12×10^4	6.94×10^4	7.14×10^4	$\mathbf{6.92\times10^4}$
	Distributions of rankings with respect to avg. of errors			
Best	**31**	23	17	29
Runner-up	16	30	**32**	22
Honorable Mention	21	**30**	20	29
Last	**32**	17	31	20

Table5.6: Comparison of the decision methods by enabling adaptive update-rate technique and the number of frequency bands is (a) 2 and (b) 7 by scheduling $N = 25$ targets with MTATBS-Type 4 within the duration of $t_{max} = 200$ s.

(a)

	Average of statistics after 100 simulations			
	CfTUL	DecP	MinTE	PurMM
# of tracking tasks	**308.11**	305.52	303.14	305.82
# of surveillances	24.53	24.64	24.58	**24.75**
# of prob. drops	43.81	**42.47**	43.75	44.03
Occupancy (%)	57.30	57.12	56.81	**57.25**
Cost (s^2)	$\mathbf{3.04\times10^5}$	3.75×10^5	3.46×10^5	3.37×10^5
Avg. of errors (m^2)	7.28×10^5	6.67×10^5	6.93×10^5	$\mathbf{6.33\times10^5}$
	Distributions of rankings with respect to avg. of errors			
Best	17	29	**33**	21
Runner-up	17	25	20	**38**
Honorable Mention	**33**	28	20	19
Last	**33**	18	27	22

(b)

	Average of statistics after 100 simulations			
	CfTUL	DecP	MinTE	PurMM
# of tracking tasks	511.81	**513.66**	512.67	512.64
# of surveillances	25.84	**25.90**	25.88	25.87
# of prob. drops	45.03	43.68	**43.40**	43.43
Occupancy (%)	81.65	**81.91**	81.76	81.78
Cost (s^2)	$\mathbf{2.12\times10^4}$	2.59×10^4	2.34×10^4	2.23×10^4
Avg. of errors (m^2)	1.51×10^5	1.46×10^5	1.43×10^5	$\mathbf{1.42\times10^5}$
	Distributions of rankings with respect to avg. of errors			
Best	17	25	**32**	26
Runner-up	21	**30**	23	26
Honorable Mention	24	**27**	23	26
Last	**38**	18	22	22

CHAPTER 6

CONCLUSIONS AND FUTURE WORK

In this work, two schedulers are examined, namely MTATBS and KS for the real-time resource management of MFPAR. A resource-aided technique called as the multi-frequency band usage, is developed to increase the applicability of task interleaving.

The KS which employs the binary integer programming is proposed to suggest a simple optimization technique for RRM. The KS is compared with TB based techniques. However, it is concluded that the computation time requirement of KS is too much for real-time operation. The higher number of targets makes the scheduling almost intractable for KS. Moreover, the resource-aided techniques except the adaptive update-rate are not applicable for it. Thus, TB based techniques comprise the main part of this work.

The MTATBS utilizes the existing ATB scheduler algorithm described in [48] with some improvements:

1. Scheduling parameters can be dynamically changed by tracker in addition to scheduler.
2. Scheduling utilizes multi-frequency bands for interleaved tasks.
3. Decision method which is previously the selection of a task with the highest priority and t_{TB}, of TB technique based schedulers is modified.

The decision process is required when there are at least two targets which satisfy the maximum priority level and t_{TB} for MTATBS. The traditional method is to choose the

target which has the smallest task id among candidate targets for track update. This does not guarantees an appropriate performance. We suggest to adopt the solution methods for the well-known machine replacement problem to the problem of target selection and track update is solved with a method called DecP. In addition to this method, two other ad hoc methods, namely MinTE and PurMM, are given.

The results show that all TB based techniques provide similar performance with minor differences. Task interleaving and the multi-frequency band usage techniques increase the tracking performance and the utilization of radar timeline effectively. Decision methods based on machine replacement and others increase the tracking performance and decrease the number probable drops. The MTATBS-Type 4 and DeCP is suggested as the scheduler and the decision method respectively. It should be noted minor performance differences not easily reflected in averaged results can be important for the practical applications. Hence, the decision policy based on track quality can be important in general.

To conduct experiments, a simulator for MFPAR system is implemented to apply RRM techniques with different optional choices, such as adaptive update-rate, dynamic task prioritization, tracking, task interleaving. The simulator which combines the model shown in Figure 2.1, is designed in a way that each of the blocks can be individually modified according to RRM constraints. Hence, the development of general purpose simulator is one of the main contributions of this work.

Among future works, it can be useful to utilize the optimization-based methods for the scheduling problem and compare the optimization-based methods and MTATBS with our simulator. In addition, the simulator can be modified to handle the radar equation, probability of detection, false alarm values and other related parameters.

REFERENCES

[1] M. I. Skolnik. *Introduction to radar systems*. Tata McGraw Hill, 772 pp., 2003.

[2] Z. Ding. A survey of radar resource management algorithms. In *Canadian Conference on Electrical and Computer Engineering, 2008. CCECE 2008*, pages 1559–1564, May 2008.

[3] S. Sabatini and M. Tarantino. *Multifunction Array Radar: System Design and Analysis*. The Artech House Radar Library. Artech House, 271 pp., 1994.

[4] B. Gillespie, E. Hughes, and M. Lewis. Scan scheduling of multi-function phased array radars using heuristic techniques. In *IEEE International Radar Conference*, pages 513–518, May 2005.

[5] A. G. Huizing and A. A. F. Bloemen. An efficient scheduling algorithm for a multifunction radar. In *IEEE International Symposium on Phased Array Systems and Technology, 1996*, pages 359–364, Oct. 1996.

[6] A. J. Orman, C. N. Potts, A. K. Shahani, and A. R. Moore. Scheduling for a multifunction array radar system. *European Journal of Operational Research*, 90(1):13–25, 1996.

[7] A. Izquierdo-Fuente and J. R. Casar-Corredera. Optimal radar pulse scheduling using a neural network. In *1994 IEEE International Conference on Neural Networks. IEEE World Congress on Computational Intelligence*, volume 7, pages 4588–4591, June 1994.

[8] W. Komorniczak and J. Pietrasiñski. Selected problems of MFR resources management. In *Proceedings of the 3rd International Conference on Information Fusion, 2000. FUSION 2000*, volume 2, pages WEC1/3–WEC1/8 vol.2, July 2000.

[9] R. Popoli and S. Blackman. Expert system allocation for the electronically scanned antenna radar. In *American Control Conference, 1987*, pages 1821–1826, Minneapolis, MN, USA, June 1987.

[10] V. C. Vannicola and J. A. Mineo. Expert system for sensor resource allocation. In *Proceedings of the 33rd Midwest Symposium on Circuits and Systems, 1990*, volume 2, pages 1005–1008, Aug. 1990.

[11] S. Miranda, C. Baker, K. Woodbridge, and H. Griffiths. Knowledge-based resource management for multifunction radar: a look at scheduling and task prioritization. *IEEE Signal Processing Magazine*, 23(1):66–76, Jan. 2006.

[12] S. L. C. Miranda, C. J. Baker, K. Woodbridge, and H. D. Griffiths. Simulation methods for prioritising tasks and sectors of surveillance in phased array radars. *International Journal of Simulation*, 5(1-2):18–25, 2004.

[13] S. L. C. Miranda, C. J. Baker, K. Woodbridge, and H. D. Griffiths. Fuzzy logic approach for prioritisation of radar tasks and sectors of surveillance in multi-function radar. *Radar, Sonar Navigation, IET*, 1(2):131–141, Apr. 2007.

[14] M. T. Vine. Fuzzy logic in radar resource management. In *IEE Multifunction Radar and Sonar Sensor Management Techniques (Ref. No. 2001/173)*, pages 5/1–5/4, Nov. 2001.

[15] D. P. Bertsekas. *Dynamic Programming and Optimal Control*, volume 1. Athena Scientific, 400 pp., Belmont, MA, USA, 1995.

[16] D. Strömberg and P. Grahn. Scheduling of tasks in phased array radar. In *Proceedings of IEEE International Symposium on Phased Array Systems and Technology*, pages 318–321, 1996.

[17] J. Wintenby and V. Krishnamurthy. Hierarchical resource management in adaptive airborne surveillance radars. *IEEE Transactions on Aerospace and Electronic Systems*, 42(2):401–420, Apr. 2006.

[18] R. Washburn, M. Schneider, and J. Fox. Stochastic dynamic programming based approaches to sensor resource management. In *Proceedings of the 5th International Conference on Information Fusion, 2002*, volume 1, pages 608–615, Annapolis, MD, USA, 2002.

[19] V. Krishnamurthy and R. J. Evans. Hidden Markov model multiarm bandits: a methodology for beam scheduling in multitarget tracking. *IEEE Transactions on Signal Processing*, 49(12):2893–2908, Dec. 2001.

[20] V. Krishnamurthy and R. J. Evans. Correction to 'Hidden Markov model multi-arm bandits: a methodology for beam scheduling in multitarget tracking'. *IEEE Transactions on Signal Processing*, 51(6):1662–1663, June 2003.

[21] B. F. La Scala and B. Moran. Optimal target tracking with restless bandits. *Digital Signal Processing*, 16(5):479–487, Sept. 2006.

[22] A. O. Hero III, D. A. Castañón, D. Cochran, and K. Kastella. *Foundations and Applications of Sensor Management*. Signals and Communication Technology. Springer, 308 pp., 2008.

[23] J. Wintenby. *Resource Allocation in Airborne Surveillance Radar*. PhD thesis, Chalmers University Of Technology, Göteborg, Sweden, 2003.

[24] A. G. Huizing and J. A. Spruyt. Adaptive waveform selection with a neural network. In *International Conference Radar 92*, pages 419–421, Oct. 1992.

[25] B. F. La Scala, W. Moran, and R. J. Evans. Optimal adaptive waveform selection for target detection. In *Proceedings of the International Radar Conference*, pages 492–496, Sept. 2003.

[26] D. Cochran, S. Suvorova, S. D. Howard, and B. Moran. Waveform libraries: Measures of effectiveness for radar scheduling. *IEEE Signal Processing Magazine*, 26(1):12–21, Jan. 2009.

[27] B. La Scala, M. Rezaeian, and B. Moran. Optimal adaptive waveform selection for target tracking. In *The 8th International Conference on Information Fusion*, volume 1, pages 552–557, July 2005.

[28] S. M. Sowelam and A. H. Tewfik. Waveform selection in radar target classification. *IEEE Transactions on Information Theory*, 46(3):1014–1029, May 2000.

[29] G. van Keuk and S. S. Blackman. On phased-array radar tracking and parameter control. *IEEE Transactions on Aerospace and Electronic Systems*, 29(1):186–194, Jan. 1993.

[30] G. A. Watson and W. D. Blair. Revisit calculation and waveform control for a multifunction radar. In *Proceedings of the 32nd IEEE Conference on Decision and Control*, volume 1, pages 456–460, San Antonio, TX, USA, Dec. 1993.

[31] H.-J. Shin, S.-M. Hong, and D.-H. Hong. Adaptive-update-rate target tracking for phased-array radar. *IEE Proceedings - Radar, Sonar and Navigation*, 142(3):137–143, June 1995.

[32] S.-M. Hong and Y.-H. Jung. Optimal scheduling of track updates in phased array radars. *IEEE Transactions on Aerospace and Electronic Systems*, 34(3):1016–1022, July 1998.

[33] W. D. Blair, G. A. Watson, and S. A. Hoffman. Benchmark problem for beam pointing control of phased array radar against maneuvering targets. In *Proceedings of the American Control Conference*, volume 2, pages 2071–2075, Baltimore, MD, USA, June 1994.

[34] W. D. Blair, G. A. Watson, G. L. Gentry, and S. A. Hoffman. Benchmark problem for beam pointing control of phased array radar against maneuvering targets in the presence of ECM and false alarms. In *Proceedings of the American Control Conference*, volume 4, pages 2601–2605, Seattle, WA, USA, June 1995.

[35] W. D. Blair and G. A. Watson. Benchmark problem for radar resource allocation and tracking maneuvering targets in the presence of ECM. Technical Report NSWCDD/TR-96/10, Naval Surface Warfare Center Dahlgren Division, Dahlgren, VA, USA, Sept. 1996.

[36] W. D. Blair, G. A. Watson, T. Kirubarajan, and Y. Bar-Shalom. Benchmark for radar allocation and tracking in ECM. *IEEE Transactions on Aerospace and Electronic Systems*, 34(4):1097–1114, Oct. 1998.

[37] S. S. Blackman, M. T. Busch, G. Demos, and R. F. Popoli. IMM/MHT tracking and data association for benchmark tracking problem. In *Proceedings of the American Control Conference*, volume 4, pages 2606–2610, Seattle, WA, USA, June 1995.

[38] Y. Bar-Shalom and X.-R. Li. *Multitarget-multisensor Tracking: Principles And Techniques*. YBS Publishing, 615 pp., Storrs, CT, USA, 1995.

[39] T. Kirubarajan, Y. Bar-Shalom, W. D. Blair, and G. A. Watson. IMMPDAF for radar management and tracking benchmark with ECM. *IEEE Transactions on Aerospace and Electronic Systems*, 34(4):1115–1134, Oct. 1998.

[40] C. Lee. *On Quality of Service Management*. PhD thesis, Carnegie Mellon University, Pittsburgh, PA, USA, Aug. 1999.

[41] R. Rajkumar, C. Lee, J. Lehoczky, and D. Siewiorek. A resource allocation model for QoS management. In *Proceedings of the 18th IEEE Real-Time Systems Symposium, 1997*, pages 298–307, Dec. 1997.

[42] S. Ghosh, J. Hansen, R. (Raj) Rajkumar, and J. Lehoczky. Integrated resource management and scheduling with multi-resource constraints. In *Proceedings of the 25th IEEE International Real-Time Systems Symposium, 2004*, pages 12–22, Lisbon, Portugal, Dec. 2004.

[43] S. Ghosh, J. Hansen, R. (Raj) Rajkumar, and J. Lehoczky. Adaptive QoS optimizations with applications to radar tracking. Technical Report 18-03-04, Institute for Complex Engineering Systems, Carnegie Mellon University, 2004.

[44] J. Hansen, R. Rajkumar, J. Lehoczky, and S. Ghosh. Resource management for radar tracking. In *IEEE Conference on Radar, 2006. RADAR '06*, pages 140–147, Verona, NY, USA, Apr. 2006.

[45] A. Ircı. *On Optimal Resource Allocation in Multifunction Radar Systems*. MSc thesis, Middle East Technical University, Ankara, Turkey, Sept. 2006.

[46] W. K. Stafford. Real time control of a Multifunction Electronically Scanned Adaptive Radar, (MESAR). *IEE Colloquium on Real-Time Management of Adaptive Radar Systems*, pages 7/1–7/5, June 1990.

[47] J. M. Butler. *Tracking and Control in Multi-Function Radar*. PhD thesis, University College London, 1998.

[48] R. Reinoso-Rondinel, T.-Y. Yu, and S. Torres. Task prioritization on phased-array radar scheduler for adaptive weather sensing. *The 26th International Conference on Interactive Information and Processing Systems (IIPS) for Meteorology, Oceanography, and Hydrology. American Meteorological Society*, Paper 14B.6, Atlanta, GA, USA, 2010.

[49] F. Opitz and T. Kausch. UKF controlled variable-structure IMM algorithms using coordinated turn models. In *Proceedings of the 7th International Conference on Information Fusion, 2004. FUSION 2004*, volume I, pages 138–145, Mountain View, CA, USA, June 2004. International Society of Information Fusion.

[50] A. J. Orman and C. N. Potts. On the complexity of coupled-task scheduling. *Discrete Applied Mathematics*, 72(1–2):141–154, 1997.

[51] G. B. Thomas and R. L. Finney. *Calculus and Analytic Geometry, 9th ed.* Addison-Wesley, 1264 pp., 1995.

[52] M. Wray. Software architecture for real time control of the radar beam within MESAR. In *International Conference Radar 92*, pages 38–41, Oct 1992.

[53] R. Reinoso-Rondinel, T.-Y. Yu, and S. Torres. Multifunction phased-array radar: Time balance scheduler for adaptive weather sensing. *Journal of Atmospheric and Oceanic Technology*, 27:1854–1867, 2010.

[54] B. Korte and J. Vygen. *Combinatorial Optimization: Theory and Algorithms*. Algorithms and Combinatorics 21. Springer Berlin Heidelberg, 597 pp., 2006.

[55] G. B. Dantzig. Discrete-variable extremum problems. *Operations Research*, 5(2):266–277, Apr. 1957.

[56] D. Pisinger. *Algorithms for Knapsack Problems*. PhD thesis, University of Copenhagen, 1995.

[57] T. Ben-Zvi and A. Grosfeld-Nir. Partially observed Markov decision processes with binomial observations. *Operations Research Letters*, 41(2):201–206, 2013.

[58] S. Anily and A. Grosfeld-Nir. An optimal lot-sizing and offline inspection policy in the case of nonrigid demand. *Operations Research*, 54(2):311–323, 2006.

[59] P. R. Kumar and P. Varaiya. *Stochastic Systems: Estimation, Identification, and Adaptive Control*. Information and System Sciences Series. Prentice-Hall, Inc., 358 pp., Englewood Cliffs, NJ, USA, 1986.

[60] R. D. Smallwood and E. J. Sondik. The optimal control of partially observable markov processes over a finite horizon. *Operations Research*, 21(5):1071–1088, 1973.

[61] M. Givon and A. Grosfeld-Nir. Using partially observed markov processes to select optimal termination time of TV shows. *Omega*, 36(3):477–485, 2008. Special Issue on Multiple Criteria Decision Making for Engineering.

[62] A. Silberschatz, P. B. Galvin, and G. Greg. *Operating System Concepts*. John Wiley & Sons, Inc., 944 pp., 2013.

[63] Y. Bar-Shalom, X.-R. Li, and T. Kirubarajan. *Estimation with Applications to Tracking and Navigation*. John Wiley & Sons, Inc., 584 pp., New York, NY, USA, July 2001.

APPENDIX A

INTERACTING MULTIPLE MODEL FILTER FOR TRACKING

The interacting multiple model (IMM) is an efficient estimation technique for maneuvering targets. The possible target maneuvers are described by a finite state model. The IMM is able to give accurate estimation results, whenever the true target maneuver fits with a single maneuver model of the implemented discrete set. The additional gain of the IMM is to extend the covered target maneuver by a statistical mixing of the elements of the model set. A widely used model set contains the constant velocity model (CV) and coordinated turn model (CT) with fixed angular velocity [49].

The evolution of the target motion model state, r_k, is modeled by a time-homogeneous (time-invariant) r-state Markov chain with the transition probabilities,

$$\pi_{ij} \triangleq \Pr\{r_{k+1} = j | r_k = i\},\ \forall\, i, j \in \{1, 2, \ldots, r\}. \tag{A.1}$$

The transition probability matrix (TPM), $\Pi = [\pi_{ij}]$ is a $r \times r$ matrix with elements satisfying $\pi_{ij} \geq 0$ and $\sum_{j=1}^{r} \pi_{ij} = 1,\ \forall\, i \in \{1, 2, \ldots, r\}$. The TPM used in this work with $r = 2$ is

$$\Pi = \begin{bmatrix} 0.99 & 0.01 \\ 0.01 & 0.99 \end{bmatrix}. \tag{A.2}$$

A.1 State Space Representations for Target Motion Models

State vector for a target moving in a 2-D plane is

$$\mathbf{x}_k = \begin{bmatrix} x_k & \dot{x}_k & y_k & \dot{y}_k \end{bmatrix}^T, \tag{A.3}$$

where x_k and y_k are the target position in Cartesian coordinates, $\dot{x}_k$ and $\dot{y}_k$ are the target velocities at time k.

The problem addressed is the estimation of the state (position) of the moving target which obeys 2 possible modes (models) that are CV with different process noise covariance, $\mathbf{Q}^j$, for $j = 1, 2$. The state space representation is considered as

$$\mathbf{x}_{k+1} = \mathbf{A}_k^j \mathbf{x}_k + \mathbf{G}_k^j \mathbf{w}_k^j, \tag{A.4}$$

$$\mathbf{y}_k = \mathbf{C}_k^j \mathbf{x}_k + \mathbf{H}_k^j \mathbf{v}_k^j, \tag{A.5}$$

where $\mathbf{w}_k^j$ is the process noise distributed with $\mathbf{w}_k^j \sim \mathcal{N}(\mathbf{w}_k^j; 0, \mathbf{Q}^j)$ and $\mathbf{v}_k^j$ is the measurement noise distributed with $\mathbf{v}_k^j \sim \mathcal{N}(\mathbf{v}_k^j; 0, \mathbf{R}^j)$ for model-j.

In (A.5), $\mathbf{y}_k$ is the 2×1 measurement vector consists only position of the moving target at time k. The coefficient parameters for state and noise vectors shown in (A.4) and (A.5) are assumed to be known. They are defined as follows:

$$\mathbf{A}_k^1 = \mathbf{A}_k^2 = \mathbf{A} = \begin{bmatrix} 1 & 0 & T & 0 \\ 0 & 1 & 0 & T \\ 0 & 0 & 1 & 0 \\ 0 & 0 & 0 & 1 \end{bmatrix}, \tag{A.6}$$

$$\mathbf{G}_k^1 = \mathbf{G}_k^2 = \mathbf{G} = \begin{bmatrix} T^2/2 & 0 \\ 0 & T \\ T^2/2 & 0 \\ 0 & T \end{bmatrix}, \tag{A.7}$$

where the sampling interval is $T = 1$ s. The other matrices are

$$\mathbf{Q}^1 = \begin{bmatrix} 0.1^2 & 0 \\ 0 & 0.1^2 \end{bmatrix} (\text{m/s}^2)^2 \quad \& \quad \mathbf{Q}^2 = \begin{bmatrix} 10^2 & 0 \\ 0 & 10^2 \end{bmatrix} (\text{m/s}^2)^2, \tag{A.8}$$

$$\mathbf{C}_k^1 = \mathbf{C}_k^2 = \mathbf{C} = \begin{bmatrix} 1 & 0 & 0 & 0 \\ 0 & 1 & 0 & 0 \end{bmatrix}, \tag{A.9}$$

$$\mathbf{H}_k^1 = \mathbf{H}_k^2 = \mathbf{H} = \begin{bmatrix} 1 & 0 \\ 0 & 1 \end{bmatrix}, \tag{A.10}$$

$$\mathbf{R}^1 = \mathbf{R}^2 = \mathbf{R} = \begin{bmatrix} \sigma_x^2 & 0 \\ 0 & \sigma_y^2 \end{bmatrix}, \tag{A.11}$$

where σ_x and σ_y are standard deviations of measurement in x and y directions, e.g. $\sigma_x = \sigma_y = 80$ m.

A.2 Interacting Multiple Model Estimator

In the interacting multiple model estimator, at time k the state estimate is computed under *each possible current model* using r filters, with each filter using a different combination of the previous model-conditioned estimates — *mixed initial conditions* [63]. The IMM estimates the posterior distribution of the state as follows:

$$p(\mathbf{x}_k|\mathbf{y}_{0:k}) = \sum_{j=1}^{r} p(\mathbf{x}_k|r_k = j, \mathbf{y}_{0:k}) P(r_k = j|\mathbf{y}_{0:k}). \tag{A.12}$$

In (A.12), $P(r_k = j|\mathbf{y}_{0:k})$ denotes the mode probability of model-j that will be derived later and $p(\mathbf{x}_k|r_k = j, \mathbf{y}_{0:k})$ is approximated as

$$p(\mathbf{x}_k|r_k = j, \mathbf{y}_{0:k}) \approx \mathcal{N}(\mathbf{x}_k; \hat{\mathbf{x}}_{k|k}^j, \mathbf{P}_{k|k}^j), \tag{A.13}$$

then (A.12) becomes a mixture of Gaussian distributions with weightings mode probabilities,

$$p(\mathbf{x}_k|\mathbf{y}_{0:k}) \approx \sum_{j=1}^{r} \mathcal{N}(\mathbf{x}_k; \hat{\mathbf{x}}^j_{k|k}, \mathbf{P}^j_{k|k})\mu^j_k, \tag{A.14}$$

where

$$\mu^j_k \triangleq P(r_k = j|\mathbf{y}_{0:k}). \tag{A.15}$$

Recursive steps to find the mode-conditioned estimate $\hat{\mathbf{x}}^j_{k|k}$, mode-conditioned covariance $\mathbf{P}^j_{k|k}$ and mode probability μ^j_k in (A.14) are briefly given with the knowledge of $\hat{\mathbf{x}}^j_{k-1|k-1}$, $\mathbf{P}^j_{k-1|k-1}$, μ^j_{k-1} and Π for $j = 1, 2, \ldots, r$.

Step 1: Mixing probability calculation.

$$\begin{aligned}
\mu^{i|j}_{k-1|k-1} &\triangleq P(r_{k-1} = i|r_k = j, \mathbf{y}_{0:k-1}), \qquad \text{(A.16)}\\
&= \frac{P(r_{k-1} = i, r_k = j|\mathbf{y}_{0:k-1})}{P(r_k = j|\mathbf{y}_{0:k-1})},\\
&= \frac{P(r_k = j|r_{k-1} = i, \mathbf{y}_{0:k-1})P(r_{k-1} = i|\mathbf{y}_{0:k-1})}{P(r_k = j|\mathbf{y}_{0:k-1})},\\
&= \frac{P(r_k = j|r_{k-1} = i, \mathbf{y}_{0:k-1})P(r_{k-1} = i|\mathbf{y}_{0:k-1})}{\sum_{\ell=1}^{r} P(r_k = j, r_{k-1} = \ell|\mathbf{y}_{0:k-1})},\\
&= \frac{P(r_k = j|r_{k-1} = i, \mathbf{y}_{0:k-1})P(r_{k-1} = i|\mathbf{y}_{0:k-1})}{\sum_{\ell=1}^{r} P(r_k = j|r_{k-1} = \ell, \mathbf{y}_{0:k-1})P(r_{k-1} = \ell|\mathbf{y}_{0:k-1})},\\
&= \frac{\pi_{ij}\mu^i_{k-1}}{\sum_{\ell=1}^{r} \pi_{\ell j}\mu^\ell_{k-1}}. \qquad \text{(A.17)}
\end{aligned}$$

Step 2: Interaction (mixing).

$$\hat{\mathbf{x}}^{0j}_{k-1|k-1} = \sum_{i=1}^{r} \hat{\mathbf{x}}^i_{k-1|k-1}\mu^{i|j}_{k-1|k-1}, \tag{A.18}$$

$$\begin{aligned}
\mathbf{P}^{0j}_{k-1|k-1} = \sum_{i=1}^{r} \mu^{i|j}_{k-1|k-1}\Big[&\mathbf{P}^i_{k-1|k-1} + \big(\hat{\mathbf{x}}^i_{k-1|k-1} - \hat{\mathbf{x}}^{0j}_{k-1|k-1}\big)\\
&\big(\hat{\mathbf{x}}^i_{k-1|k-1} - \hat{\mathbf{x}}^{0j}_{k-1|k-1}\big)^T\Big]. \qquad \text{(A.19)}
\end{aligned}$$

Step 3: Mode-matched filtering.

The estimate (A.18) and covariance (A.19) are used as input to filter M_j at time k.

Step 3a: Time update (prediction update).

$$\hat{\mathbf{x}}^j_{k|k-1} = \mathbf{A}^j_{k-1}\hat{\mathbf{x}}^{0j}_{k-1|k-1}, \tag{A.20}$$

$$\mathbf{P}^j_{k|k-1} = \mathbf{A}^j_{k-1}\mathbf{P}^{0j}_{k-1|k-1}{\mathbf{A}^j_{k-1}}^T + \mathbf{G}^j_{k-1}\mathbf{Q}^j{\mathbf{G}^j_{k-1}}^T, \tag{A.21}$$

$$\hat{\mathbf{y}}^j_{k|k-1} = \mathbf{C}^j_k\hat{\mathbf{x}}^j_{k|k-1}. \tag{A.22}$$

Step 3b: Measurement update.

$$\mathbf{S}^j_k = \mathbf{C}^j_k\mathbf{P}^j_{k|k-1}{\mathbf{C}^j_k}^T + \mathbf{H}^j_k\mathbf{R}^j{\mathbf{H}^j_k}^T, \tag{A.23}$$

$$\mathbf{K}^j_k = \mathbf{P}^j_{k|k-1}{\mathbf{C}^j_k}^T{\mathbf{S}^j_k}^{-1}, \tag{A.24}$$

$$\hat{\mathbf{x}}^j_{k|k} = \hat{\mathbf{x}}^j_{k|k-1} + \mathbf{K}^j_k(\mathbf{y}_k - \hat{\mathbf{y}}^j_{k|k-1}), \tag{A.25}$$

$$\begin{aligned}\mathbf{P}^j_{k|k} &= \mathbf{P}^j_{k|k-1} - \mathbf{K}^j_k\mathbf{S}^j_k{\mathbf{K}^j_k}^T, &\text{(A.26)}\\ &= \mathbf{P}^j_{k|k-1} - \mathbf{K}^j_k\mathbf{S}^j_k\Big[\mathbf{P}^j_{k|k-1}{\mathbf{C}^j_k}^T{\mathbf{S}^j_k}^{-1}\Big]^T,\\ &= \Big[\mathbf{I} - \mathbf{K}^j_k\mathbf{C}^j_k\Big]\mathbf{P}^j_{k|k-1}. &\text{(A.27)}\end{aligned}$$

In (A.23) and (A.24), the measurement prediction covariance (innovation[1] covariance) and Kalman filter (KF) gain are given respectively. The KF matched to each of model that gives the mode-conditioned estimate (A.25) and mode-conditioned covariance (A.27).

Step 3c: Likelihood function computation.

$$\Lambda^j_k = p(\mathbf{y}_k|r_k = j, \mathbf{y}_{0:k-1}), \tag{A.28}$$

$$\Lambda^j_k \sim \mathcal{N}(\mathbf{y}_k; \hat{\mathbf{y}}^j_{k|k-1}, \mathbf{S}^j_k), \tag{A.29}$$

$$\Lambda^j_k = \frac{1}{\sqrt{(2\pi)^2\big|\mathbf{S}^j_k\big|}}\exp\Big[-\frac{1}{2}\big(\mathbf{y}_k - \hat{\mathbf{y}}^j_{k|k-1}\big)^T\big(\mathbf{S}^j_k\big)^{-1}\big(\mathbf{y}_k - \hat{\mathbf{y}}^j_{k|k-1}\big)\Big]. \tag{A.30}$$

[1] $\mathbf{y}_k - \hat{\mathbf{y}}^j_{k|k-1}$ is called the innovation.

Step 6: Mode-probability update.

Expression for mode probability defined previously in (A.15) can be derived as

$$\begin{aligned}
\mu_k^j &= P(r_k = j|\mathbf{y}_{0:k}), \qquad \text{(A.31)}\\
&= \frac{P(r_k = j, \mathbf{y}_k|\mathbf{y}_{0:k-1})}{P(\mathbf{y}_k|\mathbf{y}_{0:k-1})},\\
&= \frac{P(r_k = j, \mathbf{y}_k|\mathbf{y}_{0:k-1})}{\sum_{j=1}^{r} P(r_k = j, \mathbf{y}_k|\mathbf{y}_{0:k-1})},\\
&= \frac{P(\mathbf{y}_k|r_k = j, \mathbf{y}_{0:k-1})P(r_k = j|\mathbf{y}_{0:k-1})}{\sum_{j=1}^{r} P(\mathbf{y}_k|r_k = j, \mathbf{y}_{0:k-1})P(r_k = j|\mathbf{y}_{0:k-1})},\\
&= \frac{\Lambda_k^j \sum_{i=1}^{r} P(r_k = j, r_{k-1} = i|\mathbf{y}_{0:k-1})}{\sum_{j=1}^{r} \Lambda_k^j \sum_{i=1}^{r} P(r_k = j, r_{k-1} = i|\mathbf{y}_{0:k-1})},\\
&= \frac{\Lambda_k^j \sum_{i=1}^{r} P(r_k = j|r_{k-1} = i, \mathbf{y}_{0:k-1})P(r_{k-1} = i|\mathbf{y}_{0:k-1})}{\sum_{j=1}^{r} \Lambda_k^j \sum_{i=1}^{r} P(r_k = j|r_{k-1} = i, \mathbf{y}_{0:k-1})P(r_{k-1} = i|\mathbf{y}_{0:k-1})},\\
&= \frac{\Lambda_k^j \sum_{i=1}^{r} \pi_{ij}\mu_{k-1}^i}{\sum_{j=1}^{r} \Lambda_k^j \sum_{i=1}^{r} \pi_{ij}\mu_{k-1}^i}. \qquad \text{(A.32)}
\end{aligned}$$

Step 7: State estimate combiner.

$$\hat{\mathbf{x}}_{k|k} = \sum_{j=1}^{r} \hat{\mathbf{x}}_{k|k}^j \mu_k^j, \qquad \text{(A.33)}$$

$$\mathbf{P}_{k|k} = \sum_{j=1}^{r} \mu_k^j \Big[\mathbf{P}_{k|k}^j + \big(\hat{\mathbf{x}}_{k|k}^j - \hat{\mathbf{x}}_{k|k}\big)\big(\hat{\mathbf{x}}_{k|k}^j - \hat{\mathbf{x}}_{k|k}\big)^T\Big]. \qquad \text{(A.34)}$$

These steps comprise the algorithm of a one cycle of IMM estimator. A block diagram summarizes the IMM estimator is shown in Figure A.1.

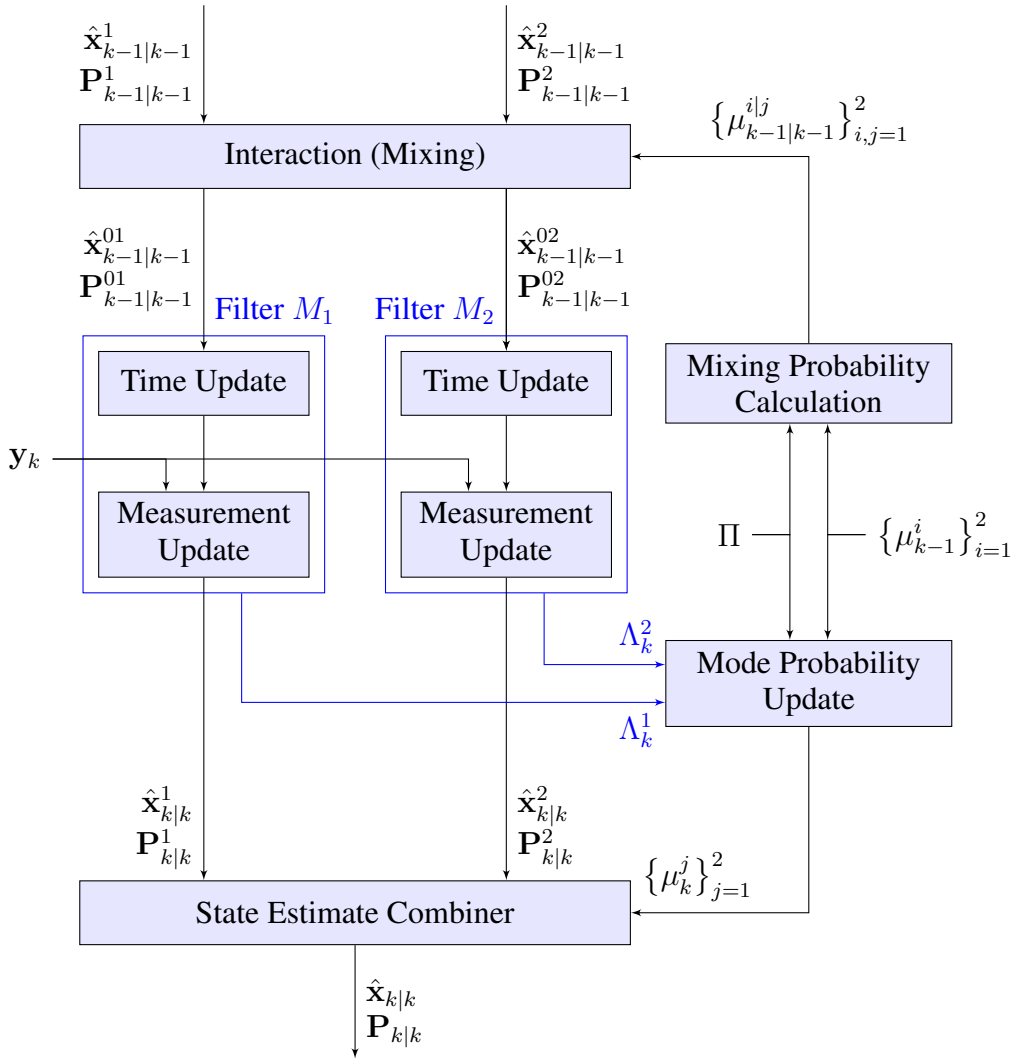

Figure A.1: Block diagram of a one cycle of IMM estimator for 2-models.

APPENDIX B

PROOFS OF LEMMAS

Lemma 1. *Both $\mathcal{H}_{gt}(\mu_k^n)$ and $\mathcal{H}_{bt}(\mu_k^n)$ are continuous and strictly increasing functions for $0 < \mu_k^n < 1$. Moreover, inverse functions $\mathcal{H}_{gt}^{-1}(\mu_k^n)$ of $\mathcal{H}_{gt}(\mu_k^n)$ and $\mathcal{H}_{bt}^{-1}(\mu_k^n)$ of $\mathcal{H}_{bt}(\mu_k^n)$ exist, and they are strictly increasing for $0 < \mu_k^n < r$.*

Proof. First derivatives of $\mathcal{H}_{gt}(\mu_k^n)$ and $\mathcal{H}_{bt}(\mu_k^n)$ are

$$\mathcal{H}'_{gt}(\mu_k^n) = \frac{\mathrm{d}\mathcal{H}_{gt}(\mu_k^n)}{\mathrm{d}\mu_k^n}, \tag{B.1}$$

$$= \frac{r\theta_0\theta_1}{\left[(\theta_0-\theta_1)\mu_k^n + \theta_1\right]^2}, \tag{B.2}$$

$$\mathcal{H}'_{bt}(\mu_k^n) = \frac{\mathrm{d}\mathcal{H}_{bt}(\mu_k^n)}{\mathrm{d}\mu_k^n}, \tag{B.3}$$

$$= \frac{r(1-\theta_0)(1-\theta_1)}{\left[1-(\theta_0-\theta_1)\mu_k^n - \theta_1\right]^2}. \tag{B.4}$$

Knowing $\mathcal{H}_{gt}(0^+) = \mathcal{H}_{bt}(0^+) = 0^+$ and $\mathcal{H}_{gt}(r) = \mathcal{H}_{gt}(r) = r$ from (4.29) and (4.31) respectively, the facts that $\mathcal{H}'_{gt}(\mu_k^n)$ and $\mathcal{H}'_{bt}(\mu_k^n)$ are continuous and not negative imply that $\mathcal{H}_{gt}(\mu_k^n)$ and $\mathcal{H}_{bt}(\mu_k^n)$ are continuous and strictly increasing functions. This also implies that $\mathcal{H}_{gt}^{-1}(\mu_k^n)$ and $\mathcal{H}_{bt}^{-1}(\mu_k^n)$ exist as

$$\mathcal{H}_{gt}^{-1}(\mu_k^n)\frac{\theta_1\mu_k^n}{(\theta_1-\theta_0)\mu_k^n + r\theta_0}, \tag{B.5}$$

$$\mathcal{H}_{bt}^{-1}(\mu_k^n) = \frac{(1-\theta_1)\mu_k^n}{(\theta_0-\theta_1)\mu_k^n + (1-\theta_0)r}, \tag{B.6}$$

respectively, and are strictly increasing for $0 < \mu_k^n < r$. □

Lemma 2. *$\mathcal{H}_{gt}(\mu_k^n)$ is strictly concave and $\mathcal{H}_{bt}(\mu_k^n)$ is strictly convex for $0 < \mu_k^n < 1$.*

Proof. Second derivatives of $\mathcal{H}_{gt}(\mu_k^n)$ and $\mathcal{H}_{bt}(\mu_k^n)$ are

$$\mathcal{H}''_{gt}(\mu_k^n) = \frac{\mathrm{d}\mathcal{H}'_{gt}(\mu_k^n)}{\mathrm{d}\mu_k^n}, \tag{B.7}$$

$$= \frac{-2r\theta_0\theta_1(\theta_0 - \theta_1)}{\left[(\theta_0 - \theta_1)\mu_k^n + \theta_1\right]^3}, \tag{B.8}$$

$$\mathcal{H}''_{bt}(\mu_k^n) = \frac{\mathrm{d}\mathcal{H}'_{bt}(\mu_k^n)}{\mathrm{d}\mu_k^n}, \tag{B.9}$$

$$= \frac{2r(1-\theta_0)(1-\theta_1)(\theta_0 - \theta_1)}{\left[1 - (\theta_0 - \theta_1)\mu_k^n - \theta_1\right]^3}. \tag{B.10}$$

The assumption, $\theta_0 > \theta_1$, claimed on page 72 guarantees that (B.8) is always negative and so $\mathcal{H}_{gt}(\mu_k^n)$ is strictly concave for $0 < \mu_k^n < 1$. That assumption also guarantees that (B.10) is always positive and so $\mathcal{H}_{bt}(\mu_k^n)$ is strictly convex for $0 < \mu_k^n < 1$. □

APPENDIX C

A VIEW TO THE RADAR SIMULATOR GUI

The radar simulator GUI is shown in Figure C.1 for MTATBS and Figure C.2 for KS. There is a plot area supports zoom in/zoom out, data cursor, rotate and pan functions. This area is very useful and informs the resource manager about how-to use or what the results. It changes interactively to correspond the operations directed by resource manager. Options which can be typed by resource manager are as follows:

- *Number of targets* is allowed between 1 and 40. The number of targets is limited to 40, since processing time becomes too much for higher values when KS is utilized. The default value is 15.
- *End time* of simulation is allowed between 10 and 1000 s. The default value is 500 s.
- *Surveillance update time* is allowed between 10 and 1000 s. This value corresponds to time that is necessary to a complete search of the region of interest, so it is namely a conventional update time. The flag named as "Surveillance is not fragmented" is used to activate this value. If this flag is disabled, the value of surveillance update time is useless. The default value is 25 s.
- *Number of frequency bands* can be used when task interleaving technique is enabled. It is allowed between 2 and 7. The default value is 2.
- *Priority threshold* is allowed between 1 and 3. The priority threshold can be set as 3 at most, instead of 5 to decrease the number of undetected targets. Simulator does not schedule the track updates of targets which have less priority than the threshold. The default value is 1.

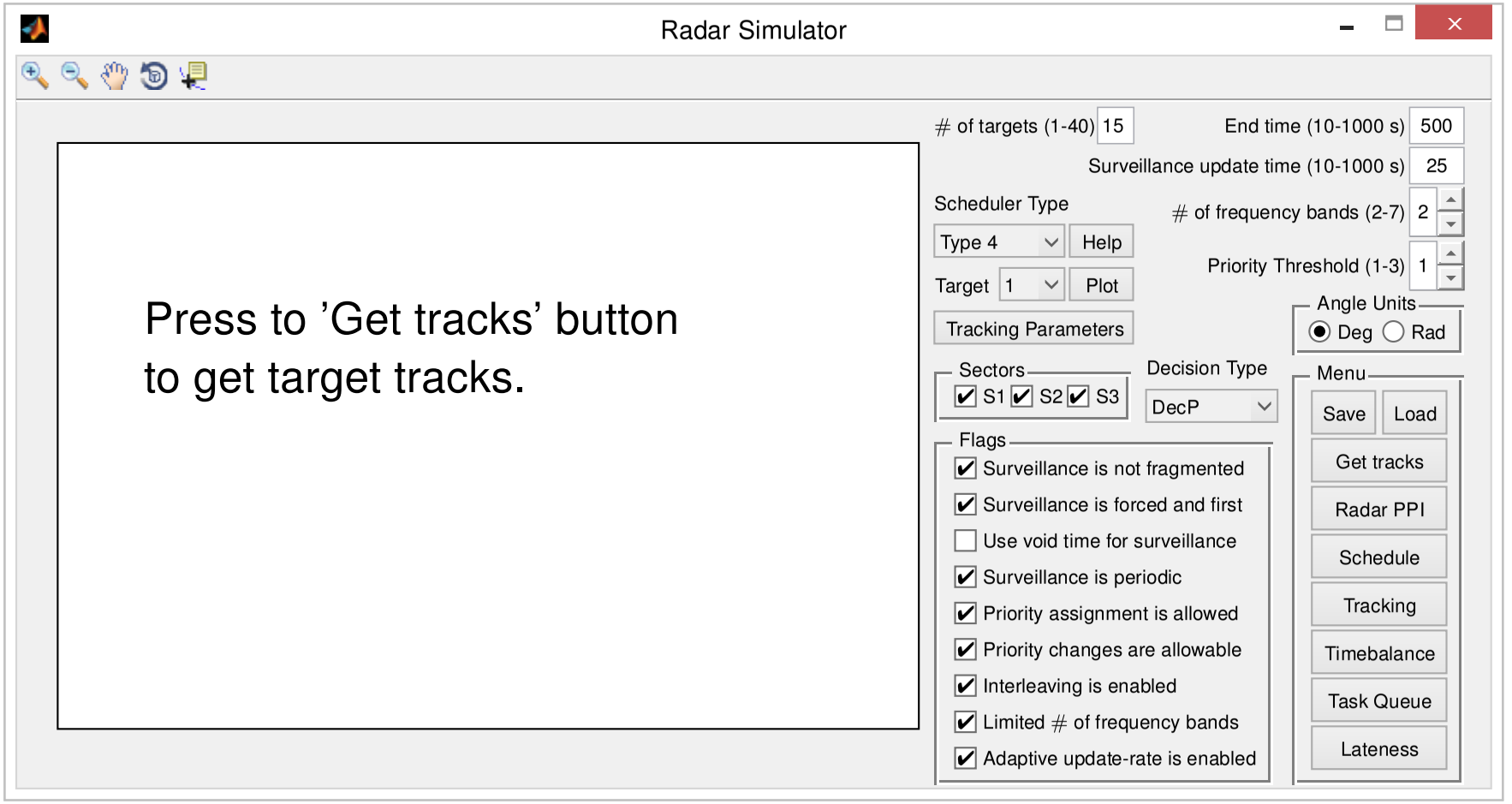

Figure C.1: Radar Simulator GUI for MTATBS.

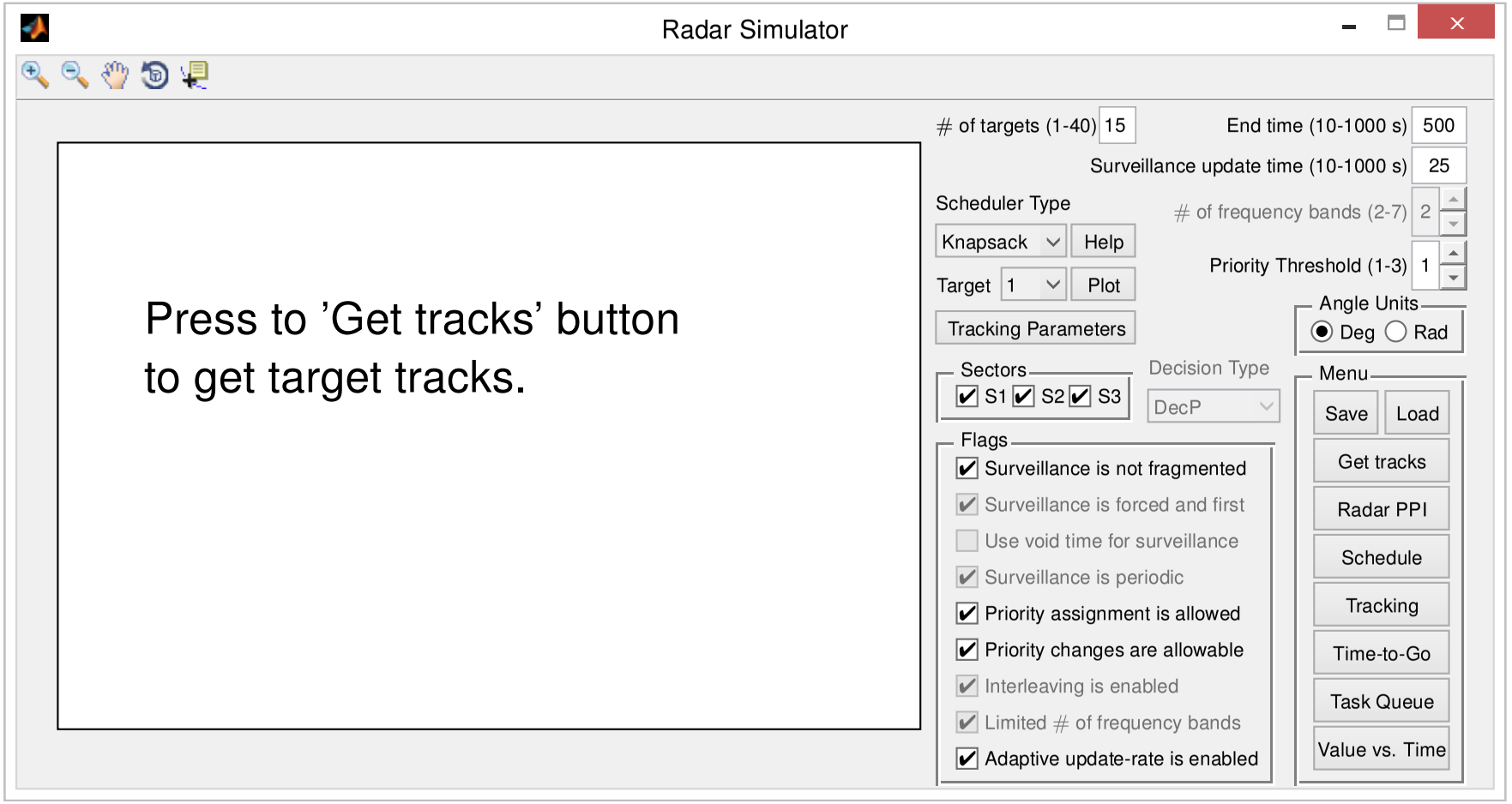

Figure C.2: Radar Simulator GUI for KS.

Scheduler type includes:

- Type 1 for MTATBS-Type 1,
- Type 2 for MTATBS-Type 2,
- Type 3 for MTATBS-Type 3,
- Type 4 for MTATBS-Type 4,
- Knapsack for KS.

Decision type includes:

- CfTUL for the method of choosing first target in the update list,
- DecP for the method of decision policy,
- MinTE the method of minimizing the tracking error,
- PurMM the method of pursuing the most maneuvering.

Angle units selection is used only for visualization of targets on "Radar PPI" and "Tracking" plots. It only changes the unit of angle for polar coordinates shown on PPI display from radians to degrees or vice versa. A sample plot is shown in Figure 2.2 when degree option is selected.

Sectors selection panel includes the sectors, where each of them corresponds to $2\pi/3$ radians or 120° and all of them are initially enabled. Visualization of sectors is shown in Figure 2.2.The sectors are

- S1 for sector 1,
- S2 for sector 2,
- S3 for sector 3.

Help button opens a help window for radar simulator.

Plot button shows the true tracks, detections, measurements and IMM tracking samples of the selected target with confidence ellipses. The sample plots are shown in Figure 4.1.

Tracking parameters button opens a window which can be utilized to change the tracking parameters, as shown in Figure C.3.

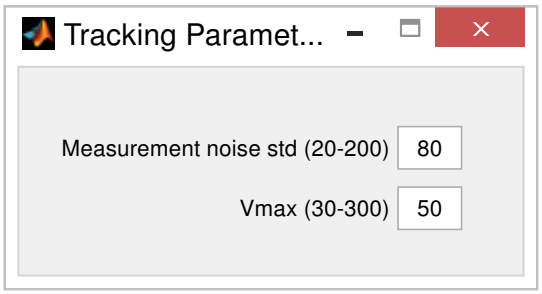

Figure C.3: Tracking parameters option.

Flags help resource manager enable or disable RRM options. Supported flags are

- *Surveillance is not fragmented*, the flag specifies the type of surveillance as conventional or fragmented. If this flag is disabled, there is no a task named as surveillance in the task list and idle time label shown in "Task Queue" plot belongs to fragmented surveillance. Flag name is changed to "Schedule surveillance, if possible", if resource manager selects the scheduler type as "Knapsack". However, KS does not guarantee to schedule surveillance task even if resource manager enables that flag, as scheduler aims only to get maximum total utility. Hence, it cannot be forced to schedule any task that does not increase the total utility desirably with KS. The sample plot is shown in Figure 2.7 when this flag is enabled.

- *Surveillance is forced and first*, the flag is supported only by MTATBS and denotes that surveillance is thought as a tracking task and each scheduling interval starts with surveillance task. Here, the scheduling interval denotes the number and identity of detected targets does not change. Hence, it is assumed that there is not any target drop or new detected target within the scheduling interval. The

time interval between two cascaded surveillance tasks can be less than the surveillance update time, if there is a target drop or detection in that interval. "Task Queue" plot is shown in Figure 2.7 that the surveillance task is the first task in radar timeline.

- *Use void time for surveillance*, the flag is supported only by MTATBS and denotes the scheduling times of surveillance task updates depend on available gaps, computed by ATB technique, on the timeline.
- *Surveillance is periodic*, the flag is supported only by MTATBS and denotes the surveillance task has a fixed task update time.
- *Priority assignment is allowed*, the flag enables the task prioritization. If it is disabled, all tasks have the priority level 1. This flag is provided to check the performance of decision methods, when there are lots of targets to make a selection. It is not suggested to disable it for general case, since the scheduling process time increases too much for target selection.
- *Priority changes are allowable*, the flag enables the dynamic task prioritization to be aware of the priority changes that affect the scheduling performance, while targets are moving in the region of interests and through the fixed priority rings. The sample plots are shown in Figure 2.5.
- *Interleaving is enabled*, the flag enables task interleaving technique.
- *Limited number of frequency bands*, the flag enables the multi-frequency bands technique.
- *Adaptive update-rate is enabled*, the flag enables the adaptive update-rate technique which modifies task update times to enhance the tracking performance.

Menu panel consists of

- *Save* button saves the targets data to a file.
- *Load* button loads the targets data from a file.
- *Get tracks* button randomly generates the targets which obey the motion models CV and CT in 2-D space.

- *Radar PPI* button shows tracks of targets. The sample plots are shown in Figure 2.2 and Figure 3.10.

- *Schedule* button schedules the tasks and shows the distribution of completed tasks. The sample plots can be found in section 3.2.

- *Tracking* button plots detected (or updated) tracks of targets. The sample plots are shown in Figure 2.5 and Figure 2.13.

- *Timebalance* button plots TB scheme of tracking and surveillance tasks. The sample plots are shown in Figure 2.12 and are found in section 3.2.1. If resource manager changes the scheduler type to "Knapsack", button plots the time-to-go scheme of tracking and surveillance tasks, as shown in Figure 3.26(a).

- *Task Queue* button plots scheduled task queue. The sample plots are shown in Figure 2.7 and Figure 2.10.

- *Lateness* button plots the histogram of lateness of tracking tasks. The sample plot for individual cumulative distribution of latenesses can be found in section 3.2.1. If resource manager changes the scheduler type to "Knapsack", button plots value vs. time graph of tracking and surveillance tasks, as shown in Figure 3.26(b).